International Journal of Comprehensive Engineering

ISSN 2186-2680

Volume 2, Number 3, September 2013

Published by
International Association of Comprehensive Engineering (IACE)

http://www.iace-journal.org/

Printed by
Diagnosis Engineering & Technology Corp., Japan

========== International Journal of Comprehensive Engineering (IJCE) ==========

International Journal of Comprehensive Engineering (IJCE) is an international interdisciplinary journal that integrates publication from aspects of research on engineering science. This journal provides a medium of communication among engineers and scientists who have engaged in research and development concerning the fields of comprehensive engineering, while maintaining a healthy balance between fundamental and experimental topics. Now, the journal has three separate fields, the scopes of which are Part A: Maintenance Engineering; Part B: Intelligent Engineering; Part C: Engineering in Agriculture, Ocean and Light Industry shown in flows, and other specialized fields will also be updated in the near future.

Part A: Maintenance Engineering

Topics of interest for submission on the field of maintenance engineering include, but are not limited to:
Condition Diagnosis Engineering and Technology; Sensing Technology; Maintenance Management; Fault Tolerant System; Fault Self-Recovery Engineering; E-Maintenance; Signal Processing; Risk, Health and Safety Management; Structural Health Monitoring; Information and Communication Technology; Data and Information Fusion; Reliability/Quality; Maintenance Robot; Data Quality and Acquisition; Human Factors; Education and Training; Risk Based Engineering; Others on Maintenance.

Part B: Intelligent Engineering

Topics of interest for submission on the field of intelligent engineering include, but are not limited to:
Application of Artificial Intelligence in Engineering; Intelligent Design, Modeling, Planning and Control for Applied Engineering; Intelligent Robot System; Intelligent Fault Diagnosis; Intelligent Signal Processing for Applied Engineering; Others on Intelligent Engineering.

Part C: Engineering in Agriculture, Ocean and Light Industry

Topics of interest for submission on the field of engineering in agriculture, ocean and light industry include, but are not limited to:
Agriculture Engineering: Agricultural Equipment and Mechanical Engineering; Agricultural Bioenvironmental Engineering; Agricultural Renewable Energy Engineering; Agricultural Produce Processing Engineering; Agricultural Information and Electrical Technologies; Others on Agricultural Engineering.
Ocean Engineering: New Ocean Energy; Ocean Maintenance Technology; Ocean Monitoring Technology; Ocean Diagnosis Method; Ocean Experimental Development; Professional Sensor Technology; Observational and Computational Tools Others on Ocean Engineering.
Light Industry Engineering: Agri-food Products Processing/Packaging Technology and Equipment; Comprehensive Utilization of Resource; Preservation; Storage and Packaging of Agri-food Products; Innovative IT Applications in Agri-food Chain; Sensing, Testing, Automation and Internet of Things Technologies; Green Environmental Protection; Energy Saving Technologies; Others on Light Industry.

========== Manuscript Submission ==========

Manuscripts should be submitted online at http://www.iace-journal.org/ by registering and logging in to the website of the IJCE. Once you have registered, please click the “Submit Manuscript” to go to the submission from. Please use the MS Word template file to prepare your manuscript. Manuscript prepared in MS Word must be converted into a single file before submission. The Microsoft Word template file can be downloaded from the website of the IJCE.

========== Submission Declaration ==========

The submission, such as articles, reviews, technical report etc., to the IJCE means these facts that the work described has not been published previously, that it is not under consideration for publication elsewhere, that its publication is approved by all authors and tacitly or explicitly by the responsible authorities where the work was carried out, and that, if accepted, it will not be published elsewhere including electronically in the same form, in English or in any other language, without the written consent of the copyright-holder.

========== Copyright ==========

Authors will be asked to complete a "Copyright Transfer Statement", when submitting the manuscript. Acceptance of the agreement will ensure the widest possible dissemination of information. Permission of the publisher is required for resale or distribution outside the institution and for all other derivative works, including compilations and translations. The "Copyright Transfer Statement" can be downloaded from the website of the IJCE as follows:
http://www.iace-journal.org/views/Copyright_Transfer_Statement.pdf.

========== Review Policy ==========

The following types of contribution to the IJCE are peer-reviewed: Articles, Reviews and Technical Reports. The articles accepted for publishing in the IJCE include regular paper and letter, which will be decided by editors according the reviewing results. All forms of published correction may also be peer-reviewed at the discretion of the editors. Other contributed types to the IJCE, particularly if they present technical information, may be peer-reviewed at the discretion of the editors. For any general questions and comments about the peer-review process, the journal or its editorial policies that are not mentioned here, please contact us using the email: ijce@nifty.com. Questions about a specific submitted manuscript should be directed to the executive editor who is handling the manuscript.

International Journal of Comprehensive Engineering (IJCE)

Volume 2, Number 3, September 2013 (ISSN 2186-2680)

International Journal of Comprehensive Engineering
Part A, 2(3), 215-222, 2013
Doi: 10.14270/IJCE2013.2.3.a215
Regular paper

ISSN 2186-2680
e-ISSN 2186-2656
www.iace-journal.org

Research of Online Detection analytical methods and Experiment for Automobile Transmission

Sheng Fu [1], Shasha Cai [1], Xiaomin Zhu [2]

[1] School of Mechanical & Electrical Engineering, Beijing University of Technology, Beijing, 100029, China
[2] Beijing Research Institute of Automation for Machinery Industry

[#] Corresponding author: fusheng@bjut.edu.cn; Tel.: 13426213281;
caishasha_work@126.com; Tel.: 13811853090

Abstract: According to the fact that transmission's test-on-line has been one important part of automobile industry production line, the paper presents the method that combines order analysis with spectrum analysis to extract characteristic signals, and combines support vector machine (SVM) with standard extremal for the quality detection. The method extracts characteristic signals by making analysis of vibration signal and speed signal, and then puts the characteristic signals into support vector machine model. While the system enriches the SVM training samples by the standard extremal to get a more complete model of support vector machine to complete the quality detection. The paper has made analytical description and experimental studies for the method of signal processing and quality detection, the result shows that the method is simple and effective and has practical value.

Keywords: Transmission, Quality Detection, Order Analysis, SVM.

Received: May 26,2012 / Accepted: May 8,2013 / Published: Sept. 10,2013

1. Introduction

As an important part of automotive driveline, the quality of transmission has very large impact on the overall performance of car. So the producer must make pre-delivery inspection to the transmission in the factory before the transmission is put into operation. The fault signal produced during pre-delivery inspection is quite complicated because there are multiple gears, shafts, bearings and other parts inside in transmission. If you want to accurately diagnose the defect type and location of the transmission, it needs to select the appropriate signal processing methods and quality testing methods. The analysis methods of noise and vibration signal usually include domain analysis, spectral analysis and order analysis. Order analysis technology is a tool that associates the spectrum and time course of the rotating parts with the RPM, which can better reveal the vibration mechanism of rotating machinery fault. The pre-delivery inspection process of automotive transmission is a nonlinear time-varying process. In order to avoid the phenomenon of frequency aliasing, and taking into account the attenuation of the vibration signal transduction process and the effects of sensor installation location, the paper combines order analysis theory with spectrum theory to extract characteristic signals. There are many theories of quality detection, such as pattern recognition, neural networks, expert systems, support vector machines and so on. The paper has selected the detection methods based on the statistical theory - support vector machine(SVM). The method can effectively solve the problems of small sample learning[1]. But when the sample data increase, the corresponding convex programming problem is more complex, computing speed will be slower[2]. The internal structure of automobile transmission is complex and types of defects are various. The premise of using SVM must guarantee the support vector machine model contains comprehensive information of defects. Therefore it needs to constantly enrich the support vector machine model in information. The system enriches the SVM training samples by the standard extremal to get a more complete model of support vector machine, so that can improve the accuracy and detection efficiency of transmission's online pre-delivery inspection.

2. The Methods of Signal Processing

2.1. Order Analysis

The substance of order analysis (also known as order tracking method) is to change time-domain non-stationary signal into angle-domain stationary signal by resampling, and the characteristic signal is more clearly shown by the Fourier transform. Shifting process of automotive transmission is a nonlinear time-varying process, there will be aliasing phenomenon using conventional power spectral analysis for the situation of speed changes[3]. Order analysis technology is a tool that associates the spectrum and time course of the rotating parts with the RPM, which can better reveal the vibration mechanism of rotating machinery fault. So the paper selects order analysis technology to analyze the vibration signal of the transmission test process. Common order tracking methods usually include hardware order tracking method and the calculating order tracking method. In this article the latter is chosen, therefore, it needs to synchronously access to the vibration signal and speed signal of the transmission. Implementation steps are as follows:

(1) Synchronously access to the vibration signal and speed signal of the transmission.

(2) Make low-pass filtering of the vibration signal

(3) Obtain the time series of angle-domain by curve fitting to speed signal

(4) Resample the vibration signal using the time series of angle-domain to obtain the periodic signal of angle-domain

(5) Make Fourier transform to the periodic signal of angle-domain to get the order spectrum

2.2. Cepstrum

Cepstrum analysis is also known as secondary spectrum analysis. It is a new technology in the science of modern signal processing, also as a useful tool to detect periodic components of the complex spectrum. The technology has been widely used in the detection and diagnosis of mechanical failure[4].The structure of transmission is so complex, that the original signal is mixed with all kinds of noise signals. Even if after filtering, there will still be multi-ingredient sideband spectrum. The sideband can be simplified to a single spectral line by spectrum analysis to facilitate the observation and analysis. The signals by processing are usually the convolution Y(t) of vibration signal X(t) and system functions H(t). But in the cepstrum, because of the function of deconvolution, the original relation of convolution between X (t) and H (t) is changed into additive relation and the separation of the signal becomes simple. The characteristics signal of transmission is retained while noise signal is eliminated in the cepstrum.

2.3. Order Cepstrum

Vibration signal obtained in the process of transmission's pre-delivery inspection is a non-stationary signals, it can not be directly analyzed by FFT, or will cause the phenomenon of "frequency aliasing". It needs to change the time-domain non-stationary signals into angle domain periodic signal by resampling. As the re-sampling signal is affected by the modulation and noise, order analysis without cepstrum analysis is difficult to produce better analysis results. The cepstrum analysis has the function of deconvolution, if cepstrum analysis is used to the angle-domain signal, the sideband can be simplified to a single spectral line, while the effect of noise is inhibited. Cepstrum analysis is introduced to order analysis in efforts to identify the periodic information hidden in the power spectrum. The theory of order cepstrum is as follows:

Set the Fourier transform of angle domain re-sampling signal x(θ)is X (f), the function of power spectral density is $S_x(f)$, make inverse Fourier transform of the logarithm of power spectrum $S_x(f)$, the function of order cepstrum $C_x(q)$ [5] is:

$$C_x(q) = F^{-1}\{\log S_x(f)\} \tag{1}$$

$F^{-1}[]$ is the inverse Fourier transform. q is the angle variable of cepstrum , referred to inverted order frequency.

3. The Theory of Quality Detection

Support Vector Machine (SVM) with excellent performance, have a wide range of applications in the field of fault diagnosis of rotating machinery components[1]. For the non-linear classification, the data samples is mapped to a high dimensional feature space Ω from the original space R^d using a nonlinear mapping ϕ ,and then seek the optimal surface in the high dimensional feature space. The high dimensional feature space can be very high, but support vector machine can cleverly solve the problem using Kernel Function. According to the functional

theory, once a kernel function satisfies Mercer condition, that is $K(x_i, y_i) = f(x_i) \cdot f(x_j)$, it simply needs the inner product in the high-dimensional space. The inner product can be implemented by the function of the original space without knowing the specific form of transformation $\phi(x)$ [7]. The optimization objective function of quadratic programming problem is:

$$Q(\partial)=\sum_{i=1}^{n}\partial_i - \frac{1}{2}\sum_{i,j=1}^{n}\partial_i\partial_j y_i y_j K(x_i, y_j) \tag{2}$$

After calculating the optimized coefficient ∂_i using the Eq.(2), the general form of support vector machine classifier function is:

$$f(x) = \mathrm{sgn}\left\{\sum_{SVM}\partial_i\, y_i K(x_i, x_j) + b\right\} \tag{3}$$

$K(x_i, x_j)$ is the kernel function.

Support vector machine is applied to the defect classification of transmission in the article. According to a small number of typical defects sample data in a given, the important objective of this detection system is to achieve fast and accurate classification. To do this, the system selects the polynomial kernel function of a smaller complexity of the algorithm to improve the detection speed. While the system enriches the SVM training samples by the standard extremal to improve the accuracy of detection. The kernel function chosen is the polynomial kernel function: $K(x,y)=(x \cdot y+1)^d$ and d=1,2,3,…, as the order of polynomial. The kernel function has a good global[8]. As shown in Fig. 1, firstly do time-domain average, order analysis and cepstrum analysis to the original signal to get the order spectrum. And extract characteristic signal from the order spectrum, that is the amplitude corresponding to characteristic order of gear and bearing and the three characteristic signals of time domain. The characteristics signal above as the test samples are entered into the support vector machine model to do the first quality detection of the current transmission. When the method of support vector machine does not detect the defects, the system will do the second judgment using the standard extremal. The order spectrum is compared with the standard extremal, if not beyond the standard extremal, the order spectrum is used to update the standard extremal; if it exceeds, find out the corresponding order of the excess part, obtain the defect type and location by querying the database. And the test samples will be used to update the training sample library, and re-train the support vector machine model to make the model contain more information. Support vector machine have the advantages of high speed and accuracy, but the internal structure of transmission is complex, the types of defects contained in training samples are not comprehensive enough. The paper enriches the SVM training samples by the standard extremal, so that support vector machine can quickly and accurately detect the type of defect to achieve the result of high speed and accuracy.

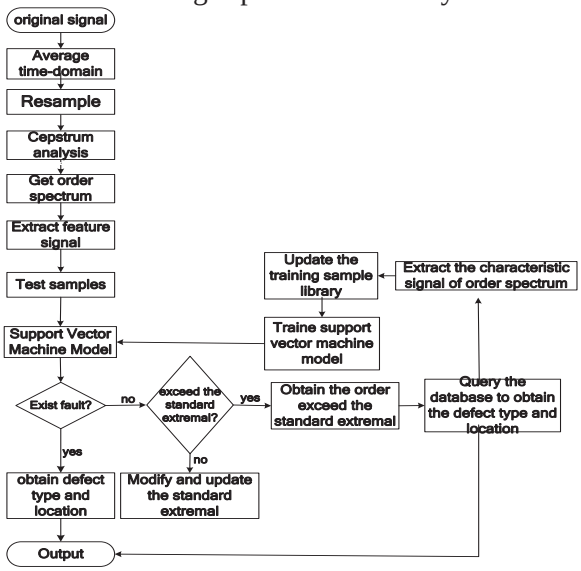

Fig. 1 The Flow Chart of Quality Detection

4. Experimental Verification

The experimental site is shown in Fig.2. The left is the pre-delivery inspection test rig, an automotive transmission is installed on the rig, and the transmission is being detection; the right is the software testing platform to detect if the transmission is eligibility.

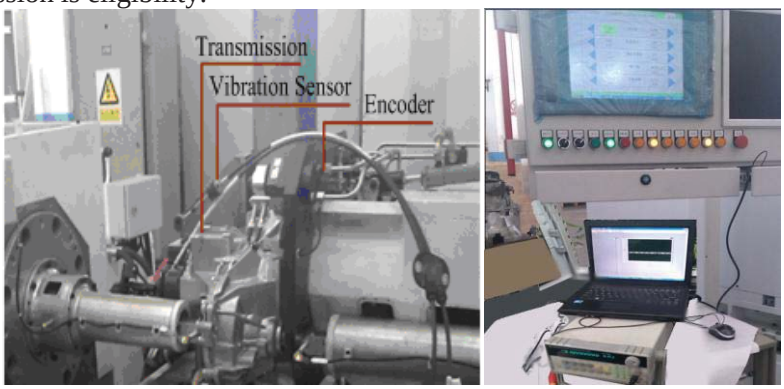

Fig. 2 The experimental site

The transmission structure diagram is shown in the Fig.3. The gear parameters are shown in Table 1, and the bearing parameters are shown in Table 2. The transmission speed is changed by the change of transmission ratio. The transmission analysis results under different rotation speed are different, so each axis of different stalls is corresponding to different standard extremal.

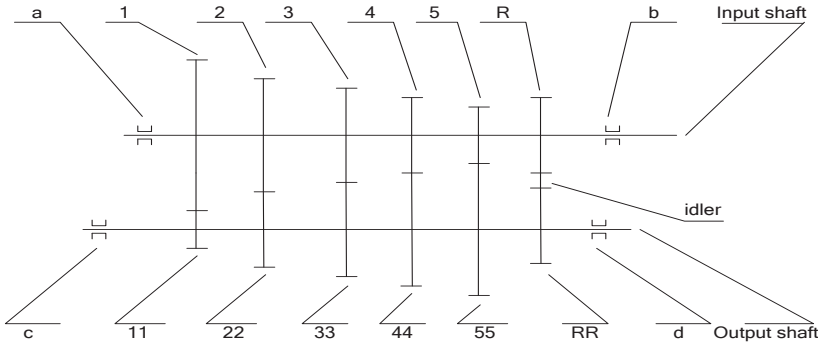

Fig. 3 The transmission structure diagram

Table 1 Gear parameters

Code	Number of teeth	Code	Number of teeth
1	11	11	40
2	22	22	45
3	29	33	41
4	39	44	41
5	41	55	35
6	13	66	47

Table 2 Bearing parameters

Code	Bearing diameter	Roller diameter	Contact angle	Number of rollers
a	24.25	2.55	1	21
b	21.24	13.8	1	7
c	39.38	5.136	1	21
d	26.16	4.16	1	14

The sampling frequency of vibration signal is 5000Hz in the experiment, and the encoder is 2000 lines / rev. The analysis object is the input shaft in raising speed state in the experiment, the number of analysis revolutions is 4, the number of time-domain average is 3, and the analysis order is 256. It intercepts the input shaft signal, and the number of pulses is $M \geq 2000 \times 3 \times 4$. Then the interception dates are uploaded to the signal processing module for analysis. The analysis points are 1024. The interpolation angle is 1.4. Data interception point is 24000. The characteristic parameters are shown in Table 3 according to Table1 and Table2 and the characteristic order formula of gear and bearing.

Table 3 Characteristic order

Order of shaft(fr)	1	Rolling body rotation order of "a" bearing(f_{1z})	8.4fr
Gear meshing order(fm)	11 f_r	The outer ring order of "b" bearing (f_{2w})	1.2fr
The outer ring order of "a" bearing(f_{1w})	9.3f_r	The inter ring order of "b" bearing (f_{2n})	5.8fr
The inter ring order of "a" bearing (f_{1n})	11.6f_r	Rolling body rotation order of "b" bearing (f_{2z})	0.4fr

The output vector SVM classification result is Y={1 2 3}. "1" represents normal transmission state; "2" represents misalignment of gear on the input shaft; "3" represents surface machining error of gear on the input shaft. The following discusses the results of the analysis of three states.

4.1 The normal state of the automotive transmission

The order cepstrums of normal state is shown in Fig.4. It can get by the above calculation of characteristic order that, it should appear peak at the axis of shaft order, second harmonic, gear mesh order and the outer ring order of "a" bearing in the normal state. Due to the function of spectrum, it makes the power spectrum effectively inhibit the effect of noise, and the power spectrum of the periodic component is simplified to a single spectral line for observations and feature extraction signal.

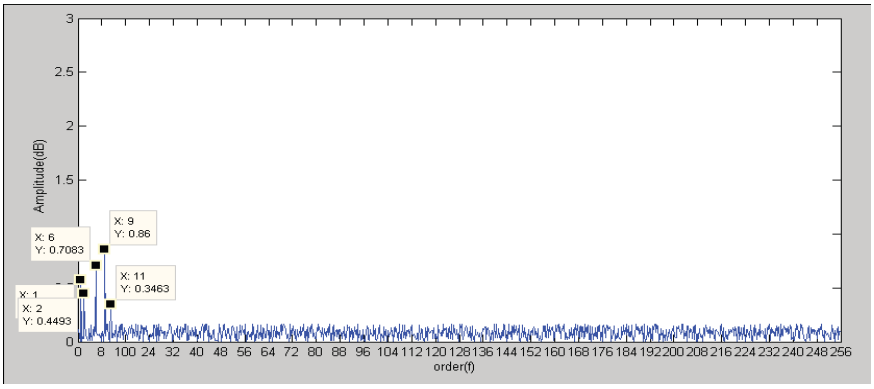

Fig. 4 The order cepstrums of normal state

The time-domain characteristic values include: RMS (x1), Peak (x2), Crest (x3). The frequency-domain characteristic values include: the shaft order (x4), the second harmonic of shaft order (x5), the outer ring order of "a" bearing (x6), the inter ring order of "a" bearing (x7), the rolling body rotation order of "a" bearing (x8), the outer ring order of "b" bearing (x9), the inter ring order of "b" bearing (x10), the rolling body rotation order of "b" bearing (x11), gear mesh order (x12), the second harmonic of gear mesh order (x13). The time-domain characteristic values and the frequency-domain characteristic values extracted are shown in Table 4.

Table 4 Characteristic values

x1			x2				x3		
0.8600			0.3641				2.3620		
x4	x5	x6	x7	x8	x9	x10	x11	x12	x13
0.1139	0.4493	0.8600	0.7702	0.0012	0.0081	0.1511	0.7083	0.3463	0.0315

In this test, the output of SVM model is "1". It indicates the transmission has no defect. On the basis of the system detection principle, if it indicates the transmission has no defect by the method of SVM, the system needs the second detection with the method of the standard extremal. The detection result is shown in Fig.5. The red line is the standard extremal, while the blue line is the order cepstrums of the transmission. We can see that

the order cepstrum did not exceed the standard extremal, so the transmission has no defect and the result of two detections is the same.

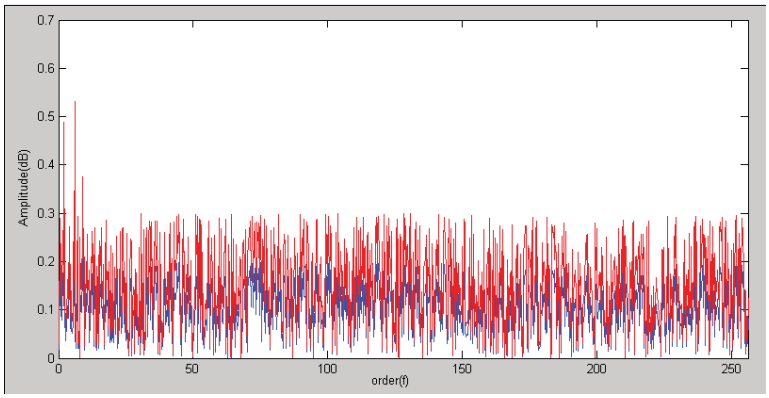

Fig. 5 The standard extremal

4.2 The misalignment of gear of the automotive transmission

The order cepstrums of misalignment is shown in Fig.6. The amplitude in Fig.6 exceeded significantly the amplitude in Fig.4. And the Fig.6 has included the second harmonic and the third harmonic of gear mesh order. The characteristic values extracted by signal processing are shown in Table 5. Put the characteristic values vector into the SVM model, the output of the model is "2". It indicates that there is the defect of misalignment in the gear.

Table 5 Characteristic values

x1			x2			x3			
1.9810			0.4165			4.7563			
x4	x5	x6	x7	x8	x9	x10	x11	x12	x13
0.5621	0.5786	0.9609	1.0716	0.1526	0.8106	0.8852	0.0153	1.9810	0.9235

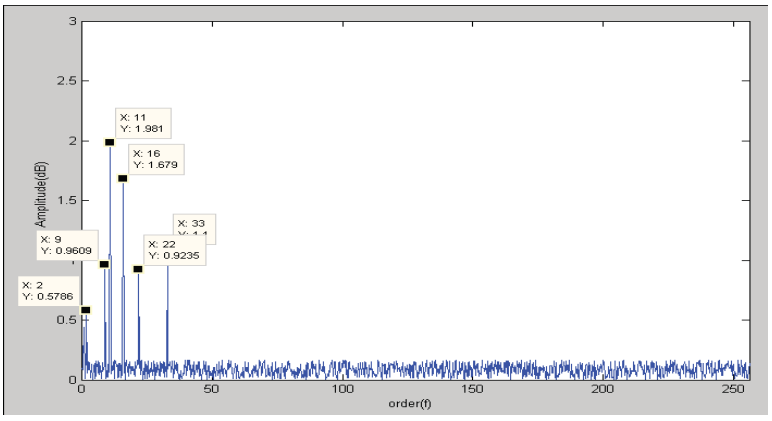

Fig. 6 The order cepstrums of misalignment of gear

4.3 The surface machining error of gear of the automotive transmission

The order cepstrums of ***s***urface machining error is shown in Fig.7. The gear mesh order and its harmonic has appeared the peak in Fig.7. In addition to this, there is also "ghost line" in Fig.7 between the gear mesh order and the second harmonic, the second harmonic and the third harmonic. As a frequency component of the power spectrum, "ghost line" is a periodic component from the machining process because of processing errors. The characteristic values extracted by signal processing are shown in Table 6. Put the characteristic values vector into the SVM model, the output of the model is "3". It indicates that there is the defect of surface machining error in the gear.

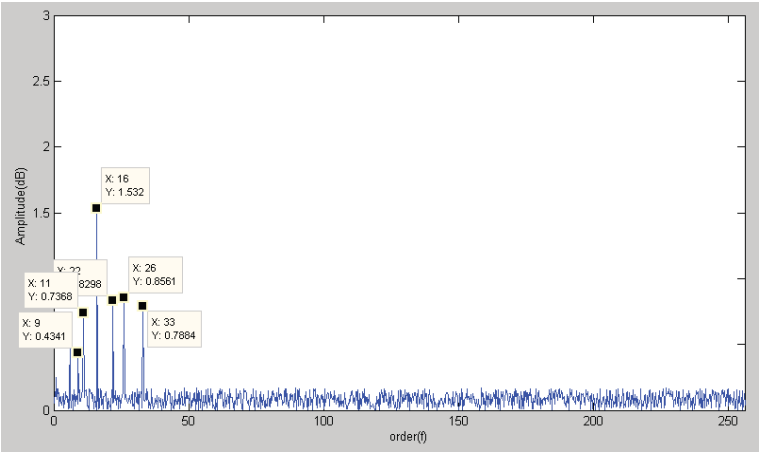

Fig. 7 The order cepstrums of surface machining error of gear

Table 6 Characteristic values

x1			x2			x3			
1.5321			0.3643			4.2056			
x4	x5	x6	x7	x8	x9	x10	x11	x12	x13
0.9275	0.7910	0.5394	0.9764	0.2017	0.7546	0.1058	0.0247	0.7368	0.8298

5. Conclusion

The running test and inspection of transmission in the factory is very important to ensure the quality of automotive transmission. An efficient and reliable quality detection method is a key technology for pre-delivery inspection. Therefore, the paper presents the method that combines order analysis theory with spectrum theory to extract characteristic signals, and combines support vector machine with standard extremal for the quality detection. According to the non-stationary vibration signals during the variable speed process of pre-delivery inspection, it has solved the phenomenon of "frequency aliasing" using the technology of order analysis and cepstrum. Meanwhile it eliminates the sideband of power spectrum and extracts effectively the characteristic signal; the input vector composed of characteristic signal will be input to the support vector machine model, while enriching the SVM training samples by the standard extremal to get a more complete model of support vector machine, so that it can realize the online quality detection of pre-delivery inspection. The experimental study also shows that the method can effectively achieve the detection of the transmission quality.

Acknowledgment

Thanks Zhiwei Zheng for the help of the language.

Thanks Xufeng Wang and Haiqiang Song for the help of writing assistance.

References

[1] Y. j Zhu. The Research on Online Automobile Transmission Fault Quick Diagnosis, *Journal of Tongji University*, 2007.

[2] G. Q Yu. Research on the Intelligent Fault Diagnosis Tcchnology Based of Support Veetor Maehine, *Journal of NanChang University*, 2007.

[3] C. H Shi, Y. P Wang and H. L Zhang. Faults Diagnosis based on Support Vector Machines and Particle Swarm Optimization, *Advancements in Computing Technology*, Vol. 3, No.5, 70-79, 2011.

[4] H. Li, H. Q Zheng and H. X Pan. Order Bicepstrum Based Fault Diagnosis Method for Roll Bearing, *Journal of North China Institute of Technology*, Vol. 29, No. 5, pp. 440-444, 2007.

[5] H. Li, H. Q Zheng and L. W Tang. Order Tracking of Instantaneous frequency Estimation of the gearbox signal, *Journal of Vibration, Measurement & Diagnosis*, Vol. 27, No. 2, pp. 125-128, 2007.

[6] G. B Zhang. Study and Development for Intelligent System of Gearbox Test.*Computer Engineering and Applications*, Vol. 46, No. 26, pp. 66-67, 2010.

[7] J. F Li and X. M Chen. Online Learning Algorithms of Direct Support Vector Machine, *Advancements in Computing Technology*, Vol. 3, No. 11, pp. 486-497, 2011.

[8] L. K Luo, M. X Luo, L. J Ye, H. Peng and Yang Fan. Maximum Robustness Criterion on Kernel Selection of Support Vector Machine, *Convergence Information Technology*, Vol. 6, No.1, pp. 294-306, 2011.

International Journal of Comprehensive Engineering
Part A, 2(3), 223-230, 2013
Doi: 10.14270/IJCE2013.2.3.a223
Regular paper

ISSN 2186-2680
e-ISSN 2186-2656
www.iace-journal.org

Fault Detection and Discrimination of Rotating Machinery Using Frequency Symptom Parameter and Bayesian Network

Haiyang Jiang [1], Ke Li [1,#] and Peng Chen [1,#]

[1] Graduate School of Bioresources, Mie University 1577 Kurimanmachiya-cho, Tsu-shi, Mie, 514-8507, Japan

[#] Corresponding author: dayanlv@live.cn; chen@bio.mie-u.ac.jp; Tel.: +81-59-231-9592

Abstract: This paper proposes a novel fault diagnosis method for rotating machinery based on symptom parameters and Bayesian Network. Non-dimensional symptom parameters in frequency domain calculated from vibration signals are defined for reflecting the features of vibration signals. In addition, sensitive evaluation method for selecting good non-dimensional symptom parameters using the method of discrimination index is also proposed for detecting and distinguishing faults in rotating machinery. Finally, the application example of diagnosis for a roller bearing by Bayesian Network is given. Diagnosis results show the methods proposed in this paper are effective.

Keywords: Non-dimensional Symptom Parameters, Vibration Signal, Bayesian Network, Rotating Machinery.

Received: May 25,2012 / Accepted: May 8,2013 / Published: Sept. 10,2013

1. Introduction

In the filed of condition diagnosis of machinery, one of effective and practical methods is vibration analysis. Using the vibration signal for the monitoring and fault diagnosis of the rotating machinery are become more and more important to prevent accidents and reduce financial loss. Furthermore, when developing intelligent condition diagnosis system by computer, Symptom parameters (SPs) used for the input of Bayesian Network system are must be defined to distinguish states of machinery beforehand. Because the accuracy of fault diagnosis depends on SPs, it is most important that excellent SPs calculated by the feature of fault states of machinery can be sensitively obtained. However, in many cases of the condition diagnosis for rotating machinery, especially in an early stage of a fault, the effect of noise in the signal measured for the diagnosis is so strong that the symptom of the fault is not evident and there are a lot of ambiguous relationships between symptom parameters and failure types of plant machinery, so failure types of plant machinery cannot be easily identified.

This paper proposes a new fault diagnosis method for rotating machinery based on non-dimensional symptom parameters and Bayesian Network. Non-dimensional symptom parameters in the frequency domain are defined to reflect the features of vibration signals measured in each state. Moreover, sensitive evaluation method for selecting good non-dimensional symptom parameters using the method of discrimination index is also proposed for detecting and distinguishing faults in rotating machinery. Practical examples of faults diagnosis for a roller bearing are provided to verify the effectiveness of the proposed method. The results verify that the faults that often occur in motor bearing, such as a outer-race defect state, a inner-race defect state and a element defect state, are effectively identified by the proposed method.

2. Symptom Parameters and Sensitivity Evaluation

2.1 Symptom Parameters (SPs) for Fault Diagnosis

For automatic diagnosis, many SPs have been defined for condition diagnosis of machinery. Here, six of the non-dimensional SPs, which are usually used to the failure diagnosis of plant machinery in the frequency domain, are considered as follows:

$$p_1 = \frac{\sum_{i=1}^{I}(f_i - \bar{f})^3 \cdot F(f_i)}{\sigma^3 I} \tag{1}$$

$$p_2 = \frac{\sum_{i=1}^{I}(f_i - \bar{f})^4 \cdot F(f_i)}{\sigma^4 I} \tag{2}$$

$$p_3 = \sqrt{\frac{\sum_{i=1}^{I} f_i^4 \cdot F(f_i)}{\sum_{i=1}^{I} f_i^2 \cdot F(f_i)}} \tag{3}$$

$$p_4 = \frac{\sum_{i=1}^{I} f_i^2 \cdot F(f_i)}{\sqrt{\sum_{i=1}^{I} F(f_i) \sum_{i=1}^{I} f_i^4 \cdot F(f_i)}} \tag{4}$$

$$p_5 = \sum_{i=1}^{I} F(f_i) \tag{5}$$

$$p_6 = \sqrt{\sum_{i=1}^{I} F^2(f_i)} \tag{6}$$

Here, I is the number of spectrum, f_i is frequency, $F(f_i)$ means the spectrum value of f_i, $\bar{f}$ is the mean value of the analysis frequency, such that $\bar{f} = \frac{\sum_{i=1}^{I} f_i \cdot F(f_i)}{\sum_{i=1}^{I} F(f_i)}$, σ is the standard deviation and $\sigma = \sqrt{\frac{\sum_{i=1}^{I}(f_i - \bar{f})^2 \cdot F(f_i)}{I}}$.

2.2 Detection Index for Evaluating Symptom Parameters

Supposing that x_1 and x_2 are values of a symptom parameter (SP) calculated from the signals measured in state 1 and state 2, respectively, and conforming respectively to the normal distributions $N(\upsilon_1, \sigma_1)$ and $N(\upsilon_2, \sigma_2)$. Here, υ and σ are the average and standard deviation of the SP. The larger the value of $|x_1 - x_2|$ is the higher the sensitivity of distinguishing the two states by the SP. Because $z = x_2 - x_1$ also conforms to the normal distribution $N(\upsilon_2 - \upsilon_1, \sigma_1 + \sigma_2)$, there is the following density function about z

$$f(z) = \frac{1}{\sqrt{2\pi(\sigma_1^2 + \sigma_2^2)}} \exp\left\{ \frac{\{z - (\upsilon_2 - \upsilon_1)\}^2}{2(\sigma_1^2 + \sigma_2^2)} \right\} \tag{7}$$

Here, $\upsilon_2 \geq \upsilon_1$ (the same conclusion can be drawn when $(\upsilon_1 \geq \upsilon_2)$. The probability can be calculated with the following formula

$$p_0 = \int_{-\infty}^{0} f(z) d_z \tag{8}$$

Here, $1-p_0$ is called the "Discrimination Rate (DR)". With the substitution

$$\upsilon = \frac{Z-(\upsilon_2-\upsilon_1)}{\sqrt{\sigma_1^2+\sigma_2^2}} \tag{9}$$

Into Formulas (7) and (8), the p_0 can be obtained by

$$p_0 = \frac{1}{\sqrt{2\pi}} \int_{-\infty}^{-DI} \exp(-\frac{\upsilon^2}{2}) d_\upsilon \tag{10}$$

Here, the DI (Discrimination Index) is calculated by

$$DI = \frac{\upsilon_2-\upsilon_1}{\sqrt{\sigma_1^2+\sigma_2^2}} \quad \text{or} \quad DI = \frac{\bar{x}_2-\bar{x}_1}{\sqrt{\sigma_1^2+\sigma_2^2}} \tag{11}$$

It is obvious that the larger the value of the DI, the larger the value of the "Discrimination Rare ($DI=1-p_0$)" will be, and therefore, the better the SP will be. Thus, the DI can be used as the index of the quality to evaluate the distinguishing sensitivity of the SP.

3. Bayesian Network

3.1 Introduce to Bayesian Network

Bayesian networks provide a means of parsimoniously expressing joint probability distributions over many interrelated hypotheses. A Bayesian network consists of a directed acyclic graph (DAG) and a set of local distributions. Each node in the graph represents a random variable. A random variable denotes an attribute, feature, or hypothesis about which we may be uncertain. Each random variable has a set of mutually exclusive and collectively exhaustive possible values. That is, exactly one of the possible values is or will be the actual value, and we are uncertain about which one it is. The graph represents direct qualitative dependence relationships; the local distributions represent quantitative information about the strength of those dependencies. The graph and the local distributions together represent a joint distribution over the random variables denoted by the nodes of the graph.

In probability theory and statistics, Bayes theorem (alternatively Bayes law or Bayes rule) is a central theorem with two distinct interpretations. In the Bayesian interpretation, it expresses how a subjective degree of belief should rationally change to account for evidence. In the frequentist interpretation, it relates inverse representations of the probabilities concerning two events. In the Bayesian interpretation, Bayes theorem is fundamental to Bayesian statistics, and is widely applied in fields including science, engineering, medicine and law. The application of Bayes theorem to update beliefs is called Bayesian inference.

Mathematically, Bayes theorem gives the relationship between the probabilities of A and B, P(A) and P(B), and the conditional probabilities of A given B and B given A, P(A | B) and P(B | A). In its most common form, it is:

$$P(A \mid B) = \frac{P(B \mid A)P(A)}{P(B)} \tag{12}$$

For proposition A and evidence B,

P(A), the prior, is the initial degree of belief in A.

P(A | B), the posterior, is the degree of belief having accounted for B.

P(B | A) / P(B) represents the support B provides for A.

In the Bayesian interpretation, probability measures a degree of belief. Bayes theorem then links the degree of belief in a proposition before and after accounting for evidence.

3.2 BN Learning

In many practical settings the BN is unknown and one needs to learn it from the data. This problem is known as the BN learning problem, which can be stated informally as follows: Given training data and prior information (e.g., expert knowledge, casual relationships), estimate the graph topology and the parameters of the JPD in the

BN. Learning the BN structure is considered a harder problem than learning the BN parameters. Moreover, another obstacle arises in situations of partial observation when nodes are hidden or when data is missing.

In general, the other learning cases are computationally intractable. In the second case with known structure and partial observation, one can use the EM (expectation maximization) algorithm to find a locally optimal maximum-likelihood estimate of the parameters. MCMC is an alternative approach that has been used to estimate the parameters of the BN model. In the third case, the goal is to learn a DAG that best explains the data. This is an NP-hard problem, since the number of DAGs on N variables is super exponential in N. One approach is to proceed with the simplest assumption that the variables are conditionally independent given a class, which is represented by a single common parent node to all the variable nodes. This structure corresponds to the BN, which surprisingly is found to provide reasonably good results in some practical problems. To compute the Bayesian score in the fourth case with partial observation and unknown graph structure, one has to marginalize out the hidden nodes as well as the parameters. Since this is usually intractable, it is common to use an asymptotic approximation to the posterior called Bayesian information criterion (BIC) also known as the minimum description length (MDL) approach. In this case one considers the trade-off effects between the likelihood term and a penalty term associated with the model complexity. An alternative approach is to conduct local search steps inside of the M step of the EM algorithm, known as structural EM, that presumably converges to a local maximum of the BIC score.

4. Diagnosis and Application

4.1 Experimental System for Fault Diagnosis

Fig. 1 shows the experiments for roller bearing fault diagnosis test. Fig. 2 shows the defect of bearing. Raw vibration signals measured in the outer-race, inner-race, rolling element states are shown in Fig. 3 at a constant speed (800 rpm). The sampling frequency of the signal measurement is 50 kHz, and the sampling time is 20 s.

Fig. 1 Experimental equipment for fault diagnosis

Fig. 2 Bearing defects (a)Outer-race defect (b)Inner-race defect (c)Roller defect

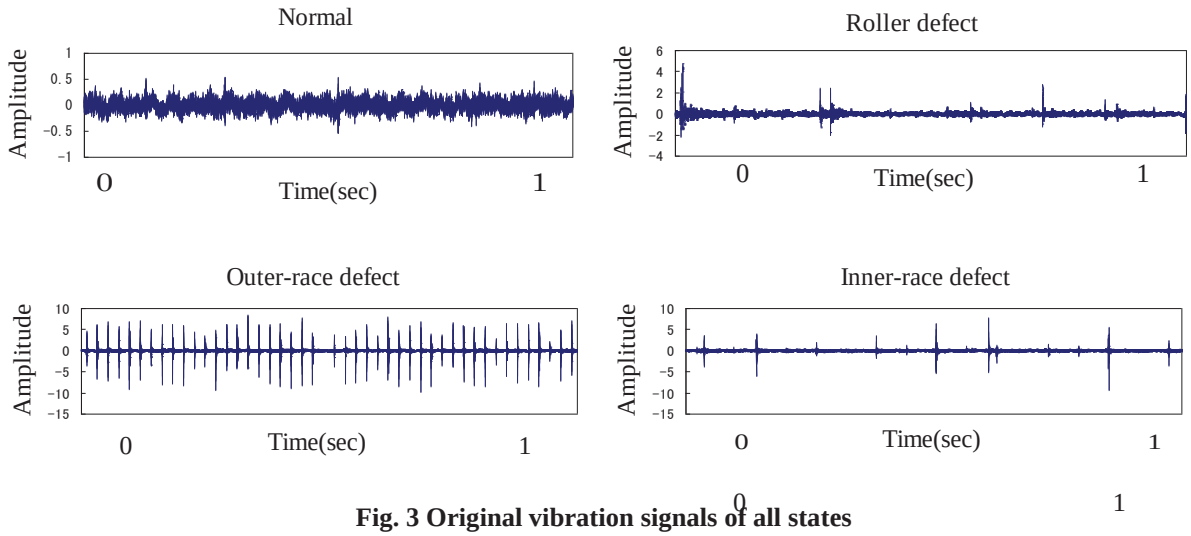

Fig. 3 Original vibration signals of all states

4.2 The evaluating results of diagnostic sensitivity

The Table 1 shows the evaluating results of diagnosis sensitivity by DI. According to the evaluating results shown in Table1, P_1, P_2 and P_4 are better for distinguishing the faults of roller bearing, because that the DI values of P_1, P_2 and P_4 are larger than those of the other.

Table 1 The evaluating result for the flaw

signal	P_1	P_2	P_3	P_4	P_5	P_6
Normal –Inner-race	2.245	3.013	0.411	4.093	3.173	0.579
Normal – Outer-race	23.006	21.182	13.092	37.879	19.856	10.941
Normal – Rolling element	7.898	4,874	4.915	9.09	1.705	2.219
Rolling element – Outer-race	3.441	1.848	3.140	14.991	9.715	5.578
Rolling element –Inner race	4.682	4.110	3.374	9.776	0.11	1.997
Inner race – Outer-race	3.057	8.951	1.519	3.588	14.134	10.405

4.3 Establishment and verification of Bayesian Network in the fault diagnosis

In this paper, the Bayesian Network model for condition diagnosis based on Bayesian Network theory are constructed, and shown in Fig. 4. In the Bayesian Network for condition diagnosis, the first layer is normal state and abnormal state, the second layer is combination of outer-race, inner-race and rolling element states, and the last layer is six symptom parameters calculated by Eq.(1-6) and the signals shown in Fig. 3.

The values and definitions of the state of each layer node respectively are shown in Tables 2-4.

In addition, before learning of Bayesian fault diagnosis Network, ensure the possible relationship between parent nodes and children nodes is very important. Table 5 shows the node possible relationship and construct model of this trial in Bayesian fault diagnosis Network. The Node in Table 5 is node name, the Model filial is the relationship of each state.

According to the model filial shown in Table 5, Bayesian fault diagnosis Network Model is built as in Fig. 4. The vibration signals measured in each state are dividing into two groups, one is used to input into the model for learning and inference, the other is for verifying the effectiveness of Bayesian Network.

The inference results of the BN model for the condition diagnosis are shown in Table 6. In the Table 6 the values are the probabilities which express the correct rate of distinguishing each state by the Bayesian Network.

Table 2 The values and definitions of the first layer

Normal States	Values of each state
state(N)	0,1(0:abnormal; 1:normal)
Abnormal state(UN)	0,1(0:normal; 1:abnormal)

According to the diagnosis results above, the normal, the outer-race defect, the inner-race defect and the

roller element defect states of the roller bearing can be automatically and correctly identified using the methods proposed in this paper.

Table 3 The values and definitions of the second layer

States	Values of each state
Outer-race	0,1(0: unknown state; 1:Yes)
Inner-race	0,1(0: unknown state; 1:Yes)
Rolling element	0,1(0: unknown state; 1:Yes)

Table 4 The values and definitions of the last layer

Symptom parameters	Values
P_1	1, 2, 3, 4, 5
P_2	1, 2, 3, 4, 5
P_3	1, 2, 3, 4, 5
P_4	1, 2, 3, 4, 5
P_5	1, 2, 3, 4, 5
P_6	1, 2, 3, 4, 5

Table 5 The relationship between nodes and model

Node	Model Filial				
N					
UN					
Inner	*UN				
Outer	*UN				
Element	*UN				
P_1	*N	*UN	*Inner	*Outer	*Element
P_2	*N	*UN	*Inner	*Outer	*Element
P_3	N	UN	Inner	Outer	Element
P_4	*N	*UN	* Inner	* Outer	* Element
P_5	N	UN	Inner	Outer	Element
P_6	*N	*UN	* Inner	* Outer	* Element

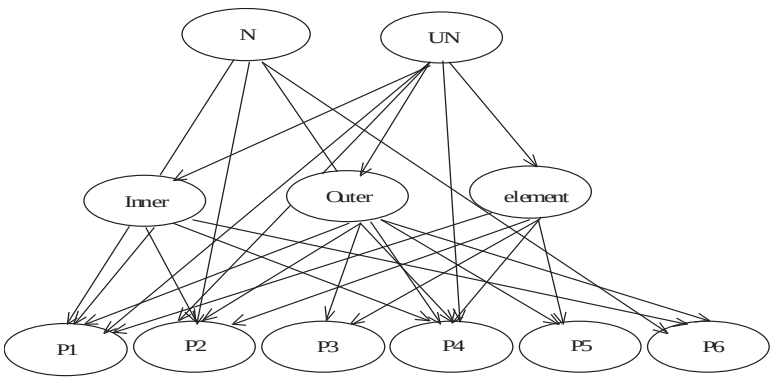

Fig. 4 Bayesian Network Model for the diagnosis

Table 6 The diagnosis results

State	Rate of distinguishing
Normal	0.985922
Outer-race	0.999965
Inner-race	0.984761
Rolling element	0.997524

5. Conclusions

In order to diagnose the faults of rotation machinery at an early stage, this paper proposed a new fault diagnosis method for rotating machinery based on non-dimensional symptom parameters and Bayesian Network. The six of non-dimensional symptom parameters were defined, which can effectively reflect the features of the vibration signals measured in each state for the fault diagnosis of rotating machinery. Detection index (DI) using statistical theory had also defined to evaluate the applicability of the NSPs for the condition diagnosis in each frequency area. Finally, the Bayesian Network for condition diagnosis was constructed, by which the fault types of rotation machinery could be identified. Practical examples of faults diagnosis for a roller bearing were provided to verify the effectiveness of the proposed method. The results verified that the faults that often occur in motor bearing, such as a outer-race defect state, a inner-race defect state and a element defect state, were effectively identified by the proposed method.

References

[1] P. Chen and T. Toyota. Fuzzy Diagnosis and Fuzzy Navigation for Plant Inspection and Diagnosis Robot, *Proc. of FUZZ-IEEE*, Vol. 1, pp.185-193, 1995.

[2] H. Q Wang and P. Chen. Fuzzy Diagnosis Method for Rotating Machinery in Variable Rotating Speed, *IEEE Sensors Journal*, Vol. 11, No. 1, pp. 23-34, 2011.

[3] P. Chen, Toshio Toyota and Z. J He. Automated Function Generation of Symptom Parameters and Application to Fault Diagnosis of Machinery under Variable Operating conditions, *IEEE Transactions On Systems*, No. 6, pp.775-781, 2001.

[4] T. Stich,T. *Bayesian networks and structure learning* [Diploma Thesis, Computer Science and Engineering]. University of Mannheim. available: http://66.102.1.104

[5] J. H Luo. The Application of Bayesian Network in the Mechanical Fault Diagnosis, Chongqing University , 2006.

[6] J. C Li and H. N Qing. Bayesian Network Theory in the Equipment Fault Device, *China Mechanical Engineert*, Vol. 10, 2000.

[7] S. Q Peng and Y. S Zhang. *Research on the Theory of Bayesian Network and Its Implication in Image Analysis*, Hefei Industial University, 2005.

[8] Wilson Quansheng Wang. Rotary Machinery Health Condition Monitoring, Fault Diagnosis, Waterloo University, 2002.

[9] N. L Zhang and D. Poole. Exploiting Causal Independence in Bayesian Network Inference, *journal of Artificial Intelligence Research*, Vol. 5, pp. 301-328, 1996.

[10] K. Murphy. A Brief Introduction to Graphical Models and Bayesian Networks, The Bayes Net Toolbox for Matlab, *Computing Science and Statistics*, 33, 2001.

[11] N. Friedman and M. d Goldszmidt. Learning Bayesian Networks with Local Structure, *in Proceedings of the 12th Conference on Uncertainty in Arificial Intelligence*, Portland, Augest 1-4, 1996.

[12] J. Pearl. *Probabilistic Reasoning in Intelligent Systems*, Morgan Kaufmann, San Francisco.

[13] M. I. Jordan. *Learing in Graphical Models*, MIT Press, Cambridge, 1999.

[14] K. Aksoy. *Parametric Models*(Bayesian Belief Networks Lecture Notes) [Department of Computer Engineering Bilkent University], available:http://www.cs.bilkent.edu.tr/ saksoy/courses/cs661/sides/cs551_parametric4.pdf

[15] C. Boutilier, N. Friedman, M. Goldszmidt and D. Koller. Context-Specific Independence in Bayesian Networks, *in Proceedings of the 12th Conference on Uncertainty in Artificaial Intelligence*, pp.115-123, Auguest 1-4, 1996, Portland.

[16] H. David. *A Tutorial on Learning with Bayesian Networks, in Learning in Graphical, M. J. Models, ed*, MIT Press, Cambridge, Also appears as Technical Report MSR-TR-95-06, Microsoft Research, March, 1995.

[17] P. Spirtes, C. Glymour and R. Schienes. *Causation Prediction and Search*, Springer-Verlag, New York.

[18] J. Pearl. Evidential Reasoning Using Stochastic Simulation of Csusal Models, *Artificial Intelligence*, Vol. 32, pp. 245-258, 1987.

[19] I. Ben-Gal, A. Shani, A. Gohr, J. Grau, S. Arviv, A. Shmilovici, S. Posch and I. Grosse. Identification of Transription Factor Binding Sites with Variable-Order Bayesian Networks, *Bioinformatics*, Vol. 21, No. 11, pp. 2657-2666, 2005.

International Journal of Comprehensive Engineering
Part B, 2(3), 231-240, 2013
Doi: 10.14270/IJCE2013.2.3.b231
Regular paper

ISSN 2186-2680
e-ISSN 2186-2656
www.iace-journal.org

Intelligent Diagnosis Method for Rotating Machinery Using Non-dimensional Symptom Parameter and Particle Swarm Optimization

Ke Li [1], Peng Chen [1, #], Hao Sun [2]

[1] Department of Environmental Science and Engineering, Faculty of Bioresources, Mie University, 1577 Kurimamachiya-cho, Tsu-shi, Mie-ken, 514-8507, Japan
[2] School of Mechanical Engineering, Jiangnan University, 1800 Li Hu Avenue, Wuxi, Jiangsu Province, 214122, China

[#] Corresponding author: chen@bio.mie-u.ac.jp; Tel.: +81-59-2329592; Fax: +81-59-2329592

***Abstract*:** This paper proposes a novel method of intelligent condition diagnosis for rotating machinery using non-dimensional symptom parameter (NSP) and particle swarm optimization (PSO) to detect faults and distinguish fault types at an early stage. NSPs in the time domain are defined for reflecting the features of vibration signals measured in each state. The state identification for the condition diagnosis of rotating machinery is converted to a clustering problem of the values of the NSPs, calculated from vibration signals in different states of the machine. PSO is also introduced for this purpose. Moreover, synthetic detection index (*SDI*) using statistical theory has also defined to evaluate the applicability of the NSPs for the condition diagnosis measured in each state. The *SDI* can be used to indicate the fitness of a NSP for PSO. A practical example of condition diagnosis for a rolling bearing used in the centrifugal fan system verifies that the method is effective.

Keywords: Fault Diagnosis, Particle Swarm Optimization, Non-dimensional Symptom Parameter, Synthetic Detection Index.

Received: May 3,2012 / Accepted: May 8,2013 / Published: Sept. 10,2013

1. Introduction

In the field of condition-based maintenance, vibration diagnosis is often used for fault detection and state discrimination for rotating machinery. The condition diagnosis of rotating machinery depends largely on the feature analysis of vibration signals measured for the condition diagnosis because the signals carry dynamic information about the machine state [1]-[3]. The vibration signals in different states show different features, that is, when plant machinery is in an abnormal state, it will output sign sets corresponding to different faults . If the vibration signals in each state can be automatically identified and classified using these features, intelligent condition diagnosis for plant machinery can be achieved [4]-[6].

Roller bearings are an important part of and widely used in rotating machinery. The failure of a rolling bearing may cause the breakdown of a rotating machine, and furthermore, serious consequences may arise due to the failure. Therefore, fault diagnosis of rolling bearings is most important for guaranteeing production efficiency and plant safety. Although fault diagnosis of rolling bearings is often artificially carried out using time or frequency analysis of vibration signals, there is a need for a reliable, fast automated diagnosis method.

For above reasons, this paper proposes a novel method of intelligent condition diagnosis for rotating machinery using NSP and PSO to detect faults and distinguish fault types at an early stage. The ten NSPs in the time domain are defined for reflecting the features of vibration signals measured in each state. The state identification for the condition diagnosis of rotating machinery is converted to a clustering problem of the values of the NSPs, calculated from vibration signals in different states of the machine. PSO is also introduced for this purpose. Moreover, *SDI* using statistical theory has also defined to evaluate the applicability of the NSPs for the condition diagnosis measured

in each state. The *SDI* can be used to indicate the fitness of a NSP for PSO. A practical example of condition diagnosis for a rolling bearing used in the centrifugal fan system verifies that the method is effective.

2. Non-dimensional Symptom Parameters (NSPs) and Sensitivity Evaluation

2.1 Non-dimensional Symptom Parameters (NSPs) for Fault Diagnosis

When a computer is used for condition diagnosis of plant machinery, symptom parameters (SPs) are required to express the information indicated by a signal measured for diagnosing machinery faults. A good symptom parameter can correctly reflect states and the condition trend of plant machinery [7]-[9]. Many symptom parameters have been defined in the pattern recognition field. Here, eight NSPs in the time domain, commonly used for the fault diagnosis of plant machinery, are considered.

$$P_1 = \frac{\sigma}{\bar{x}} \tag{1}$$

$$P_2 = \frac{\sum_{i=1}^{N} x_i^2}{\sigma^2} \tag{2}$$

$$P_3 = \frac{\left|\sum_{i=1}^{N} (x_i - \bar{x})^3\right|}{N\sigma^3} \tag{3}$$

$$P_4 = \frac{\sum_{i=1}^{N} (x_i - \bar{x})^4}{N\sigma^4} \tag{4}$$

Here, x_i is digital data of vibration signal. $\bar{x}$ is the mean value of x_i, $\bar{x} = \frac{\sum_{i=1}^{N} x_i}{N}$. σ is standard deviation of x_i, $\sigma = \sqrt{\frac{\sum_{i=1}^{N} (x_i - \bar{x})^2}{N-1}}$.

$$P_5 = \frac{\overline{x_p}}{\bar{x}} \tag{5}$$

$$P_6 = \frac{\overline{x_p}}{\sigma} \tag{6}$$

$$P_7 = \frac{\left|\sum_{i=1}^{N_p} (x_{pi} - \overline{x_p})^3\right|}{N_p \sigma_p^{\,3}} \tag{7}$$

$$P_8 = \frac{\left|\sum_{i=1}^{N_p} (x_{pi} - \overline{x_p})^4\right|}{N_p \sigma_p^{\,4}} \tag{8}$$

Here, x_{pi} is the peak value of x_i. $\overline{x_p}$ and σ_p are the mean value and standard deviation of x_{pi}, respectively.

$$P_9 = \frac{\left|\sum_{i=1}^{N_v}(x_{vi} - \overline{x_v})^3\right|}{N_v \sigma_v^{\ 3}} \tag{9}$$

$$P_{10} = \frac{\left|\sum_{i=1}^{N_v}(x_{vi} - \overline{x_v})^4\right|}{N_v \sigma_v^{\ 4}} \tag{10}$$

Here, x_{vi} is the valley value of x_i. $\overline{x}_v$ and σ_v are the mean value and standard deviation of x_{vi}, respectively.

2.2. Detection Index

Supposing that x_1 and x_2 are values of a symptom parameter (SP) calculated from the signals measured in state 1 and state 2, respectively, and conforming respectively to the normal distributions N(μ_1,σ_1)and N(μ_2,σ_2). Here, μ and σ are the average and the standard deviation of the SP. The larger the value of $|x_2 - x_1|$ is, the higher the sensitivity of distinguishing the two states by the SP. Because $z = x_2 - x_1$ also conforms to the normal distribution N($\mu_2 - \mu_1$,$\sigma_1 + \sigma_2$), there is the following density function about z:

$$f(z) = \frac{1}{\sqrt{2\pi(\sigma_1^{\ 2} + \sigma_2^{\ 2})}} \exp\{\frac{\{z - (\mu_2 - \mu_1)\}^2}{2(\sigma_1^{\ 2} + \sigma_2^{\ 2})}\} \tag{11}$$

Here, $\mu_2 \geq \mu_1$ (the same conclusion can be drawn when $\mu_1 \geq \mu_2$). The probability can be calculated with the following formula

$$P_0 = \int_{-\infty}^{0} f(z) d_z \tag{12}$$

Here, 1-P_0 is called the "Discrimination Rate (*DR*)". With the substitution

$$\mu = \frac{z - (\mu_2 - \mu_1)}{\sqrt{\sigma_1^{\ 2} + \sigma_2^{\ 2}}} \tag{13}$$

into (11) and (12), the P_0 can be obtained by

$$P_0 = \frac{1}{\sqrt{2\pi}} \int_{-\infty}^{-DI} \exp(-\frac{\mu^2}{2}) d_\mu \tag{14}$$

Here, the *DI* (Discrimination Index) is calculated by

$$DI = \frac{\mu_2 - \mu_1}{\sqrt{\sigma_1^{\ 2} + \sigma_2^{\ 2}}} \quad \text{or} \quad DI = \frac{\overline{x_2} - \overline{x_1}}{\sqrt{\sigma_1^{\ 2} + \sigma_2^{\ 2}}} \tag{15}$$

It is obvious that the larger the value of the *DI*, the larger the value of the "Discrimination Rate (*DR*=1-P_0)" will be, and therefore, the better the SP will be. Thus, the *DI* can be used as the index of the quality to evaluate the distinguishing sensitivity of the SP.

The number of symptom parameters used for the diagnosis and fault types are *M* and *N*, respectively, and the synthetic detection index (*SDI*) is defined as follows:

$$SDI = \sum_{i=1}^{N-1} \sum_{j=i+1}^{N} \sum_{k=1}^{M} \frac{|\mu_{ik} - \mu_{jk}|}{\sqrt{\sigma_{ik}^2 + \sigma_{jk}^2}} \tag{16}$$

Table 1 lists the diagnosis sensitivity standard for condition diagnosis.

Table 1 Diagnosis sensitivity for condition diagnosis

Detection Index	Discrimination Rate	Sensitivity
< 0.85	< 80%	Low
0.85 - 1.30	80% - 90%	Slightly low
1.30 - 1.65	90% - 95%	Middle
1.65 - 2.33	95% - 99%	High
> 2.33	> 99%	Very high

3. Particle Swarm Optimization for Condition Diagnosis

In this study to effectively and automatically distinguish faults for condition monitoring of rotating machinery, a new intelligent condition diagnosis method is proposed based on the NSPs and the PSO, the problem of state identification for the condition diagnosis is converted into the clustering problem of the NSPs calculated by vibration signals measured in different states, which will be solved by the PSO.

3.1 Brief of Particle Swarm Optimization

Particle swarm optimization (PSO) is a population based stochastic optimization technique developed by Dr. Eberhart and Dr. Kennedy in 1995, inspired by social behavior of bird flocking or fish schooling [10]. In past several years, PSO has been successfully applied in many research and application areas [11]-[13].

PSO algorithm is based on the groups, and according to the environmental fitness, individual in groups will be moved to the good region. The algorithm evaluates the optimal result by using evolutionary fitness function of group, and each particle in the algorithm has a fitness value determined by the fitness function, two properties of position and speed that are used to show the location and moving speed of the current articles in the solving space, by the fitness function value corresponding to particle position coordinate determines the performance of particles. In PSO algorithm, each particle adjusts its location according to its own experience, and according to the experience of a neighboring particle, making use of the best location encountered by itself and its neighbor.

In the R-dimensional search space, the *i* particle's space location is defined as follows

$$P(i).location = [X_{i1}, X_{i2} \cdots X_{iR}] \tag{16}$$

The velocity of particle i is defined as follows

$$P(i).velocity = [V_{i1}, V_{i2} \cdots V_{iR}] \tag{17}$$

The best previous location of particle i is defined as follows

$$P(i).best = [P_{i1}, P_{i2} \cdots P_{iR}] \tag{18}$$

The best location among all particles experienced is defined as follows

$$g(i).best = [g_{i1}, g_{i2} \cdots g_{iR}] \tag{19}$$

The particle updates the position and velocity according to the following equations:

$$\begin{aligned} P(i).velocity(t+1) = \omega P(i).velocity(t) + \eta_1 r_1 [P(i).best(t) - P(i).location(t)] \\ + \eta_2 r_2 [g(i)best(t) - P(i).location(t)] \end{aligned} \tag{20}$$

$$P(i).location(t+1) = P(i).location(t) + P(i).velocity(t+1) \tag{21}$$

where r_1 and r_2 are the random numbers between (0, 1), and η_1 and η_2 are the acceleration which constants the

control of how far a particle moves in a single generation. Eberhart *et al*. suggested the values of $\eta_1 = \eta_2 = 2$. The inertia weight ωcontrols the previous velocity of particle, and it is defined as follows

$$\omega = 0.5 + \frac{rand}{2} \tag{22}$$

where *rand* is random generated number between 0 to 1.

3.2 Weight Particle Swarm Optimization

Although PSO algorithm is easy to realize, the method is easy to trap into local optimum. Shi and Eberhart proposed a linearly decreasing weight particle swarm optimization (WPSO) of which, a linearly decreasing inertia factor was introduced into the velocity of the updated equation from the original PSO [14],[15]. The performance of WPSO is significantly improved over the original PSO because WPSO balances out the global and local search abilities of the swarm effectively. In WPSO, ω_l is the inertia weight which linearly decreases from 0.9 to 0.4 through the search process . The equation for the linearly decreased weight is defined as follows

$$\omega_l = \omega_{max} - iteration \frac{\omega_{max} - \omega_{min}}{iteration_{max}} \tag{23}$$

In Eq. (23), ω_{max} is 1, ω_{min} is 0.1 and *Iterationmax* is the maximum number of the allowed iterations. The velocity of the updated equation for WPSO is defined as follows

$$\begin{aligned} P(i).velocity(t+1) = \omega_l P(i).velocity(t) + \eta_1 r_1 [P(i).best(t) - P(i).location(t)] \\ + \eta_2 r_2 [g(i)best(t) - P(i).location(t)] \end{aligned} \tag{24}$$

3.3 Fitness function for WPSO

Assume that *N* is the sample set of vibration signals measured in *m* different states, the length of *N* is *n*, $N=\{s_1, s_2 \ldots s_n\}$. Every sample signal has *t* identified symptoms (in this paper, the symptoms are P_1-P_{10}). Then, the clustering analysis is to divide *n* sample data into *m* states, such that the objective function *F* shown in (21) is minimized.

$$\min F = \sum_{j=1}^{m} \sum_{i=1}^{n} \sum_{k=1}^{t} a_{ij} \left\| S_{ik} - X_{jk} \right\|^2 \tag{25}$$

$$X_{jk} = \frac{\sum_{i=1}^{n} a_{ij} S_{ik}}{\sum_{i=1}^{n} a_{ij}} \qquad (j = 1,2 \cdots m; k = 1,2 \cdots t) \tag{26}$$

$$a_{ij} = \begin{cases} 1 & if \quad S_i \in state j \\ 0 & if \quad S_i \notin state j \end{cases} (i = 1,2 \cdots n; j = 1,2 \cdots m) \tag{27}$$

In this paper, the procedure for applying the PSO for the condition diagnosis is as follows:

(1) NSPs used for reflecting the features of sample signals are inputted into the PSO;
(2) Sample signals are randomly classified by PSO, and the clustering centers are calculated by Formula (26);
(3) According to the clustering centers, locations of particles are initialized;
(4) Initializing particles speed;
(5) Evaluating the fitness value of each particle by Formula (25);
(6) To each particle, its adaptive value will compare with the best position *Pbest (t)* experienced, if the adaptive value is better, will be regarded as the best present position *Pbest (t)*.
(7) To ach particle, its adaptive value will compare with the best position *gbest (t)* overall situation experienced, if better, then reset the index of *gbest(t)*

(8) According to the Equations (21) and (24) update the location and the speed of particles;
(9) Steps (5) – (8) are looped until the ending condition is satisfied.

4. Diagnosis and Verification

Fig. 1 shows the centrifugal fan system for rolling bearing fault diagnosis test. The most commonly occurring faults in a rolling element bearing are the outer-race defect, the inner-race defect, and the roller element defect. These fault bearings are shown in Fig. 2 and were artificially made with the use of a wire-cutting machine. The bearings were utilized, and specifications of the test bearing, the size of the faults, and other necessary information are listed in Table 2.

In this work the accelerometer (PCB MA352A60) with a bandwidth from 5 Hz to 60 kHz and 10 mV/g output was used to measure the vibration signals of the vertical direction in the normal(N), the outer-race defect(O), the inner-race defect(I), and the roller element defect(R) respectively. The vibration signals measured by the accelerometer were transformed into the signal recorder (Scope Coder DL750) after being magnified by the sensor signal conditioner (PCB ICP Model 480C02). The original vibration signals in each state shown in Fig. 3 were measured at a constant speed (800 rpm). The sampling frequency of the signal measurement was 50 kHz, and the sampling time was 20 s.

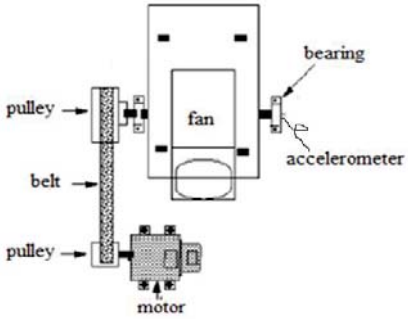

Fig. 1 Experimental system for bearing fault diagnosis

Fig. 2 Bearing defects (a) Outer-race defect. (b) Inner-race defect. (c) Roller defect

Table 2 Bearing Information for verification

Contents	Parameters
Bearing outer diameter	52 mm
Bearing inner diameter	25 mm
Bearing width	15 mm
Bearing roller diameter	7 mm
The number of the rollers	11
Contact angle	0 rad
Outer-race defect	0.3 * 0.25 mm (width * depth).
Inner-race defect	0.3 * 0.25 mm (width * depth)
Rolling element defect	0.5 * 0.15 mm (width * depth)

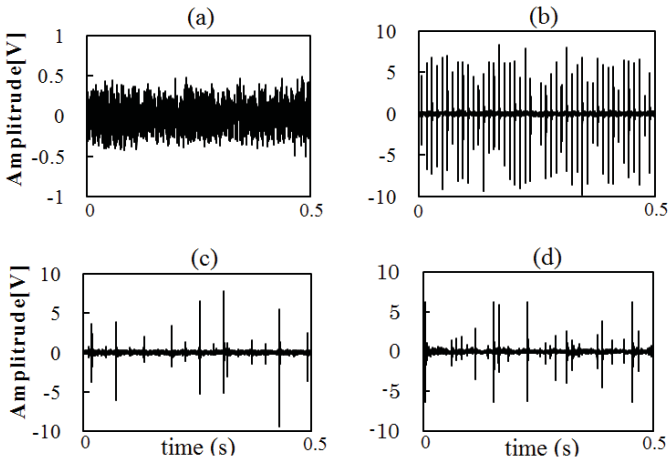

Fig. 3 Raw vibration signals of the bearing used in the centrifugal fan system (a) in the normal state (b) in the Outer-race defect state (c) in the Inner-race defect state (d) in the Roller defect state.

Table 3 *SDI* of each NSP

NSPs	SDI	DI_{max}	DI_{min}
$P_1P_2P_3$	40.35	15.31	0.26
$P_1P_2P_4$	37.68	12.56	0.26
…	…	…	…
$P_5P_6P_7$	99.17	45.39	0.852
$P_5P_6P_8$	110.85	45.39	1.35
…	…	…	…
$P_7P_8P_9$	50.84	11.04	0.55
P_8P_9 P_{10}	55.83	11.04	0.86

In this study the good NSPs which have high sensitivity for distinguishing each fault state of the bearing are selected by the method of *SDI*. As an example, Table3 lists parts of *SDI*s of NSPs calculated by formulas (1)-(10). The maximum value (110.85) of *SDI* is obtained in the case of the combination of P_5, $P_6$and P_8, and when P_5, $P_6$and P_8 are used for distinguishing each state separately, the *DI*s are larger than 1.35, all of the *DR*s are larger than 90%. Therefore, the combination of P_5, $P_6$and P_8 has high sensitivity for distinguishing each fault state of the bearing.

In this research, the state identification for the condition diagnosis is converted to a clustering problem for the values of the NSPs calculated from vibration signals measured in different states of the bearing. The PSO automatically finds the optimal clustering centers and classify all sample data according to the amount of information around the clustering centers. The purpose of training the PSO is the acquisition of optimum clustering centers. The NSPs calculated using the signals measured in each state were input into the PSO. The PSO converged to the optimum clustering centers. As an example, parts of the training data and their clustering centers are shown in Table 4.

Table 4 Parts of acquired data of diagnosis for the PSO. (a) Normal state, (b) Outer-race defect state, (c) Inner-race defect state, (d) Roller element defect state.

(a) Normal state

NSPs			Clustering Center		
P_5	P_6	P_8			
2.878453	1.068688	1.312963	2.88	1.39	1.37
3.025416	1.854305	2.155492			
2.841769	1.037276	1.087691			
…	…	…			

(b) Outer-race defect state

NSPs			Clustering Center		
P_5	P_6	P_8			
6.101696	6.648086	7.03251	6.09	6.53	7.07
6.099626	6.325836	7.13369			
6.10457	6.836914	7.142626			
…	…	…			

(c) Inner-race defect state

NSPs			Clustering Center		
P_5	P_6	P_8			
3.314811	19.654	25.194396	3.99	18.98	20.30
3.510085	20.814144	24.373076			
4.094827	17.659119	20.85357			
…	…	…			

(d) Roller element defect state

NSPs			Clustering Center		
P_5	P_6	P_8			
5.190183	14.140374	14.449141	5.13	12.94	11.58
5.276201	10.818479	9.008349			
5.24421	9.354266	9.880798			
…	…	…			

(e) Table 5 Diagnosis result using proposed method

NSPs			Judge States	Diagnostic accuracy
P_5	P_6	P_8		
2.729195	0.907776	0.818102	N	100%
2.924529	1.228315	1.235438	N	
2.878453	1.068688	1.312963	N	
3.025416	1.854305	2.155492	N	
2.841769	1.037276	1.087691	N	
…	…	…	…	
6.072179	6.501908	7.523308	O	100%
6.075658	6.563426	7.348812	O	
6.096211	6.436205	7.199994	O	
6.101696	6.648086	7.03251	O	
6.099626	6.325836	7.13369	O	
…	…	…	…	
4.050713	21.129965	21.718092	I	92.5%
3.314811	19.654	25.194396	I	
3.510085	20.814144	24.373076	I	

4.094827	17.659119	20.85357	I	
4.227996	17.521754	16.876144	I	
…	…	…	…	
4.407554	24.91525	16.203999	R	
5.297461	11.250889	8.976939	R	
5.261556	10.148004	8.690489	R	
4.260219	26.053496	25.076406	R	87.5%
5.359627	9.92814	9.362753	R	
…	…	…	…	

After training the PSO, to verify the diagnostic capability of the proposed method in this paper, the test data measured in each known state that had not been used to train the PSO were used. When inputting the test data into the trained PSO, the PSO classified the test data according to the information of the optimum clustering centers shown in Table 4 and correctly and quickly output identification results. As an example, some diagnosis results are listed in Table 5. These results verified the efficiency of the intelligent diagnosis method using NSPs and the PSO proposed in this paper.

5. Conclusions

In order to diagnose faults of rotation machinery at an early stage, this paper proposed a novel method of intelligent condition diagnosis for rotating machinery using NSP and PSO to detect faults and distinguish fault types at an early stage. The ten NSPs in the time domain were defined for reflecting the features of vibration signals measured in each state. The state identification for the condition diagnosis of rotating machinery was converted to a clustering problem of the values of the NSPs, calculated from vibration signals in different states of the machine. PSO was also introduced for this purpose. Moreover, *SDI* using statistical theory had also defined to evaluate the applicability of the NSPs for the condition diagnosis measured in each state. The *SDI* could be used to indicate the fitness of a NSP for PSO. A practical example of condition diagnosis for a rolling bearing used in the centrifugal fan system verified that the method is effective.

References

[1] B. Liu, S. F. Ling. On the Selection of Informative Wavelets for Machinery Diagnosis, *Mechanical Systems and Signal Processing*, Vol.13, pp.145-162, 1999.

[2] L. Jing and L. S Q. Feature Extraction Based on Morlet Wavelet and Its Application For Mechanical Fault Diagnosis, *Journal of Sound and Vibration*, Vol. 234, pp. 135-148, 2000.

[3] Q. B. Zhu. Gear Fault Diagnosis System Based on Wavelet Neural Networks, *Dynamics of Continuous Discrete and Impulsive Systems-series A-Mathematical Analysis. Part 2*, Vol. 13, pp. 671-673, 2006.

[4] P. Chen, T. Toyota and Z. J. He. Automated Function Generation of Symptom Parameters and Application to Fault Diagnosis of Machinery in Variable Operation-conditions, *IEEE Transactions on System, Man, and Cybernetics (Part A)*, Vol. 31, No. 6, pp. 775-781, 2001.

[5] P. Chen and T. Toyota. Fuzzy Diagnosis and Fuzzy Navigation for Plant Inspection and Diagnosis Robot, *International Joint Conference of the Fourth IEEE International Conference on Fuzzy Systems and The Second International Fuzzy Engineering Symposium*, pp.185-192, IEEE xplore, March 20-24, 1995, Yokohama, Japan.

[6] K. Li and P. Chen. Intelligent Method for Diagnosing Structural Faults of Rotating Machinery Using Ant Colony Optimization, *Sensors*, No.11, pp. 4009-4209, 2011.

[7] H. Matuyama. Diagnosis Algorithm, *Journal of JSPEl*, Vol. 75, No. 3, pp. 35-37, 1991.

[8] K. Fukunaga. *Introduction to Statistical Pattern Recognition*, Academic Press, San Diego, CA, USA, 1972.

[9] J. Kennedy and R. Eberhart. Particle Swarm Optimization, *Proceedings of IEEE International Conference on Neural Networks*, pp.1942-1948, IEEE xplore, Nov 27- Dec 1, 1995, Perth, Western Australia.

[10] J. Kennedy. The Particle Swarm: Social Adaptation of Knowledge, *Proceedings of IEEE International Conference on Evolutionary Computation*. pp.303-308, Aprile13-16,1997, Indianapolis, USA.

[11] R. C. Eberhart and Y. Shi. Particle Swarm Optimization: Developments, Applications, and Resources. *Proceedings of the IEEE Congress on Evolutionary Computation*, pp. 81-86, IEEE Service Center, Piscataway NJ, May27-30, 2001, Seoul, Korea.

[12] X. Xie, W. Zhang and Z. Yang. Dissipative Particle Swarm Optimization, *In Proceedings of the IEEE congress on evolutionary computation (CEC)*, pp.1456-1461, IEEE xplore, May12-17, 2002, Honolulu, Hawaii, USA.

[13] Y. Shi and R.C. Eberhart. Empirical Study of Particle Swarm Optimization, *Proc. of Congress on Evolutionary Computation*, pp.1945-1949, July6-9, 1999, Washington, USA.

[14] Y. Shi and R. C. Eberhart. A Modified Particle Swarm Optimizer, *IEEE International Conference on Evolutionary Computation*, pp. 69-73, IEEE xplore, May 4-9, 1998, Anchorage, Alaska.

International Journal of Comprehensive Engineering
Part B, 2(3), 241-252, 2013
Doi: 10.14270/IJCE2013.2.3.b241
Regular paper

ISSN 2186-2680
e-ISSN 2186-2656
www.iace-journal.org

The Research of Reliability Assessment Technology for Key Parts of Equipment Based on Weibull Distribution

Min Zhou [1], Jianfeng Yang [2], Wenbin Liu [2,#], Wei Xu [2] and Xiyong Ke [2]

[1] China National Petroleum Corporation, Beijing, 100007, China
[2] Chemical Safety Engineering Research Center of the Ministry of Education, Beijing University of Chemical Technology, Beijing, 100029,China

[#] Corresponding author: liuwb1437@263.net

Abstract: An important issue in the lifetime data analysis of key parts of equipment is to specify the most appropriate life distribution model. In this paper, weibull distribution as one of the most widely-used reliability models is used for reliability assessment, which is based on the failure data obtained from measurements or simulations. The unary two-parameter or three-parameter weibull model is applied in a system in which the components are independent of each other, and the genetic algorithm(GA) which can search the globally optimal solution is put forward to estimate the unknown parameters. Meanwhile, the Monte Carlo(MC) simulation is adopted to analyze the failure rate under the breakdown and periodic maintenance strategy respectively. Furthermore, so as to model the possibility of multiple failures more vigorously, the mixed weibull model is introduced, and the expectation maximization(EM) algorithm which repeats the iteration process to convergence is presented for the mixed parameters estimation. Finally, the relationship between model and parameters is utilized to assess various reliability characteristic quantities. The results of case studies show that our method can provide the decision-makers with quantitative references to improve the reliability, availability and safety of equipment.

Keywords: Weibull Distribution, Key Parts, Genetic Algorithm, Monte Carlo Method, Expectation Maximization Algorithm, Reliability Assessment.

Received: July 1,2012 / Accepted: May 8,2013 / Published: Sept. 10,2013

1. Introduction

A mechanical equipment is generally made up of several key parts, while the failures which happen among them may result in machine stoppage or even system breakdown. Therefore, it is very important to carry out reliability assessment for key parts of equipment [1]. In practical engineering projects, we often statistically analyze reliability data to find out the failure distribution rule that can exactly reflect failure mechanism and failure analysis result, and then perform reliability assessment and reliability prediction by fitting failure data into certain distribution [2]. Based on statistical analysis results of the mean time between failure (MTBF) of bearings, gears and other typical components, we find that the life expectancy of components, parts, equipment or systems that suffer from partial fatigue failure or global failure all follow weibull distribution, so that it is more comprehensive to analyze early fault, occasional fault and wearout fault using weibull distribution [3].

In recent years, researches on equipment reliability assessment which are based on weibull distribution model have increased greatly and have achieved considerable results. There are several methods available in published literatures to estimate weibull distribution parameters from a failure data set, such as the least square method, the maximum likelihood estimation method, the graphic analysis method and so on, which, have been improved constantly, thus making reliability assessment more accurate [4-6]. However, since the least square method mainly depends on the empirical distribution function, the maximum likelihood method may not be solvable or have more than one solution, and the accuracy of graphic analysis method is not high enough, a more robust

method is needed. In this paper, GA and EM algorithm are proposed to overcome those shortcomings, with examples showing that they can complete the task better.

Besides, it is well known that the reliability can be described by reliability index, and the failure rate is often used as characteristic parameters to describe the failure behavior of equipment, so that we can find out failure distribution by analyzing the change of failure rate, which is helpful for decision-makers to formulate maintenance plans. Generally speaking, the changing trends of failure rate can be analyzed based on the relationship between the model and parameters, but given the difficulty of solving the model, the scarcity of reliability data and the complexity of traditional Markov process [7], it is necessary to find a method that is independent of the states and subject to fewer conditions. A Monte Carlo method is used for this purpose, and once the random variables are generated, we are able to conduct simulation and estimation [8].

The paper is structured as follows. Section 2 introduces the basic theories of the proposed method, and focuses on the GA and the EM algorithm to estimate the parameters. Meanwhile, it shows how the Monte Carlo simulation can be exploited to analyze the failure rate under the breakdown or preventive maintenance strategy. Section 3 illustrates the effectiveness of the proposed methods using engineering cases. Section 4 concludes with discussions and analysis.

2. Basic Theories

2.1 Reliability Index

From an engineering point of view, qualitative analysis of equipment reliability is far from satisfying engineering demands, so it is necessary to carry out quantitative analysis. Only if we get reliability quantitatively assessed, can we possibly propose the clear and unified requirements for equipment reliability management. Those quantities which can measure reliability are called reliability index(RI) [9]. Commonly used reliability index include reliability level, failure rate and life expectancy, etc.

Reliability level is described in Eq.(1).

$$R(t)=P(E)=p(T\geq t),0\leq R(t)\leq 1. \tag{1}$$

The failure rate is described in Eq.(2).

$$\lambda(t)=\lim_{\substack{N\to\infty\\ \Delta t\to 0}}\frac{\Delta n(t)}{[N-n(t)]\cdot\Delta t}. \tag{2}$$

Where N is the number of total products, n(t) is the number of failure products at time t, Δt is the interval between two failures, and $\Delta n(t)$ is the number of failure products in Δt.

The average life expectancy can be described in Eq.(3).

$$T=\int_0^\infty R(t)dt\ . \tag{3}$$

For non-repairable systems, T is the exact failure time , which is mean time to failure(MTTF); for repairable systems, T stands for the time between two consecutive failures, which is mean time between failures(MTBF).

In order to improve the reliability of key parts of equipment, it is necessary to investigate failure causes and to master failure mechanism. Only by comprehensively understanding these knowledge can we adopt effective measures to improve the reliability.

2.2 The unary weibull distribution model

The following expression is applied to define the probability density function of the unary weibull distribution.

$$f(t)=\begin{cases}\dfrac{b}{a}\left(\dfrac{t-r}{a}\right)^{b-1}\exp\left[-\left(\dfrac{t-r}{a}\right)^{b}\right] & (\mathrm{t}\geq \mathrm{r})\\ 0 & (\mathrm{t}<\mathrm{r})\end{cases} \tag{4}$$

Where t is the average life, which may be the time between failures or the time to failure, a, b and r are the scale, shape and location parameter respectively. When r=0, Eq.(4) will become two-parameter weibull distribution.

Different values of shape parameter b (b<1, b=1, b>1) are corresponding to different stages of the bathtub curve separately, as shown in Fig.1. If we change the value of b, we can get different failure rate functions, so that the unary weibull distribution is one of the most commonly used distributions in reliability assessment and life expectancy analysis [9].

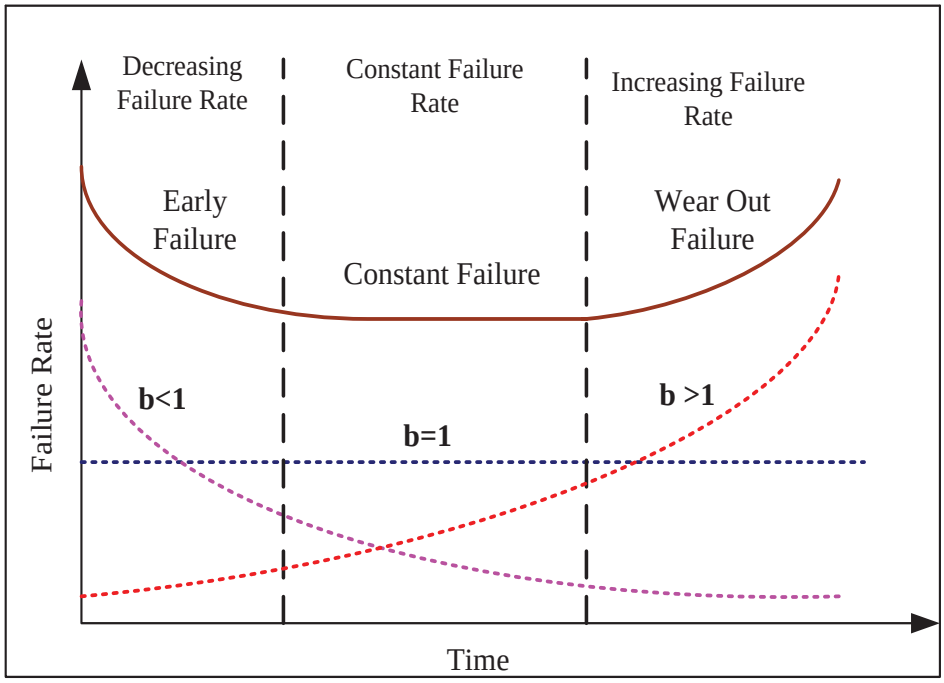

Fig. 1 The bathtub curve and the failure rate curve of weibull distribution

2.2.1 Parameter estimation of the unary weibull distribution

Using the "survival of the fittest" principle, the genetic algorithm(GA) starts to produce a group of individuals that are more adapted to the environment from any initial population. By random selection, crossover and mutation, the groups could evolve into an area that is better and better from one generation to anther, until they are converged to the individuals who are the most adapted to the environment, namely globally searching to the optimal solution of the problem is accomplished [10].

The procedures of using GA to estimate the parameters are as follows.

(1) Establish the objective function, and we get the optimal parameters when Eq.(5) is minimal.

$$\min\ f(x) = -\sum_{i=1}^{n} \ln\left[f(t_{i,}Q)\right] \tag{5}$$

Where $f(t_{i,}Q)$ is the probability density function of the unary weibull distribution, Q is the parameters of the model and t_i (i=1,2,…,n) is the observed values of the sample;

(2) Determination of the decision variations and its constraints: the decision variations in three-parameter weibull distribution can be expressed as x=[x1,x2,x3]=[r,a,b]. However, it is difficult to determine the parameter ranges, if the ranges are too wide, it may take longer time to converge and it is more likely to converge to local maximum, while if ranges are too narrow, true parameter values may not be included. Based on previous research achievements [11], the ranges can be set as 0<x1<t1 ,0<x2<tn and 0<x3<5. If it's two-parameter weibull distribution we can just set r as 0;

(3) Producing the initial population: N initial string structure data are generated randomly, where each string structure is an individual, and N structures form a group. Meanwhile, the maximum genetic algebra T is determined (between 200 to 500);

(4) Coding: variables are converted into binary string, and the length of which depends on the desired accuracy;

(5) Fitness evaluation: calculate the inferiority of individual or solution in a group;

(6) Selection, crossover and mutation: individuals of inferior fitness are phased out, and individuals of superior fitness are retained, thus getting new generation of groups;

(7) Judging the terminal condition and deciding the optimal solution: when the iteration times T is reached, stop iteration process (otherwise go to step (3)), and ultimately the individual of maximal fitness is the optimal solution of the objective function;

(8) Decoding: transform the binary string of the optimal solution into a practical value.

2.3 Mixed weibull distribution model [12]

The unary two-parameter or three-parameter weibull distribution model can analyze the failure rate of the system of which the component is independent of each other. However, with the complexity of equipment growing, the unary weibull distribution could not reflect the true failure mechanism of system accurately. For this reason, the mixed weibull distribution is introduced.

The probability density function of mixed weibull distribution is expressed as $f_k(t) = \sum_{j=1}^{k} w_j f_j(\mathrm{t})$, and we can write the corresponding cumulative distribution function as $F_k(t) = \sum_{j=1}^{k} w_j F_j(\mathrm{t})$, where k is the number of mixtures, and constant w_j stands for a weighting factor, satisfying $\sum_{j=1}^{k} w_j = 1$.

A mixed probability density function of two-parameter weibull distribution is described as below:

$$f_j(t_i|b_j, a_j) = \frac{b_j}{a_j}\left(\frac{t_i}{a_j}\right)^{b_j-1} \exp\left\{-\left(\frac{t_i}{a_j}\right)^{b_j}\right\} \tag{6}$$

2.3.1 Parameter estimation of the mixed weibull distribution

The aim of expectation maximization (EM) algorithm is to search for the maximum likelihood estimation of parameters, and it is very effective when dealing with incomplete data and when the likelihood function expression is too complex [13-14].

The unknown parameters in mixed weibull distribution could be estimated using EM algorithm, the main steps of which are shown as follows.

(1) Give the initial value of parameters;

(2) E step (expectation);

$$Q(\Theta, \Theta^{(s)}) = \sum_{i=1}^{n}\sum_{j=1}^{k} f(j|t_i, \Theta^{(s)}) \log\left\{w_i f_j(t_i|\theta_j)\right\} \tag{7}$$

According to Bayesian's viewpoint, we calculate the posterior probability of model j given a group of failure data t_i:

$$f(j|t_i, \Theta^{(s)}) = \frac{w_j^{(s)} f_j(t_i|\theta_j^{(s)})}{\sum_{j=1}^{k} w_j^{(s)} f_j(t_i|\theta_j^{(s)})} \tag{8}$$

Where $w_j^{(s)}$ is the current coefficient, $\theta_j^{(s)}$ is the current unknown parameters;

(3) M step (maximization); re-estimation of model parameters, maximize Eq. (7) to obtain new parameters estimation $\Theta^{(s+1)}$,where $\Theta^{(s+1)} = \arg\max_{\Theta} Q(\Theta, \Theta^{(s)})$, and estimate the maximum likelihood function of parameters by the combination of Eq.(6), (7) and (8). Finally, we can get the new parameters as follow:

$$w_j^{(s+1)} = \frac{1}{n}\sum_{i=1}^{n} f(j|t_i, \Theta^{(s)}) \tag{9}$$

$$f(j|t_i, \Theta^{(s)}) = \frac{w_j^{(s)} f_j(t_i|\theta_j^{(s)})}{\sum_{j=1}^{k} w_j^{(s)} f_j(t_i|\theta_j^{(s)})} \tag{10}$$

$$\frac{\sum_{i=1}^{n} f(j|t_i, \Theta^{(s)}) \log(t_i)}{\sum_{i=1}^{n} f(j|t_i, \Theta^{(s)})} - \frac{\sum_{i=1}^{n} f(j|t_i, \Theta^{(s)}) t_i^{b_j^{(s+1)}} \log(t_i)}{\sum_{i=1}^{n} f(j|t_i, \Theta^{(s)}) t_i^{b_j^{(s+1)}}} + \frac{1}{b_j^{(s+1)}} = 0 \tag{11}$$

(4) Judge whether convergence is reached: if the convergence criterion $\left|Q(\Theta, \Theta^{(s)}) - Q(\Theta, \Theta^{(s+1)})\right| \le e$ is satisfied, stop the iteration, otherwise, return to step (2), where accuracy e can be set to 0.0001.

Repeating E step and M step in an iterative manner until the calculation converges to the maximum likelihood solution, thus getting the optimal parameters.

2.4 Monte Carlo Simulation

It is important to find a appropriate method to carry out quantitative reliability analysis. In this section, a Monte Carlo (MC) approach is selected to analyze the failure rate for a systems under periodic maintenance strategies, which is not easily done by analytical model.

Based on the principle of a statistical sampling, the Monte Carlo method, using the random number, counts, samples or simulates randomly the relevant random variables to obtain statistical characteristic value as the numerical solution of to-be-answered problem [15]. When the training samples are enough, the frequencies of certain event will be close to its probability, and therefore it is feasible to apply the Monte Carlo method to analyze the failure rate.

The model here proposed is based on the following assumptions: (a) the fault distribution has been clear, and the occurrence of failure is random; (b) the maintenance process is short, which means the time of fault diagnosis, fault orientation, maintenance or replacement can all be neglected; (c) the repaired component can be restored to an "as good as new"condition [16].

The main process to simulate the failure rate is given as below:

(1) Generate a group of uniform random numbers ε_i and $0 < \varepsilon_i < 1$,(i=1,2,…,n);

(2) Assume that the probability density function of $f(t)$ working life or maintenance time of the mechanical system follows the weibull distribution, and then the random sampling value can be obtained directly from $t' = r + a \cdot \sqrt[b]{-\ln(1-\varepsilon_i)}$;

(3) Calculate each model according to the maintenance strategy and the corresponding condition;

(4) Repeat the process above N times (for example 10000 in this paper);

(5) For each simulation period, divide the simulation time lim into the j intervals denoted by Δt_j (j=1,2,…), count the number h (failure times) in each interval, and then use the number h divided by the total failure times N, to get the failure rate.

The simulation process is shown in Fig.2.

3. Case studies

3.1 Example No.1

A group of fatigue data of specimens from literature [17] is listed in Table 1.

(1) Model establishment and parameters estimation

The data set is presented in the form of a convex curve on the weibull probability plot, based on which we can establish the unary three-parameter weibull model [18]. The relationship between the iteration number and the objective function values obtained by the GA can be observed from Fig.3, and when the number is close to 20, the objective function gradually reaches its minimal value, in other words, convergences to the optimal solution of the problem, but the average value of population is different due to the production of various random number.

Table 1 The fatigue data of specimens

Fatigue life statistics (h)						
350	380	400	430	450	470	480
500	520	540	550	570	600	610
630	650	670	730	770	840	

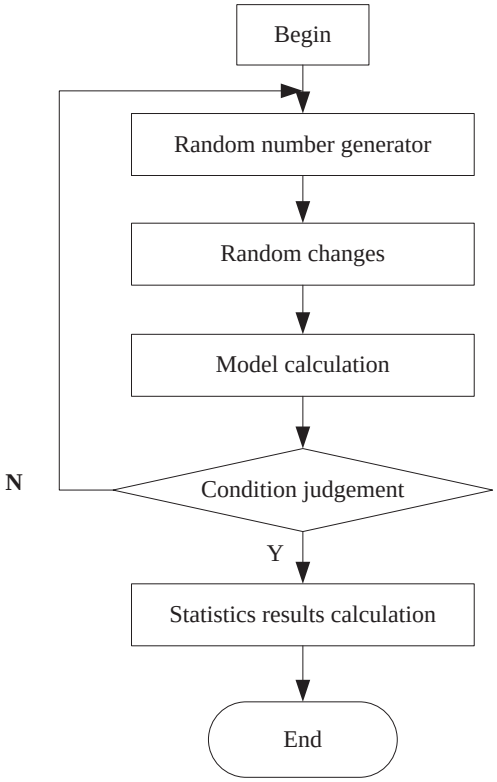

Fig. 2 The flow diagram of the MC simulation

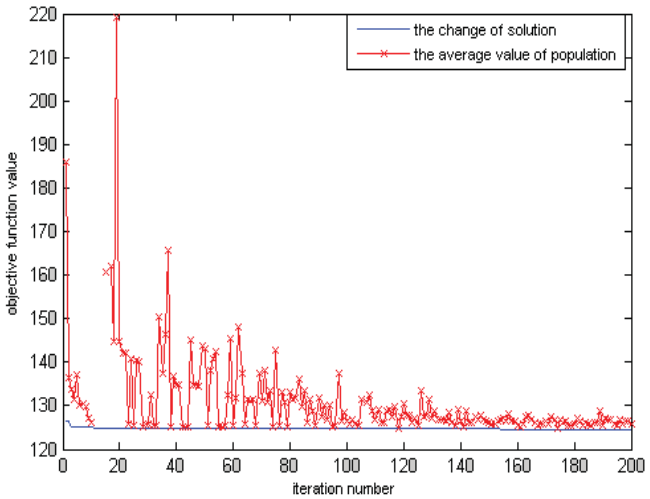

Fig. 3 The change of objective function values based on GA

The estimated shape parameters b is 2.0512, scale parameter a is 283.2524 and position parameter r is 306.8157; the optimal values of objective function is 124.5816, while the fitting results show that the data generally fall on the fitting line (see Fig.4), so the application of three-parameter weibull to model the complete life of a system is suitable.

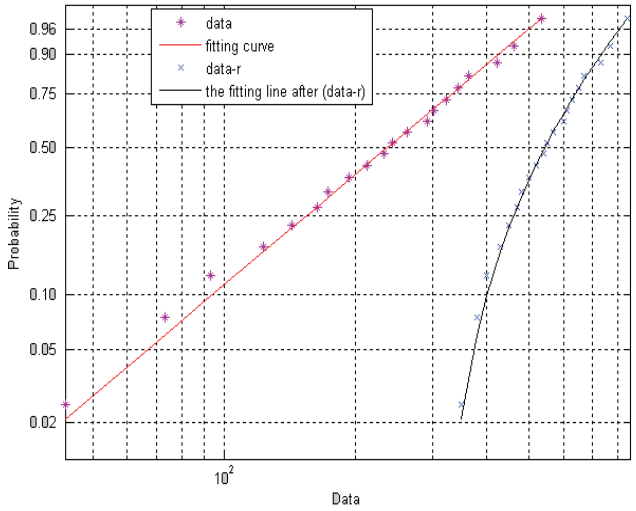

Fig. 4 The fitting result based on GA

Using the relation between the model and parameters, the mean time between failure can be determined from:

$$MTBF = r + a\Gamma\left(1+\frac{1}{b}\right) = 557.7456h \tag{12}$$

Finally, the theoretical failure rate is obtained by

$$\lambda = \frac{1}{MTBF} = 0.0018/h \tag{13}$$

(2) Monte Carlo simulation to analyze the failure rate

In the simulation, we conduct random sampling on a weibull distribution with the scale, shape and location parameter of 283.2524, 2.0512 and 306.8157 respectively, and then generate n random numbers as failure times of components. The maximum simulation time lim is 3000h, during which period we count the number of failure in each time interval Δt =200h when N=10000. We can divide this number by total simulation number, and the result is the failure rate we wanted, which can be expressed by $\Delta\lambda$. The simulation result is shown in Fig.5.

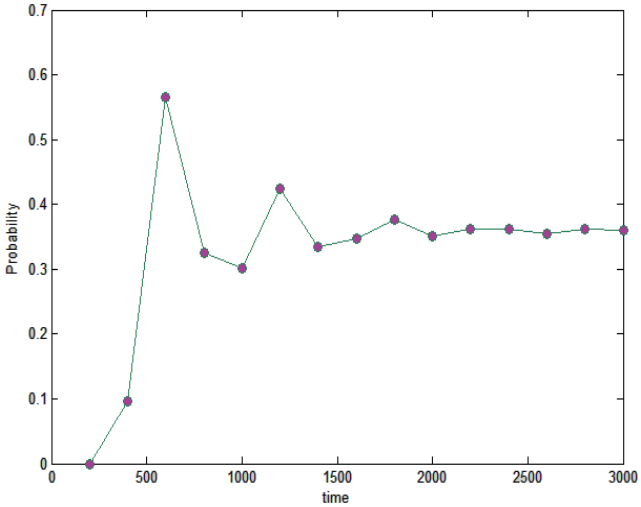

Fig. 5 The failure rate of component via MC simulation under the breakdown maintenance strategy

We notice that failure rate gradually becomes a constant with the simulation time increasing under the breakdown maintenance strategy, and the true value via Monte Carlo simulation is

$$\hat{\lambda} = \Delta\lambda_i / \Delta t_i \tag{14}$$

We can get the deviation between two methods.

$$\ell = \frac{|\lambda - \hat{\lambda}|}{\hat{\lambda}} \times 100\% \tag{15}$$

Comparing the analytical results above with those obtained by the Monte Carlo simulation, we can derive some facts as shown in Table 2.

Table 2 The comparison between the simulation value and the theoretical value

Δt_i	[1800, 2000]	[2000, 2200]	[2200, 2400]	[2400, 2600]	[2600, 2800]	[2800, 3000]
$\Delta\lambda$	0.35104	0.36134	0.36170	0.35376	0.36222	0.35986
$\hat{\lambda}$	0.00176	0.00181	0.00181	0.00177	0.00181	0.00180
λ	0.0018	0.0018	0.0018	0.0018	0.0018	0.0018
ℓ	0.0249	0.0037	0.0047	0.0173	0.0062	0.0004

It can be seen from Table.2 that the maximum deviation is 2.49% between the real value and theoretical value. Obviously, the real value of the Monte Carlo simulation is very close to its theoretical value, so the deviation can be neglected, which, validates the correctness and effectiveness of Monte Carlo method.

The Monte Carlo simulation is therefore introduced for age and batch replacement under preventive maintenance strategy (their principles are shown in Fig.6 and 7), the initial conditions of which stay as same as those mentioned above. We set regular maintenance period T to 600h. As can be observed from Fig.8 and 9, the failure rate changes periodically with the amplitude diminishing under the age replacement maintenance strategy, but repeats the same periodical changes under the batch replacement maintenance strategy. It is clear that the failure rate is influenced by the maintenance strategy. If no maintenance action is taken, the failure rate is a constantly 0.0018/h. Given the preventive maintenance period T=600, the failure rate decreases significantly, and can be improved greatly after each half period under batch replacement strategy. So, the development trend of failure rate can be changed by the maintenance activities. Indeed, efficient maintenance policies could ensure the improvement of reliability. Based on this thought, various preventive maintenance strategies have been set up, such as the Reliability Centered Maintenance (RCM) method, a very successful systematic method for establishing maintenance programs, which has been applied in many industries [19] in order to repair before the failure.

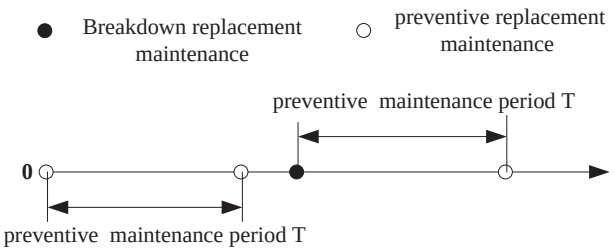

Fig. 6 The age placement maintenance strategy

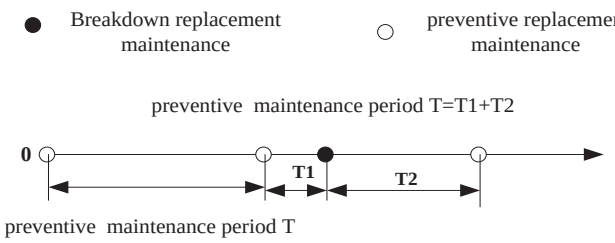

Fig. 7 The batch placement maintenance strategy

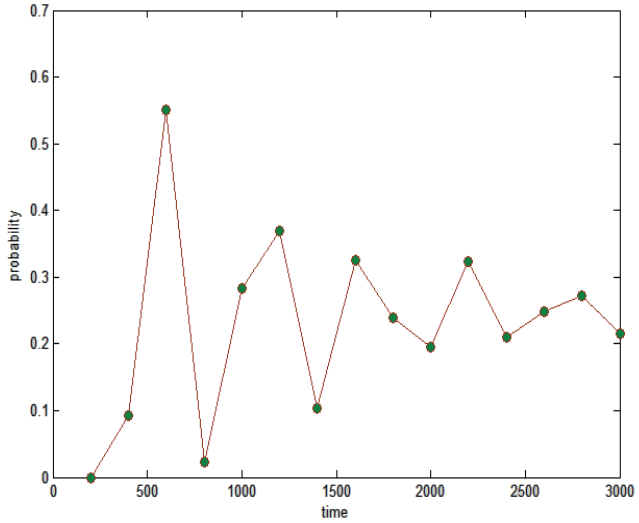

Fig. 8 The failure rate of component by MC simulation under the age replacement strategy

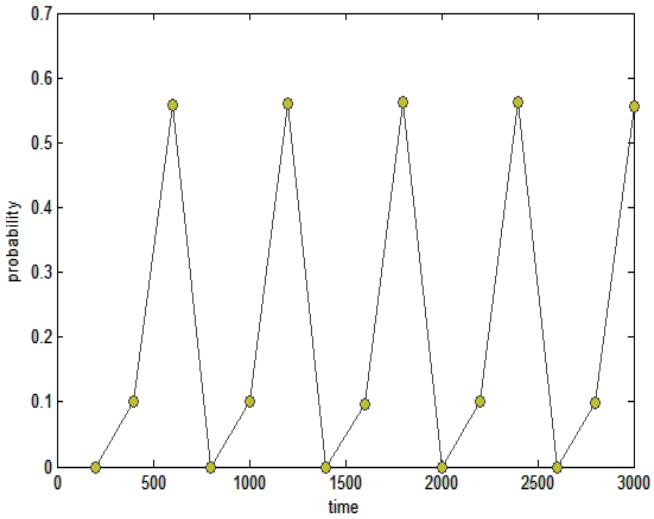

Fig. 9 The failure rate of component via MC simulation under thebatch replacement strategy

The advantage of Monte Carlo approach be come more apparent when the real data is hard to acquire. Besides, the Monte Carlo simulation can also analyze the failure rate of components under different maintenance strategies. This example is quoted exactly to explain the availability of Monte Carlo simulation in the failure rate analysis.

3.2 Example No.2

Reliability data on van section valve (see Table 3) is obtained from literature [20].

Table 3 Reliability data of the van section valve

Life data statistics(km)						
478	583	753	753	801	834	944
959	1377	1534	2400	2639	2944	2981
3392	3392	3904	4829	5328	5562	6122
6331	6531	11019	12986			

(1) Model establishment and parameters estimation

It can be observed that these data are not on one straight line on the weibull probability plot, but rather show the trend of two branchs, so that the unary weibull distribution model is not feasible any more. We can consider using two-fold weibull distribution model to model the lifetime data[18].

Fig.10 reflects the relationship between the likelihood function value and its iteration number, with the iteration number increasing, the objective function value is gradually close to its maximum, and the iteration process ends when the function value of two successive iterations is less or equal to the given error precision (e=0.0001). The result shows that the objective value converges to the stability points of its likelihood function.

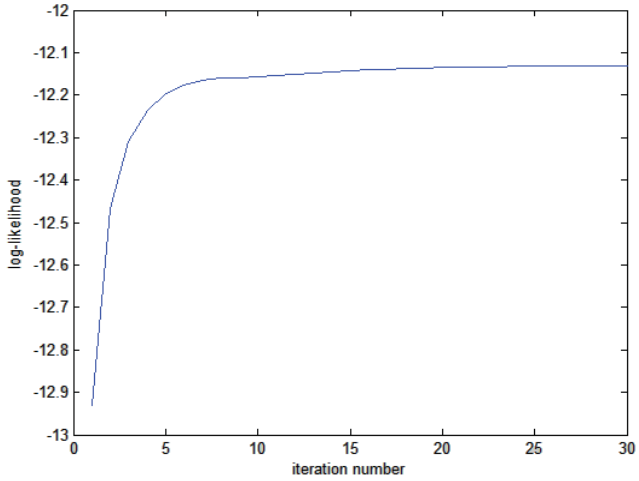

Fig. 10 The log-likelihood as a function of iteration number

The parameters estimated by EM algorithm are: weight coefficient w1=0.2697, w2=0.7303; shape parameters b1= 6.6416, b2= 1.5610; scale parameter a1= 831.8250, a2 = 5151.9142. Data fitting result (as shown in Fig.11) proves that establishing two-fold mixed weibull model is reasonable.

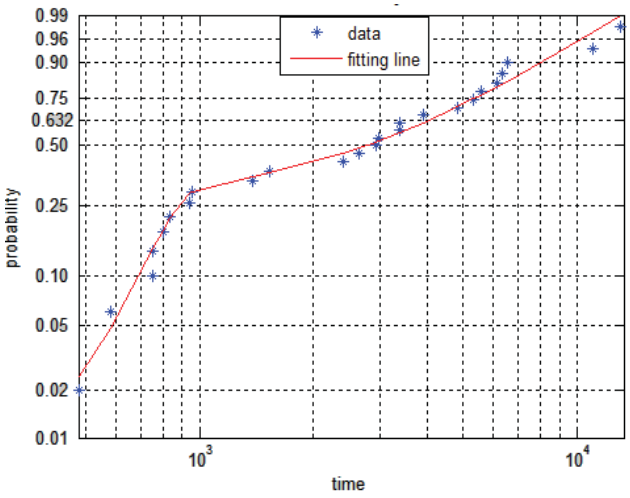

Fig. 11 The fitting result of two-fold mixed weibull

(2)Analysis of failure rate based on the relation between the model and parameters

By incorporating the estimated parameters of mixed weibull model, we can obtain the reliability $R(t) = w_1 \exp\left[-\left(\frac{t}{a_1}\right)^{b_1}\right] + w_2 \exp\left[-\left(\frac{t}{a_2}\right)^{b_2}\right]$, the failure rate $\lambda(t) = \frac{w_1 f_1(t) + w_2 f_2(t)}{w_1 R_1(t) + w_2 R_2(t)}$ as well as the mean time between failure $MTBF = w_1 a_1 \Gamma(1+1/b_1) + w_2 a_2 \Gamma(1+1/b_2)$ for the van section valve at anytime.

From the analysis above, we know that there are mainly two types of failure modes for the section valve: one is early failure, the failure distribution of which can be described by $f_1(t)$ and the probability of occurrence is 26.97%; another is the normal failure, the failure distribution of which can be represented by $f_2(t)$ and the probability of occurrence is 73.03%. As a result, to improve the reliability of the section valve, we should emphasis on the data of which the failure time is less than 1000 (km), analyze their failure mechanisms and then take effective measures to solve the problem of early failure.

4. Conclusions

(1) The research of reliability assessment technology for key components of equipment is based on the reliability data. The main thought of this research is to exploit the data shape on the weibull probability plot to establish the unary weibull or mixed weibull model, and then assess the rationality of model selection according to the inferiority between the data and the fitting curve. Two cases have demonstrated how to use the proposed GA and EM algorithm to estimate the unknown parameters, which could ensure the correctness of reliability assessment. Up to now, the development of efficient parameter estimation methods for weibull distribution and its application in reliability assessment are still a topic for further study.

(2) Once the parameters are estimated, it is possible to apply the weibull model for the calculation of various reliability index such as failure rate, reliability, life expectancy, etc. For the unary weibull model, the failure rate is analyzed in terms of the model itself and the Monte Carlo simulation, and the results show that under the breakdown maintenance strategy, the real failure rate of Monte Carlo simulation is similar to its theoretical value, which has verified the correctness of Monte Carlo method Introducing the theory into the analysis of failure rate under the preventive maintenance strategy, we can find that without any maintenance actions taken in the operation process of equipment, the failure rate is a constant, but if preventive methods are taken, the failure rate will no longer be a stable value, but rather varies with different maintenance period. Generally speaking, the failure rate decreased significantly compared with the breakdown maintenance strategy. As to the mixed weibull model, the failure behavior can be analyzed based on the relationship between the model and parameters, and the data which needs careful analysis are also determined by the fault probability and the size of scale parameter, so that effective measures can be taken to prevent the failure from happening.

(3) Overall, the information obtained from this study can be referred to by the maintenance managers, planners and operators to grasp the failure rule and the fault mechanism of equipment, and can provide the quantitative reference value in objective decision-making.

Acknowledgements

This project is supported by National Key Technologies R&D Program (Grant No. 2011BAK06B03-05)

References

[1] X. Zhong, M. Ichchou and A. Saidi. Reliability Assessment of Complex Mechatronic Systems Using a Modified Nonparametric Belief Propagation Algorithm, *Reliability Engineering and System Safety*, Vol. 95, No. 11 , pp. 1174-1185, 2010.

[2] M. Edimu, C. T Gaunt and R. Herman. Using Probability Distribution Functions in Reliability Analyses, *Electric Power System Research*, Vol. 81, No. 4 , pp. 915-921, 2011.

[3] LIU W X. *The mechanical reliabilitydesign*, Tsinghua University press, 1996.

[4] A. Saghafi, A. R Mirhabibi and G. H Yari. Improved Linear Regression Method for Estimating Weibull Parameters, *Theoretical and Applied Fracture Mechanics*, Vol. 52, No. 3 , pp. 180-182, 2009.

[5] N. Balakrishnan and M. Kateri. On the Maximum Likelihood Estimation of Parameters of Weibull Distribution Based on Complete and Censored Data, *Statistics and probability letters*, Vol. 78, No. 17 , pp. 2971-2975, 2008.

[6] R. Ross. Graphical Methods for plotting and Evaluating Weibull Distributed Data, *Proceedings of the 4th International Conference on Properties and Applications of Dielectric Materials*, pp. 250-253, IEEE xplore, Jul 3-8, 1994, Brisbane, Qld.

[7] Sandra Fortini, Lucia Ladelli, Giovanni Petris and Eugenio Regazzini. On Mixtures of Distributions of Markov Chains, *Stochastic Processes and their Applications*, Vol. 100, No. 1-2 , pp. 147-165, 2002.

[8] NagarajBalijepalli, Subrahmanyam S.Venkata and Richard D.Christie. Modeling and Analysis of Distribution Reliability Indices. *IEEE Transactions on power delivery*, Vol. 19, No. 4 , pp. 1950-1955, 2004.

[9] Y. Zhao, J. Yang and X. B Ma. *Reliability Analysis Tutorial*, Beijing University of Aeronautics and Astro-nautics Press, 2009.

[10] Elisaveta G. Shopova and Natasha G. Vakieva-Bancheva. Basic-A Genetic Algorithm for Engineering Problems Solution, *Computers and Chemical Engineering*, Vol. 30, No. 8 , pp. 1293-1309, 2006.

[11] David W.Coit, Alice E.Smith. Genetic Algorithm to Maximize a Lower-Bound for System Time-to-Failure with Uncertain Component Weibull Parameters, *Computer & Industrial Engineering*, Vol. 41, No. 4 , pp. 423-440, 2002.

[12] Marko Nagode and MatijiaFajdiga. An Improved Algorithm for Parameter Estimation Suitable fFor Mixed Weibull Distributions, *International Joural of Fatigue*, Vol. 22, No. 1 , pp. 75-80, 2000.

[13] D. N. Prabhakar Murthy, X. Min and Y. J Ren, *WeibullModels*, Wiley, 2003.

[14] T. Bucar, M. Nagode and M. Fajdiga. Reliability Approximation Using Finite Weibull Mixture Distributions, *Reliability Engineering and System Safety*, Vol. 84, No. 3 , pp. 241-251, 2004.

[15] A. A.Chowdhury, L. Bertling, B. P. Glover and G. E. Haringa. A Monte Carlo Simulation Model for Multi-Area Generation Reliability Evaluation, *9th International Conference on Probabilistic Methods Applied to Power Systems*, pp.1-10, IEEE xplore, June 11-15, 2006, Stockholm.

[16] E. Borgonovo, M. Marseguerra and E. Zio. A Monte Carlo Methodological Approach to Plant Availability Modeling With Maintenance, Aging and Obsolescence. *Reliability Engineering and System Safety*, Vol. 67, No. 1 , pp. 61-73, 2000.

[17] H. M Fu, Z. T Gao. Optimization Method of Correlative Coefficient Determining the Threeparameter Weibull Distribution, *AstronauticaSinica*, Vol. 11, No. 7 , pp. 233-237, 1990.

[18] D. N. Prabhakar Murthy, Michael Bulmer and John A.Eccleston. Weibull Model Selection for Reliability Modeling, *Reliability Engineering and System Safety*, Vol. 86, No. 3 , pp. 257-267, 2004.

[19] Robison TirreRibeiro, Nancy Flora Alves Pinto,etc. Reability Centered Maintenance(RCM), Gain and Result 3Years after Implementation, *Proceedings of IPC2004 International Pipeline Conference*, pp.1977-1981, ASME, October 4-8, 2004, Calgary, Alberta, Canada.

[20] R. Y Jiang. *Weibull model¬characteristics,parameter estimation and application*, Science publishing company, 1998.

International Journal of Comprehensive Engineering
Part C, 2(3), 253-260, 2013
Doi: 10.14270/IJCE2013.2.3.c253
Regular paper

ISSN 2186-2680
e-ISSN 2186-2656
www.iace-journal.org

Preparation of Phytase Feed Pellets by Extrusion-Spheronization

Huanxin Jiang [1], Zhengwei Cui [2, #]

[1] Packaging Engineering & Machinery Group, School of Mechanical Engineering, Jiangnan University, Wuxi, Jiangsu, 214122, China
[2] Food Engineering & Machinery Group, School of Mechanical Engineering, Jiangnan University, Wuxi, Jiangsu, 214122, P. R. China

[#] Corresponding author: cuizhengwei.sytu @yahoo.com.cn; Tel.: +86-510-85912082; Fax: +86-510-85912082

Abstract: The aim of this study was to develop extrusion-spheronization technology for preparation of the phytase pellets in size about 40 meshes as feed additive. The activity of fermented liquid phytase was about 950 U/mL, and it was microfiltrated through a ceramic membrane (0.5μm) to remove the cells, and then ultrafiltered to a concentration of liquid phytase of about 12200 U/mL. The concentrated liquid phytase was blended with different constituents of the powder (such as maize starch, maize cob flour and maltodextrin) for preparation of the plastic mass, and then the wet mass were shaped into long rods using a basket extruder. Subsequently, the long rods were dumped onto the spinning plate of spheroniser, where the extrudate was broken up into smaller cylinders with a length equal to their diameter, and those plastic cylinders were rounded due to frictional forces. Finally, the pellets were dried at about 50 ^{o}C in a fluidized bed dryer. The composition of supplementary materials was extensively chosen and tested. The particle size distribution, physical quality of pellets and retention of the phytase activity were determined. The results showed that the particle size distribution was narrow, less friable dosage formed and almost no activity lost in the process of extrusion-spheronization. The composition of supplementary materials influenced the concentration of phytase, and the phytase activity in final product reached about 5000 U/g which was sufficient for commercial production by adding stated quantity of maize cob flour or silica powder.

Keywords: Extrusion, Spheronization, Pellet, Granulation, Phytase.

Received: May 23,2012 / Accepted: May 8,2013 / Published: Sept. 10,2013

1. Introduction

Phytase (*myo*-inositol hexakisphosphate 3-phosphohydrolase, EC 3.1.3.8) belongs to the family of histidine acid phosphatases [1]. It catalyzes the hydrolysis of phytates (*myo*-inositol hexakisphosphate) to inositol and *ortho*-phosphoric acid. Phytate, the major storage form of phosphorous in plant seeds [1-3], is regarded as an antinutrient factor since it forms insoluble complexes with proteins and a variety of nutritionally important metal ions such as calcium, zinc, magnesium, and iron, and decreasing the bioavailability of phourous [4-5]. Monogastric animals are unable to utilize phytic acid phosphorus since they have very low or no levels of phytase activity in their digestive tracts and inorganic phosphate (Pi) is commonly added into the feed for the purposes of phosphorous supplementation. Supplemental microbial phytase present in corn-or soybean-based feed for pigs or poultry has been demonstrated to effectively improve phosphorous utilization and performance and reduce fecal phosphorous excretion and pollution potential of phosphorous returned to soil and/or water [6-7]. Therefore, decreasing the phytate content in plant materials to increase their nutritional values and thus reduce environmental eutrophication is advisable. This helps explain why the phytase has attracted great global attention in the animal feed business.

Phytases are typically found in plants, certain animal tissues and many microorganisms [5, 8-10]. Endogenous intestinal phytase can be found, but have very low activity. Most phytases added into feeds are of microbial origin [11]. The optimal temperature for phytase activity is between 45 ^{o}C and 60 ^{o}C, declining rapidly

at higher temperatures [12]. Phytase is usually mixed with other supplementary materials such as starch, sugar and fibre content, and then pelletized instead of being added into feed directly. Granulation and its products (granulates, pellets) offer a product form that has many advantages over powder [13], and resulting in its application both for feed additives and animal feeds. Some advantages are:

- Pellets have better flow properties, and the quantity of phytase with the activity about 5000U/g added into animal feed is generally 100~200g per ton feed. The more uniformity mixed product can be obtained when pellets substitute the powder of enzyme. Moreover, pellet with better gravitation discharging behavior is necessary for good transport in conveying equipments.
- The bulk density of pellets is higher than that of powder so that it is not easy to be carried out in a mixer due to ventilation, and the dust possibly being breathed into body is avoided.
- Prevent the enzyme from separating from the mixed ingredients.
- Prevention of the static, conglutination and grume.
- Improve solubility.
- The higher value of the products can be obtained.
- If the pellet enzymes are coated with a polymer film, it can be released in lower speed or released in special location of animal vitro.

Rotor disk fluid-bed technology is a popular method for the preparation of pellets in pharmaceutical and enzyme industries. It is a one-step closed process in which the binder solution is added at a fixed rate onto the powder blend in the fluid bed rotor (a kind of spheronizer), and the particles are agglomerated and spheronized simultaneously, then this is followed by drying (by inlet air) of spherical particles until the desired final moisture is reached [14-15]. The fluid-bed technology has been developed to involve the rotor module for several different manufacturing processes, which now include spheronization.

Usually, tangential spraying and top spraying are two typical fluidized-bed granulation technologies. The tangential spraying has been shown to be good choices for producing spheroids that can be coated for controlled release in the same rotor insert [15]. Moreover, the prepared spheroids by tangential spraying are reported to have a surface morphology (less porous and more spherical) that is more suitable for coating than that of spheroids prepared through a top-spray process. But rotor disk fluid-bed granulator is very expensive and complicated for controlling work parameters during granulation process, and the output of fluid-bed granulation is also limited. In contrast, Extrusion-spheronization has been described as another traditional and popular method of producing pellets [14], and this method produce pellets in higher output suited for preparation of feed enzymes which are usually in great yield. However, this traditional spheronization method involves four different steps: granulation, extrusion, spheronization, and drying. The success or failure of each of these steps affects greatly the quality of the final pellets or spheres. Currently, very limited literature sources are available for enzyme products pelletized by extrusion-spheronization.

The objective of this study was to develop the method of preparing the micro-pellets of feed enzymes by extrusion-spheronization, and the composition of supplementary materials. The physical quality of phytase pellets and retention of its activity were also studied and evaluated.

2. Material and Methods

2.1 Enzyme assay

Phytase activity was determined according to the technique of Bae et al.[16]. One unit of phytase activity was defined as the amount of activity that releases 1 μmol of phosphate per min at 37 ^{o}C.

2.2 Preparation of liquid phytase

The culture of phytase was done in Luliang Enzymes Co. Ltd, Yunnang Province, China. The specific microbe was cultured in a 15 m^3 fermentor with relevant temperature, pH, stirring speed and airflow during fermentation. Then the fermented liquor was pumped to microfiltration equipment with ceramics membrane (HeFei ShiJie Membrane Engineering Co., Ltd, Hanhui province, China) to remove the cells. The phytase activity was tested to be 950 U/mL in the fermentation liquor. Such a concentration level was not sufficient for commercial production for feed additive applications by the extrusion and rolling method because the final phytase activity could not reach about 5000 U/g required by commercial product. Therefore, it was needed to be concentrated by ultrofiltration. The whole treatment was as following:

Fermented liquid (950 U/mL)

↓

Microfiltration (0.50 μm)

↓

Ultrofiltration

↓

Ultrofiltrated liquid (12210 U/mL)

2.3 Equipment used during an extrusion-spheronisation cycle

2.3.1 Mixer

The first step of an extrusion-spheronization cycle consisted of the preparation of the plastic mass. A special feature of this step was the homogeneous distribution of the enzyme liquid phase throughout the wet powder mass. Different types of mixers can be used to perform the mixing of the powder blend and the concentrated enzyme liquid. Here, a single-shaft paddle batch mixer was used (Model: SLHJ1, Jiangsu MuYang Group Co., Ltd, Jiangsu province, China.)

2.3.2 Extruders

The second step of the process was the shaping the wet mass into long rods during extrusion. The extrusion process, widely used in the pharmaceutical, food, ceramics and polymer industries, can be performed using four main classes of extruders: screw, sieve and basket, roll and ram extruders [14]. The screw extruder consists of one or two (twin-screw) Archimedes screws feeding the plastic mass to an axial or radial extrusion screen. In the axial type, the screen is placed at the end of the screw, perpendicularly with the axis of the screw in contrast to the radial type where the dies are placed around the screw, discharging the extrudate perpendicularly to the axis of the screw. In the current study, the basket extruder (Fig. 1(a, b)) was designed and fractured, and the vertical walls of the extrusion chamber made up the extrusion screen. The mass was fed by a screw (driven by motor 2) and gravity into the extrusion chamber, where a rotating or oscillating device pushed the plastic mass through the screen. The Fig. 1(c) shows the size and distribution of dies in extrusion screen.

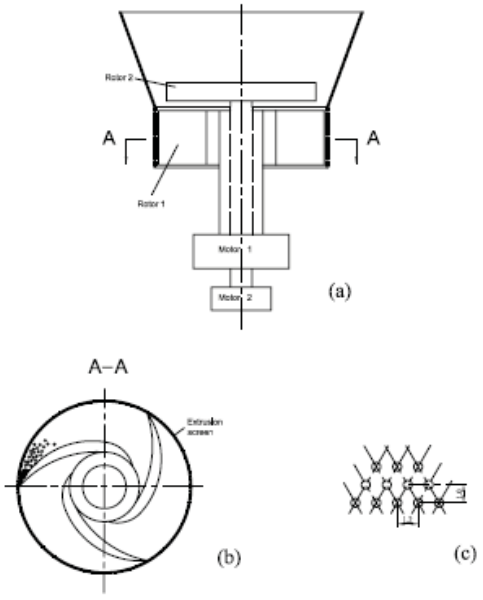

Fig. 1 Schematic view of a basket extruder. (a) View of extruder; (b) A-A section view; (c) Outspread view of extrusion screen

2.3.3 Spheronizer

After extruding, the cylinders were dumped onto the spinning plate of the spheronizer, called the friction plate with a grooved surface, where the extrudate was broken up into smaller cylinder with a length equal to their diameter [17]. Subsequently, those plastic cylinders were rounded due to frictional forces. During this spheronization process, the shape of the particles started from a cylinder over a cylinder with rounded edges, dumb-bells and elliptical particles to eventually perfect spheres. The spheronizer was also designed and constructed by us in this study.

2.4 Spheroid production

The following conditions were chosen after a series of preliminary experiments:

Wet massing (single-shaft paddle mixer): rotation speed, 50 rpm; wetting time, 10 min; enzyme liquid proportion, 20% ~ 60% (% w/w); wet massing, 2 min.

Extrusion (basket extruder): extrusion speed, 40 rpm; diameter of die, 0.6 mm; thickness of extrusion screen, 0.6 mm.

Spheronization (spheronizer; diameter of friction plate, 400 mm): time, 3 min; rotation speed, 700~900 rpm; load, 2000 g.

Drying (fluidized-bed dryer): temperature, 50±3 oC ; relative humidity, ≤3%.

2.5 Testing

2.5.1 Particle size distribution

Sphere size distribution was determined using conventional sieve analysis as described in Barrau et al.[18] (1993). The apparatus containing a set of sieves with apertures of 30, 40, 50, 60, 70 and 80 mesh were employed.

2.5.2 Friability measurement

Friability tester (Model: CS—1, Tianjin Gumin Pharmaceutics Equipment Co. Ltd., Tianjin, China) was used for the evaluation of durability of pellets. In principal, this device brings about attrition stresses that are exerted to pellets, due to either mechanical or pneumatic transportation. Friability is determined by inducing fines through an abrasion action of pellets shearing over each other and over the wall of drums. The procedure is standard by using a drum with specified dimensions, in which 200 g of sieved pellets are inserted. After tumbling for 10 min at 50 rpm, the pellets are subsequently sieved and the amount of fines passing a sieve with a grid size "just smaller than the nominal pellet diameter" is determined. Friability/or durability is normally expressed as a percentage which gives the amount of fines returned or the amount of pellets recovered. Friability measurement of sample was replicated three times.

2.5.3 Sphericity measurement

Sphericity was determined using an image analyzer (Quantimet 500, Leica, Cambridge, UK) interfaced with a microscope (Model: WV-CP 430/CH, Panasonic Electric Equipment Co. Ltd, Japan) in which the roundness, perimeter (P_M) and particle projected area (A) were measured. These were used to calculate the sphericity (S), as shown in equation below [19]:

$$S = \frac{4A \times 3.142}{P_M{}^2} \tag{1}$$

2.5.4 Flowability measurement

The repose angle φ was employed to indicate of the sphericity of a pellet indirectly. Tangent φ is the ratio of the pile height and the pile radius measured after a certain amount of pellets are allowed to fall from a given height onto a hard surface through a specified orifice [19].

$$\varphi = arctg(\frac{H}{R}) \tag{2}$$

Where φ is the angle of repose, and H and R are the height and radius, respectively, formed by the spheroids.

3. Results

3.1 Compositions of supplementary materials on the concentration of phytase

Usually, maize starches, binders such as cyclodextrin and CMC are basic components for feed enzyme additives. When the rapid-solubility of enzyme pellets is required, a quantity of sucrose is often added. Some optimized compositions and extrusion status are presented in Table 1. When the ultra-fine silica powder or maize cob flour were added into compositions, it was noticed that more liquid enzyme was absorb and/or stored without excessive water being present on the surface of particles during extrusion, while the phytase activity in final product was over 5000 U/g (Table 1). This can be explained that the structure of the silica is in tiny-hole and the maize cob is classified as fibrin with much hydrophilic-group such as hydroxyl. Consequently, more

enzymes were able to get into the internal structure of components resulting in the higher enzyme concentration in final product.

Table 1 Effect of compositions of supplementary materials on the concentration of phytase

Experiment	1	2	3	4
Activity of concentrated phytase solution （U/ml）	12210±10.44	12210±10.44	12210±10.44	12210±10.44
Compositions	80g maize starch : 20g maltodextrin : 20 mL phytase solution	83g maize starch: 9 g cyclodextrin : 8 g silica powder: 45 mL phytase solution	78g maize starch : 3g CMC : 9g silica powder : 10g sucrose : 45 mL phytase solution	72g maize starch :18g maize cob flour : 10g maltodextrin : 63 mL phytase solution
Extrusion status	good	very good	very good	very good
Activity of phytase in product after drying (U/g)	2385±7.14	5400±5.41	5412±6.32	7560±8.54
Sphericity(S)	0.74±0.01	0.85±0.02	0.81±0.02	0.79±0.01
Flowability(φ)	20.54±1.21	21.45±1.56	22.01±0.92	23.31±1.02
Friablility	1.60±1.12	1.75±1.62	1.45±1.09	2.60±1.52

3.2 Retention of phytase activity

The extrusion temperature and retention of phytase activity are illustrated in Tab. 2. The extrusion temperature could be controlled below 50 °C in our basket extruder whose structure and work parameters were optimized and as shown in Fig. 1 and *Section 2.4*. In the process of optimization, many experiments were performed, and it was noticed that the distributing density of dies on screen and thickness of extrusion screen had significant influence on the extrusion process. In fact, extrusion stress and the shearing strength had less impact on enzyme activity, but the subsequent drying temperature had marked effects on retention of phytase activity as Tab. 3 shows. Therefore, the temperature for drying phytase pellets should be below 55 °C.

Table 2 Effect of extrusion process on retention of phytase activity

Liquid phytase activity （U/ml）	Extrusion temperature （°C）	Composition	Phytase activity after pellet（U/g）	Ratio of retention of phytase activity （%）
12210±10.44	42±3.5	72g maize starch +18g maize cob flour+ 10g maltodextrin+63 mL liquid phytase	5416±2.3	98.5

Table 3 Effect of drying temperature on retention of phytase activity

Drying temperature	Ratio of retention of phytase activity（%）
50 °C	96.4±2.4
60 °C	85.6±4.2

3.3 Particle size distribution

In these experiments, the starting raw materials were kept uniform by sieving the powders through an 80-mesh size prior to blending. Fig. 2 shows particle size distributions for four groups of experiments. The 40 mesh size die is about 0.35 mm. It is evident from Fig. 2 that the size of the most finial phytase pellets were between 30 meshes and 50 meshes which were desirable and eligible size and they added up to about 90% even if the size distributions were not the same. Therefore, the particle size and its distribution were mainly determined by the size of dies. In this four groups of composition, maltodextrin, cyclodextrin and CMC were respectively employed as binder and their quantity in each composition were carefully chosen by a series of

preliminary experiments. The Fig. 2 also indicts that the quantity of binder had greatly impact on size and its distribution whereas the kind of binder had little influence. The experiment 4 in Fig. 2 also shows that the maize cob flour, as a kind of dissolved plant fiber, mighty lead to more fine particles, implying it is beneficial to break the cylinders due to their stiffness and elasticity during spheronization. Therefore, the quantity of fibers in the mass should be carefully chosen.

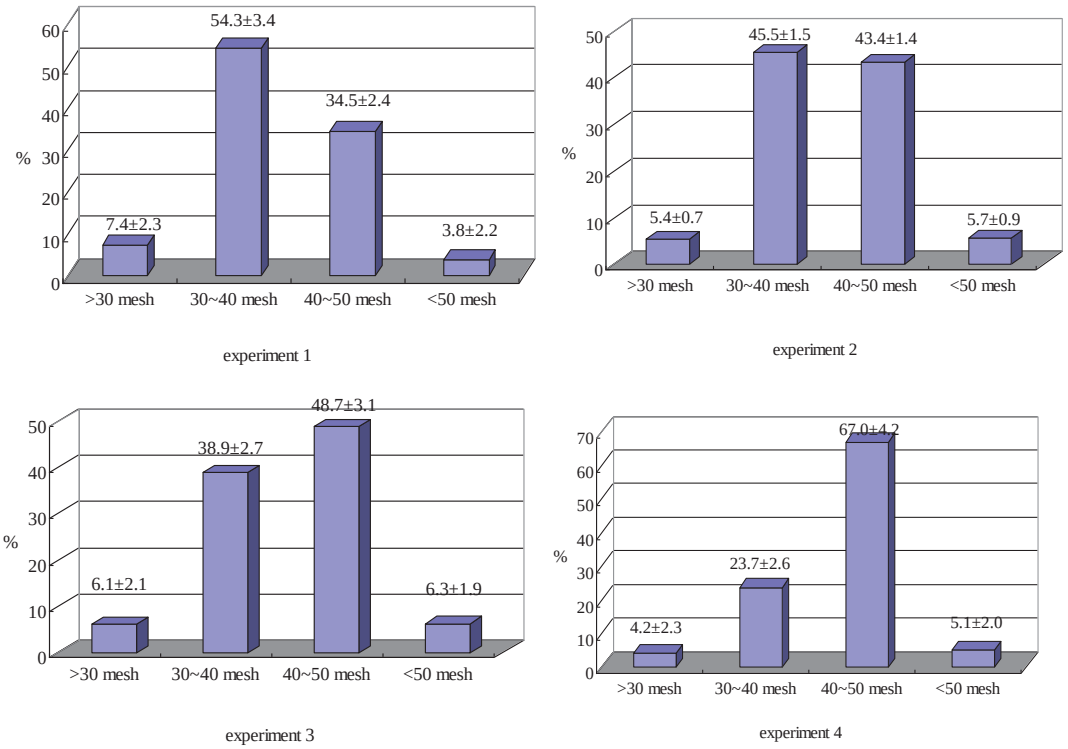

Fig. 2 Particle size distributions of four groups of experiments. (Expt. 1: 80g maize starch : 20g maltodextrin : 20 mL phytase solution; Expt. 2: 83g maize starch: 9 g cyclodextrin : 8 g silica powder : 45 mL phytase solution; Expt. 3: 78g maize starch : 3g CMC : 9g silica powder: 10g sucrose: 45 mL phytase solution; Expt. 4: 72g maize starch : 18g maize cob flour : 10g maltodextrin : 63 mL liquid phytase)

3.4 Physical quality (Sphericity, Flowability and Friability)

Fig. 3 shows the pellets photograph prepared in our current study. The sphericity of the pellets was in the range of 0.74 to 0.85, which is approximately 1.0, the optimal value for sphericity. The percentage weight loss from the batches was less than 5% as shown in Tab. 1. However, increased rotor speed, use of the maize cob, and use of rougher plate contours increased the friability due to attrition and weakly agglomerated particles. The angle of repose of all the formulations was less than 30^{o} as shown in Tab. 1, indicating good flow behavior of the spheroids.

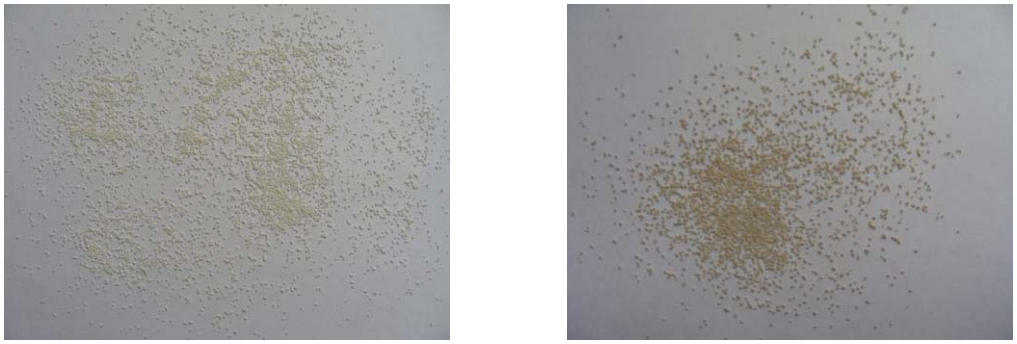

(a) (b)

Fig. 3 Typical photograph of particles.(Composition: (a) 83g maize starch : 9 g cyclodextrin : 8 g silica powder : 45 mL phytase solution, (b) 72g maize starch : 18g maize cob flour : 10g maltodextrin : 63 mL liquid phytase)

4. Discussion

The composition is one of key factors for successful pellet preparation by the current method, and the results show a strong correlation between the concentration of phytase and the compositions. Traditionally, it was considered that it was difficult to prepare enzyme pellets in higher concentration by extrusion-spheronization. If that, the mass will be too moistening to shape because of the need to add more liquid enzyme. The cultured phytase activity was reported at 950 U/mL in our current study. Such a level was not sufficient for commercial production for feed enzymes additive applications by the extrusion-spheronization method because the phytase activity after drying cannot reach about 5000 U/g which is required for commercial products. Although ultrafiltration was employed to concentrate liquid phytase, the concentration was limited by the ultrafiltration membrane and the cost increased with the increasing concentration of phytase. Therefore, it was necessary to add the components which were able to store and immobilize more water during granulation.

In fact, compositions are very complex and diverse because many components can be used for this propose. The compositions shown in Tab. 1 were determined through thorough preliminary studies with an aim to prepare pellets with a higher enzyme concentration and uniform size and shape distribution. Enzyme concentration and extrusion statue (long rods discharged from the dies smoothly, not too wet and not too dry) determined the compositions. The fiber material, such as maize cob flour availability and low-cost, is an ideal additive component for this proposes.

The extrusion temperature has much impact on the retention of enzymes activity in the whole process of extrusion-spheronization. Furthermore, it was strongly related to structure parameters such as diameter, density and thickness of the die of extrusion screen as well as work parameters such as the rotate speed of the roller, the distance between the edge of the roller and the screen. In addition, the subsequent drying temperature had marked impact on the retention of enzymes activity due to its sensitivity to temperature.

During the extrusion-spheronization process the cylinders were broken up into smaller pieces with a length generally equal to their diameter, and then those plastic cylinders were rounded due to frictional forces. Therefore, the size of the die on the screen of basket extruder determined the size of the final pellet as well as its size distribution. Certainly, size distributions were also related to the formulation components characteristics and process variables [20]. Water content, spheronizer speed, spheronization time and plate types also influenced the particle size as well as its distributions. Usually, the more surface free water will lead reuniting of particles; the increased rotor speed decreased the mean diameter due to surface defects on the pellets by the high speed, thereby producing more fines. Their impacts on pellet size distributions were similar to other reports [14, 21]. The particle size distribution experiments demonstrated that the desirable particle size distribution could be obtained if these sound composition and processing parameters were imposed in current studies.

Transportation and handling in both the factory and on the farm requires pellets of certain integrity without fines being produced by attrition stresses. In general, pellet quality depends on the combination of raw materials used, the process technology and the different operating/processing variables during pelleting. All these variables affect pellet integrity, sphericity, flowability and durability. Due to the complexity of the feed enzyme mash (blends of several raw materials that differ in composition and functional properties), processing condition and interaction between composition and processing parameters, quantitative descriptions of effect of the formulation components on particle size distribution were acquired differently.

5. Conclusion

Pellets as an enzyme delivery system offer many technological advantages, and the size of pellets is usually about 40 meshes. Pellets of uniform size, low porosity, and regular shape can be produced via properly formulated and conducted extrusion/spheronization process. During the extrusion phase, extrusion temperature can be controlled below 50 ^{o}C by use of our basket extruder which's structure and work parameters were optimized, and almost no activity lost in this process of extrusion. The fermented liquid phytase was concentrated to about 12000 U/mL using microfiltration by ultrafiltration. The compositions of supplementary materials influenced the concentration of phytase, and the phytase activity in final product can reach to about 5000 U/g which was sufficient for commercial product by adding quality of maize cob flour or silica powder. Narrow particle size distributions, less friable dosage form and flow-preference pellets can be provided in large scale by the current method.

References

[1] D. B. Mitchell, K. Vogel, B. J. Weimann and L. Pasamontes. The Phytase Subfamily of Histidine Acid Phosphatases: Isolation of Genes for Two Novel Phytases from the Fungi Aspergillus Terreus and Myceliophtora Thermophila, *Microbiology*, Vol.143, pp. 245-252, 1997.

[2] P. Vohra, G. A. Gray and F. H. Kratzer. Phytic Acid-Metal Complexes, *Proceedings of the Society for Experimental Biology and Medicine*, Vol. 120, pp. 447-449, 1965.

[3] J. N. A. Lott, I. Ockenden, V. Raboy and G. D. Batten. Phytic Acid and Phosphorus in Crop Seeds and Fruits: A Global Estimate, *Seed Science Research*, Vol. 10, pp. 11-33, 2000.

[4] M. Torre, A. R. Rodriguez and F. Saura-Calixto. Effects of Dietary Fiber and Phytic Acid on Mineral Availability, *Critical Reviews in Food Science and Nutrition*, Vol. 30, pp. 1-22, 1991.

[5] B. L. Liu, A. Rafiq, Y. M. Tzeng and A. Rob. The Induction and Characterization of Phytase and Beyond, *Enzyme and Microbial Technology*, Vol. 22, pp. 415-424, 1998.

[6] K. Zyla. Mould Phytases and Their Application in the Food Industry, *World Journal of Microbiology and Biotechnology*, Vol. 8, pp. 467-472, 1992.

[7] J. Juanpere, A. M. Perez-Vendrell and J. Brufau. Effect of Microbial Phytase on Broilers Fed Barley-Based Diets in the Presence or Not of Endogenous Phytase, *Animal Feed Science and Technology*, Vol. 115, pp. 265-279, 2004.

[8] M. Wyss, L. Pasamontes, A. Friedlein, R. Remy, M. Tessier and A. Kronenberger. Biophysical Characterization of Fungal Phytases(*Myo*-Inositol Hexakisphosphate Phosphohydrolases): Molecularsize, Glycosylation Pattern, and Engineering of Protoelitic Resitance, *Applied and Environmental Microbiology*, Vol. 65, pp. 359-366, 1999.

[9] M. Wyss, R. Brugger, A. Kronenberger, R. Remy, R. Fimbel and G. Oesterhelt. Biochemical Characterization of Fungal Phytases(*Myo*-Inositol Hexakisphosphate Phosphohydrolases): Catalytic Properties, *Applied and Environmental Microbiology*, Vol. 65, pp. 367-373, 1999.

[10] E. Frossard, M. Bucher, F. Machler, A. Mozafar and R. Hurrell. Potential for Increasing the Content and Bioavailability of Fe, Zn and Ca in Plants for Human Nutrition, *Journal of the Science of Food and Agriculture*, Vol. 80, pp. 861-879, 2000.

[11] V. Ravindran, W. L. Bryden and E. T. Kornegay. Bioavailability and Implications in Poultry Nutrition, Avian and Poultry Biology Reviews, Vol. 6, pp. 125-143, 1995.

[12] R. J. Wodzinski and A. H. J. Ullah. Phytase, *Advances in Applied Microbiology*, Vol. 42, pp. 263-302, 1996.

[13] M. Tomas and A. F. B. van der Poel. Physical Quality of Pelleted Animal Feed 1. Criteria for Pellet Quality, *Animal Feed Science and Technology*, Vol. 70, pp. 59-78, 1998.

[14] C. Vervaet, L. Baert and J. P. Remon. Extrusion Spheronization: a Literature Review, *International Journal of Pharmaceutics*, Vol. 116, pp. 131-146, 1995.

[15] D. P. Rubino. Fluid-Bed Technology: Overview and Criteria for Process Selection, *the Journal of Pharmacy and Technology*, Vol. 23, pp. 104-113, 1999.

[16] H. D. Bae, L. J. Yanke, K. J. Cheng and L. B. Selinger. A Novel Staining Method for Detecting Phytase Activity, *Journal of Microbiological Methods*, Vol. 39, pp. 17-22 ,1999.

[17] J. W. Conine and H. R. Hadley. Preparation of Small Solid Pharmaceutical Spheres, *Drug and Cosmetic Industry*, Vol.106, pp. 38-41, 1970.

[18] J. P. Barrau, B. Bataile and M. Jacob. The Influence of Spheronizer Load in Extrusion/Spheronization, *Pharmaceutical Technology International*, Vol. 5, pp. 66-70, 1993.

[19] B. N. Chukwumezie, M. Wojcik and M, C. Adeyeye. Feasibility Studies in Spheronization and Scale-Up of Ibuprofen Microparticulates Using the Rotor Disk Fluid-Bed Technology, *AAPS Pharmscitech*, Vol. 3, No. 1, pp. 1-13, 2002.

[20] L. Hellen, J. Yliruui, P. Merkku and E. Kristoffersson. Process Variables of the Radial Screen Extruder: Shape, Surface, and Flow Properties of Pellets, *Pharmaceutical Technology International*, Vol. 5, pp. 38-48, 1993.

[21] D. Sonaglio, B. Bataille, C. Ortigosa and M. Jacob. Factorial design in the feasibility of producing Microcel MC 101 pellets by extrusion/spheronization, *International Journal of Pharmaceutics*, Vol. 115, pp. 53-60, 1995.

International Journal of Comprehensive Engineering
Part C, 2(3), 261-267, 2013
Doi: 10.14270/IJCE2013.2.3.c261
Regular paper

ISSN 2186-2680
e-ISSN 2186-2656
www.iace-journal.org

Establishment of Tillage Soil Contact Model And Uniaxial Compression Test Based On EDEM

Jianping Hu, Yongliang Zhang #, Chunjian Zhou and Chuantong Lu

Key Laboratory of Modern Agricultural Equipment and Technology, Ministry of Education&Jiangsu Province, Jiangsu University, Zhenjiang, 212013, China

Corresponding author: Yongliang Zhang,yy19860922@126.com; Tel.: +86-13656136423

Abstract: Tillage soil is a typical discrete particulate material, and it is the key of soil analysis of dynamic changes that the simulation for the generation and fracture of soil agglomerate with adhesive particle DEM. In this paper, we introduced bond model add to existing dry granular discrete element contact mechanical model of soil to express water adhesion, builded wet granular soil contact mechanics model. Through the soil specimen uniaxial compression test method for calibrating the model bonding parameter. In EDEM software, using the wet granular soil contact mechanical model which has been established to simulate the soil uniaxial compression test, and the simulation results were compared with the experimental results. As results show, the compression curves of simulation and experiment are in good agreement, and these two curves both increase linearly to a peak, followed by decreasing smoothly. The compression strengths for experiment and simulation were 33.68N and 32.66N respectively, and the simulative strength is 3% lower than that of experiment.

Keywords: Discrete Element Method, Tillage Soil Particle Contact Model, Uniaxial Compression, EDEM Simulation.

Received: May 11,2012 / Accepted: May 8,2013 / Published: Sept. 10,2013

1. Introduction

Discrete element method(referred to as DEM) was put forward by the America scholar Professor Cundall [1] in 1971, which based on molecular dynamics principle, and is widely used in rock mechanics, pharmaceutical, agriculture and other fields of a uncontinuous numerical simulation method, the theory is based on the second law of thermodynamics and has a solid theory foundation.

At present, many scholars has analysed arable soil particle discrete element model. Xu Yong [2] and his colleagues put forwarded new ideas which based on particle contact mechanics principle of discrete element method on tillage soil dynamics numerical simulation, and discuss the discrete element method for soil dynamics simulation feasibility and some key technology problems and Countermeasures. Oda [3] using discrete element method simulation of soil uniaxial compression broken problem, considering the contact point of the rolling resistance of granular discrete element model to simulate the soil in the process of uniaxial compression, resulting in the macroscopic shear band deformation mechanism, model does not involve adhesion. Zhang Rui [4] and his collaborators by introducing parallel constraint to the characterization of soil particle in liquid bridge between viscous effects, established the soil particle contact nonlinear mechanical model, and a discrete element macroscopic and mesoscopic simulation model, but only in the particles into contact with each other to produce parallel constraint, do not conform to the real effect of the moisture in the soil. Liu [5] considered the band adhesion force of the spring - damper model analysis of unsaturated granular soil aggregation process of disintegrating, and combined test, research the compacted unsaturated clay three axial compression and biaxial shear problem, but its adhesion model modeling complex, general discrete element software can not meet the requirements of modeling simulation. Li Yanjie and Xu Yong [6] used adhesion particle discrete element model for soil uniaxial compression tests were simulated, simulation values higher than test value 11.6%.

2. Establishment of tillage soil discrete element contact mechanics model

According to the different soil moisture content, soil particle discrete element model including dry particle model and wet particle model, the latter including liquid bridge and immersion type two forms. As shown in figure 1. Dry particle model for loose sand, liquid bridge wet particle model suitable for general cultivation soil or rheology liquid wet soil, immersion type particle model in paddy soil[2].

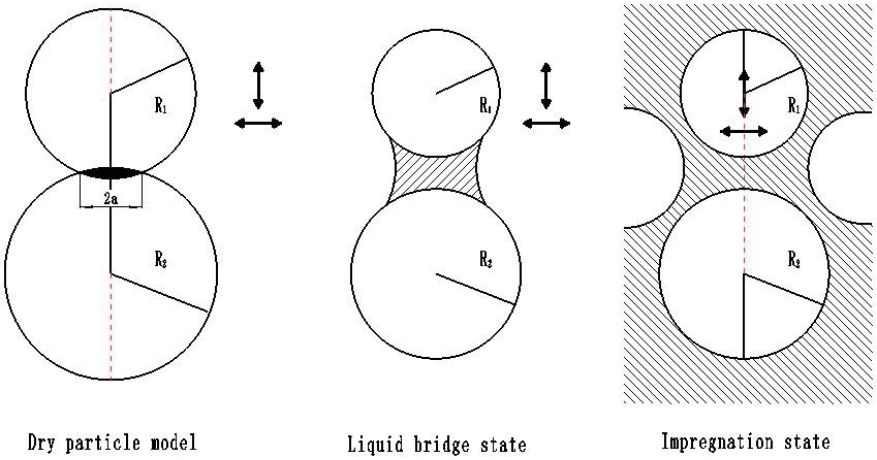

Fig. 1 Soil particle contact model

The soil in addition to soil particles as a skeleton, liquid water is a important component, it is usually to moisture, water film, capillary water and gravity water exist in the form of [7]. Among them, capillary water in soil particle spaces form a discontinuous liquid bridge, the liquid bridge between soil particles produced in viscous effects which is the impact force between soil particles are important factors. This article in dry granular soil contact model is based on the introduction of bonding constraints, composed of particles of wet soil contact mechanics model to represent the result of water present in the soil contact mechanics model. As shown in figure 2.

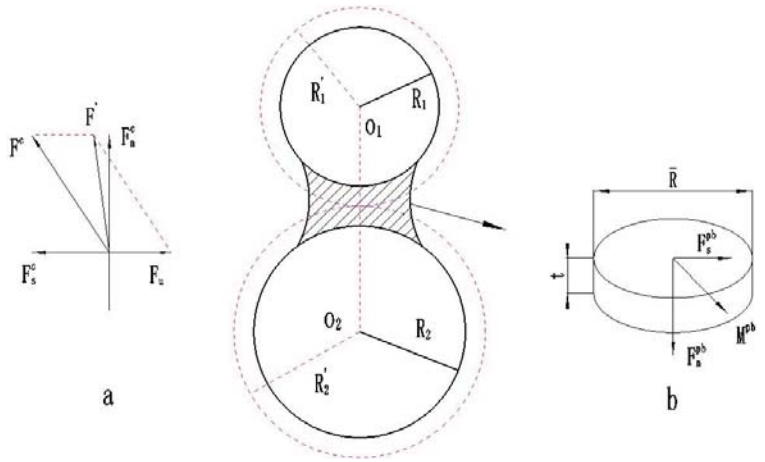

Fig. 2 Wet granular discrete element contact mechanical model of soil

In wet granular soil contact mechanics model, soil particle interactions include granular contact force, adhesive binding force and friction force, the performance equation for:

$$[F]=[F^{c}]+[F^{pb}]+[F_{\mu}] \tag{1}$$

In the equation, $[F]$ is soil particle interaction total force. $[F^{c}]$ is soil particle contact force, including the normal contact force and tangential contact force, among them, sliding model control tangential contact force. $[F^{pb}]$ is binding constraint force, including normal force, tangential force and adhesive bonding constraints constraint force moment. $[F_{\mu}]$ is Friction force.

The following content will introduction to bond model which is the author originality:

Binding constraints is established between particles, this relationship run together with linear stiffness model and the slip model [8]. Binding constraints occurs in the soil particles without contact time. This paper introduces the bonding radius, soil moisture much influence the size of it. Each particle has set a bond radius When model building. bond radius is larger than the particle radius, when two discrete particles between the centroid distance is less than or equal to the setting of the two particle bonding radius, that is $o_1o_2 \le R_1' + R_2'$, the bonding constraints will formed between particles. As shown in figure 2. Formation of the binding constraint can transfer the forces and torque. When the two bound particles have relative movement, either the maximum normal or tangential stress than their corresponding constraint strength, bonding constraints fracture.

Binding constraint forces including normal force and tangential force, that is:

$$F^{\text{pb}} = F_{\text{n}}^{\text{pb}} + F_{\text{s}}^{\text{pb}} \tag{2}$$

Binding constraints are generated after, The outside to soil particles F_{n}^{pb}, F_{s}^{pb} and torque M_{n}^{pb}, M_{s}^{pb} with the time step increasing. According to formula (1.3) starting from zero increase:

$$\begin{cases} \delta F_{\text{n}}^{\text{pb}} = -\upsilon_n S_n A \delta t \\ \delta F_{\text{s}}^{\text{pb}} = -\upsilon_t S_t A \delta t \\ \delta M_{\text{n}}^{\text{pb}} = -\omega_n S_t J \delta t \\ \delta M_{\text{s}}^{\text{pb}} = -\omega_t S_n \dfrac{J}{2} \delta t \end{cases} \tag{3}$$

In the equation, A is the contact area, $A = \pi R_B^2$; $J = \dfrac{1}{2}\pi R_B^2$, R_B is Bond radius. S_n and S_t were normal and tangent stiffness. δt is time step. υ_n and υ_t as the particles of normal and tangential velocity. ω_n and ω_t for normal and tangential velocity.

When the normal force and tangential force is greater than a defined value, bond was broken. Therefore, the definition of normal and tangential stress maximum value is as follows:

$$\begin{cases} \sigma_{\max} < \dfrac{-F_{\text{n}}^{\text{pb}}}{A} + \dfrac{2M_{\text{s}}^{\text{pb}}}{J} R_B \\ \tau_{\max} < \dfrac{-F_{\text{s}}^{\text{pb}}}{A} + \dfrac{M_{\text{n}}^{\text{pb}}}{J} R_B \end{cases} \tag{4}$$

When the external force destroys the soil particles between the binding constraint, interactions among soil particles will be dry granular soil discrete element contact mechanics model in the form of action.

3. Determination of contact mechanics model parameters

By using EDEM software to simulation dynamic behavior of soil, establishing a simulation system need to enter the soil contact model parameters are many. So far, there have been many scholars on the soil of these physical properties are studied. Some of these parameters reference the soil testing manual [9] and granular material mechanics[10]. This parameter values as shown in table 1.

Table 1 Some Model parameters

Soil particle radius/mm	Soil particle density/kg/m^3	Poisson's ratio	Shear modulus/Pa	The coefficient of restitution	Coefficient of friction	Normal stiffness/N/m	Shear stiffness /N/m
1	2680	0.3	1e+08	0.3	0.5	1e+08	5e+07

Bonding radius, Cirtical normal stress and Cirtical shear stress are through the following method to derive. In which of them, soil moisture much influence the size of it. The higher Water content, the biger bonding radius. In this paper, according to the general tillage soil water content of 15% calculated the size of the radius of the particle bonding: $R_1' = 1.3mm$.

This paper through the soil in uniaxial compression test critical bond law of corresponding force and critical bond shear stress used by Changchun Branch of new test equipment limited production of type WDW-300 universal material test machine. Firstly, the soil sample made of soil mechanics standard cylinder specimens (diameter 39.1mm, high 80mm), then the test piece mounted on the compression apparatus, and in the sample around with vaseline to prevent evaporation. Prior to the start of test specimen and pressurized columns, adjust good contact, the stress and displacement are set to 0. Click the start button to test, pressure column to 10mm / min rate on compression, recording of stress and displacement change value, until the test piece ruptures or slip to fall apart. As shown in figure 3.

Fig. 3 The normal and shear direction of the broken of soil uniaxial compression method

The measured stress and time curves as shown in figure 5 and figure 6.

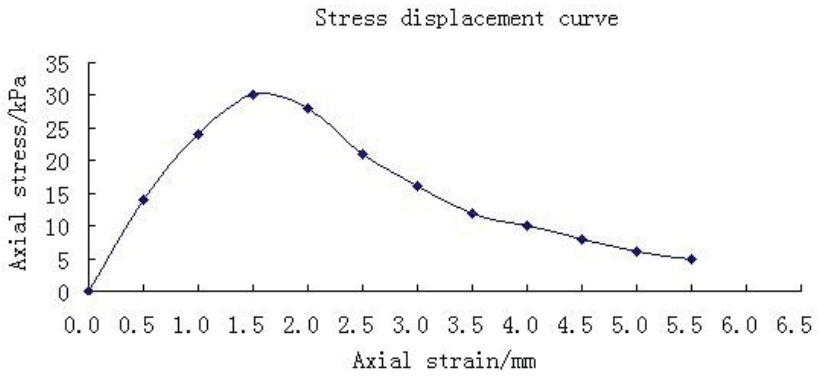

Fig. 5 Normal stress and time curves of soil uniaxial compression method

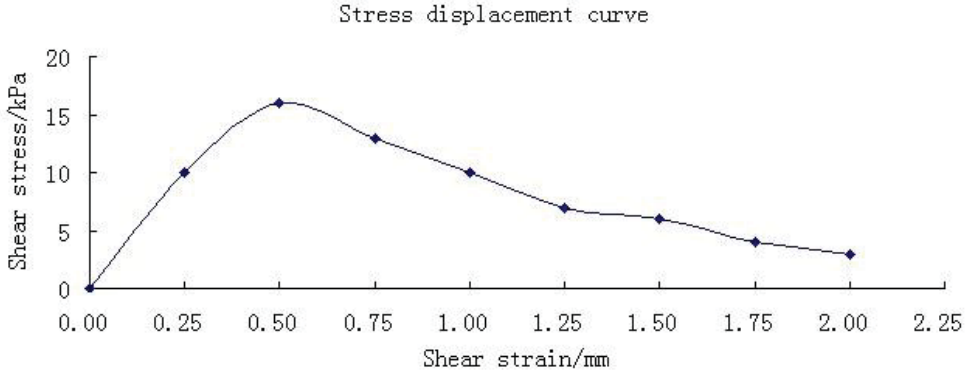

Fig. 6 Shear stress and time curves of soil uniaxial compression method

In the test, the specimen sides free, bearing the axial pressure when the sample partial yielding and failure, after the destruction of soil bearing capacity decreased, so the specimen subjected to axial stress (axial pressure) has a maximal value, consistent with the test curves shown in figure 4. The stress displacement curve graph we can see, farming soil maximum bonding method corresponding to force 30kPa. Farming soil maximum tangential stress is in 16kPa bonding.

4. EDEM simulation and analysis

In recent years, with the development of computer technology, the discrete element software applications have been developed to a new stage. On behalf of new discrete element analysis software is EDEM[11]. In this paper, using the discrete element simulation software EDEM to simulate three-dimensional soil in uniaxial compression. The simulation system of soil model parameters according to the determined parameters set. Soil particles in diameter is 39.1mm, height 100mm soil cylinder to generate, soil cylinder on the length of 400mm simulation on a flat plate. According to the test of soil column density calculation, using a total of 12000 particles, particle radius 1mm. Soil particles in 3S is generated when finished, soil column height of 80mm. Parallel constraint set in 3.1s effect, so that the soil particles cohere. Then the soil barrel upward movement, leaving the simulating soil column. As shown in figure 7

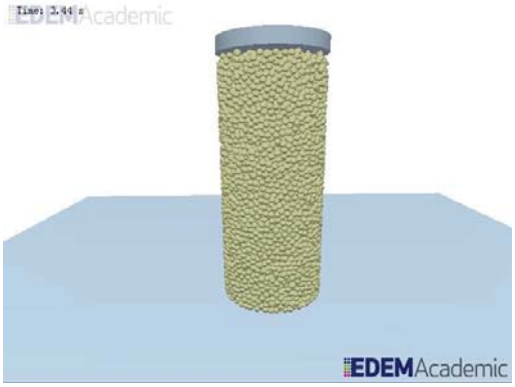

Fig. 7 Simulation of soil specimen in uniaxial compression test

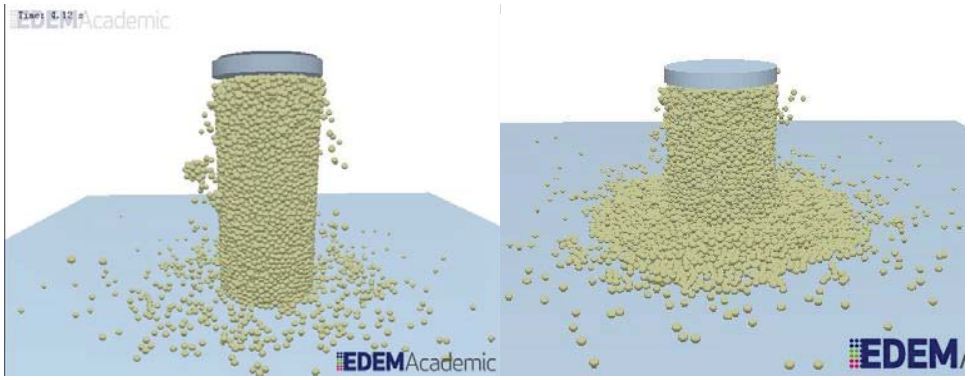

Fig. 8 Simulation of soil specimen in uniaxial compression test of broken

Continue to simulation, pressure plate and soil column simulated equal in diameter, located in the simulated soil column above 15mm, at time 3 seconds, pressure plate with 10mm / min speed to the soil column simulated movement, until the simulation soil column specimens completely rupture or slip lost. As shown in figure 8.

Simulation and test of soil uniaxial compression stress - strain curve comparison. As shown in figure 9. Through the experiment and simulation of soil uniaxial compression stress - strain curve contrast, found the simulated values at the peak is slightly smaller than the experimental values. The axial strain in 2.5mm, analog values are slightly higher than the experimental values. But in the axial strain4mm, test values again higher than simulation value. On the whole, the simulation results of the axial pressure curve and the test curve basically coincide, and these two curves both increase linearly to a peak, followed by decreasing smoothly. The compression strengths for experiment and simulation were 33.68N and 32.66N respectively, and the simulative strength is 3% lower than that of experiment. Prove that the construction of tillage soil contact mechanics model and model parameter

selection are correct and the simulation of EDEM feasibility. Provides soil particle discrete element development a useful contact model and simulation method.

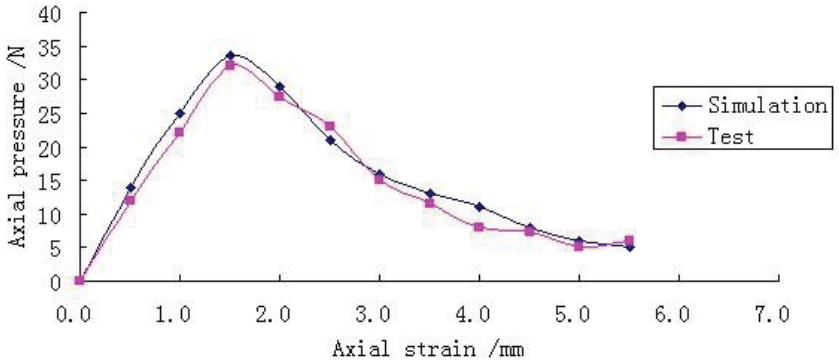

Fig. 9 Test and Simulation of soil uniaxial compression stress - strain curve comparison

5. Conclusions

(1) This paper put bond constraints are added to dry granular soil contact mechanics model, bonding radius which in the binding constraints should be larger than the particle radius, according to the soil moisture content of different size can be adjusted. Compared to the Zhang Rui building soil particle contact nonlinear mechanics model, the model more accord with the real soil due to the moisture arising from the presence of the particles between bonding, and the use of the classical soil mechanics test soil specimen uniaxial compression test calibration the maximum bonding normal stress and tangential stress.

(2) Using discrete element software EDEM to simulate soil uniaxial compression, simulation of the axial strain stress curve results agree with the experimental results, the simulated curves in peak less than the experimental value of 3%, the simulation results close to the real soil uniaxial test results. Contrast Xu Yong used the adhesion particle discrete element model for soil uniaxial compression test numerical simulation analysis results, in this paper, the simulation results of higher accuracy.

(3) Successfully simulated by using bonding constrained particle discrete element model for soil agglomerate breaking, prove this paper using the methods of establishing farming soil contact model is correct and the simulation analysis of the feasibility of using EDEM. For the use of discrete element method for the dynamic behavior of soil provides a new model and method.

(4) Through this kind of soil contact model can solve the problem of agricultural mechanical rotary tillage. In EDEM software, using the wet granular soil contact mechanical model which has been established to simulation and optimization choose the best machine forward velocity, rotary blade speed, cover grid position and rotary tillage knife deep tillage and so on. This model will have a wide application in development of the agricultural machinery

Acknowledgment

This work was financially supported by the Priority Academic Program Development of Jiangsu Higher Education Institutions((Su financial teacher(2011)no.8), Qing Lan Project of Jiangsu Province (Su teacher (2010)no.27) and Three Engineering of Agricultural Machinery(NJ2009-21).

References

[1] P. A Ctmdall. A Discrete Nunzrieal Model for Granular Assembles. *Ceotechnical*, Vol. 291, pp. 47-65, 1979.

[2] Y. Xu, H. Y Li and W. B Huang. Modeling and Methodological Strategy of Discrete Element Method Simulation for Tillage Soil Dynamics, *Transactions of the CSAE*, Vol. 3, pp. 34-38, 2003.

[3] K. Iwashita and M. Oda. Micro-Deformation Mechanism of Shear Banding Process Based on Modified Distinct Element Method, *Powder Technology*, Vol. 109, No. (1-3), pp. 192-205, 2000.

[4] R. Zhang, J. Q Li, Y. W Li, Z. B Liu and B. Chen. Dem Macroscopic and Mesoscopic Analysis in Disturbed Behavior of soil Acted by Part with Complex Surface, *Journal of Jilin University (Engineering*

and Technology Edition), 2009.
[5] S. H Liu, D. A Sun and Y. S Wang. Numerical Study of Soil Collapse Behavior by Discrete Element Modeling, *Computers and Geotechnics*, Vol. 30, No. 5, pp. 399-408, 2003.
[6] Y. J Li and Y. Xu. Comparison Study Between the Soil Uniaxial Compression Test and the Discrete Element Simulation, *Journal of China Agricultural University*, Vol. 14, No. 4, pp. 103-108, 2009.
[7] Y. Jiang. *Soil*, Jilin people's Publishing House, 1983.
[8] L. X Zhai and C. Q Ji. Foundation of Dynamic Soil Model Based on Distinct Element Method, *Acta Agriculturae Jiangxi*, Vol. 20, No. 9, pp. 108-111, 2008,
[9] Nanjing Hydraulic Research Institute. *Soil test technical manual*, China Communications Press, 2007.
[10] Q. C Sun and G. Q Wang. *Granular material mechanics*, Science Press, 2009.
[11] G. Q Wang, W. J Hao and J. X Wang. *Discrete Element Method and its Practice on EDEM*, Northwestern Polytechnical University press, 2010.

International Journal of Comprehensive Engineering
Part C, 2(3), 268-274, 2013
Doi: 10.14270/IJCE2013.2.3.c268
Regular paper

ISSN 2186-2680
e-ISSN 2186-2656
www.iace-journal.org

Design of Feeding System with Remote Monitoring in Marine Ranching

Weifeng Peng [1], Shaojie Jiang [2, #]

[1] College of Engineering, Shanghai Ocean University, Shanghai, 201306, China

[#] Corresponding author: sjjiang@shou.edu.cn; Tel.: +86-156-9216-5367

Abstract: In order to reach the need of the systematic fishery production and management by marine ranching, a feeding system with remote monitoring was designed. A programmable internet controller was used as a control core in the system, and technologies about auto-feeding, underwater cameras, sensors and wireless network are involved in. Problems of precise feeding, audible acclimatization and underwater video monitor were solved to meet the request of marine ranching. Remote control and management were achieved finally.

Keywords: Marine Ranching, Feeding Machine, Remote Monitoring, System Design.

Received: May 21,2012 / Accepted: May 8,2013 / Published: Sept. 10,2013

1. Introduction

The key of construction of marine ranching is to solve the construction and improvement of artificial interest-bearing field, behavior control of object, environmental regulation, the monitoring of biological resources and so on. Therefore, to achieve the systematic fishery production and management of marine ranching, developing a bait-throwing system which has the function of remote monitoring has important significance. Although there are several kinds of automatic bait- throwing systems for large-scale anti-wave net cage breeding in China, they are difficult to achieve micro-baiting, and they have huge volume, complex structure and high maintenance costs, so it can't be remotely controlled on land and monitored on real-time, it cannot reach the requirement of ocean ranching also. Overseas, automatic bait-throwing system with technologies of micro baiting, sound trace domestication and underwater monitoring has been widely in application. However, its higher technical requirements and complex structure, high cost, also can't adapt to the needs of marine fishery production inland.

2. Development Scheme

The marine ranching technology in China is still in its initial stage, based on the current situation and the user's economic situation as well as the technical requirements of marine ranching; high cost of equipment is difficult for users to accept. Therefore, the development of marine ranching feeding system with remote monitoring mainly solves the following problems:

(1) Playing a certain frequency of the acoustic wave, aggregating fry in certain range;

(2) Improving feed utilization and controlling the behavior of fish, regular quantitative and precise feeding combined with acoustic taming to make fish form conditioned reflections;

(3) Real-time observation of size, quantity and scope of fish;

(4) Realizing feeding, acoustic taming and remote monitoring to reduce human labor and improve piscatorial utilization.

The overall structure of the feeding system is like a tower (Fig.1), which consists of a solar power, feeding machine, a float, a programmable Ethernet controller, several underwater sensors, an underwater camera, an audio sound device and a remote monitoring terminal. Float, fixed to the sea ranch by an anchor, works as an offshore work platform with a feeding machine installed on the upper, and the programmable logic controller installed in the float can realize automatic regular quantitative bait-throwing for all-weather.

Because it is difficult and unsafe to arrange cable between the remote monitoring terminal and the feeding machine, a solar photovoltaic power is used in the system. While it is operated, the solar panels can convert solar energy to electricity to supply power to the system, some electric power is also utilized to charge the storage battery in cloudy day and night to energize the system.

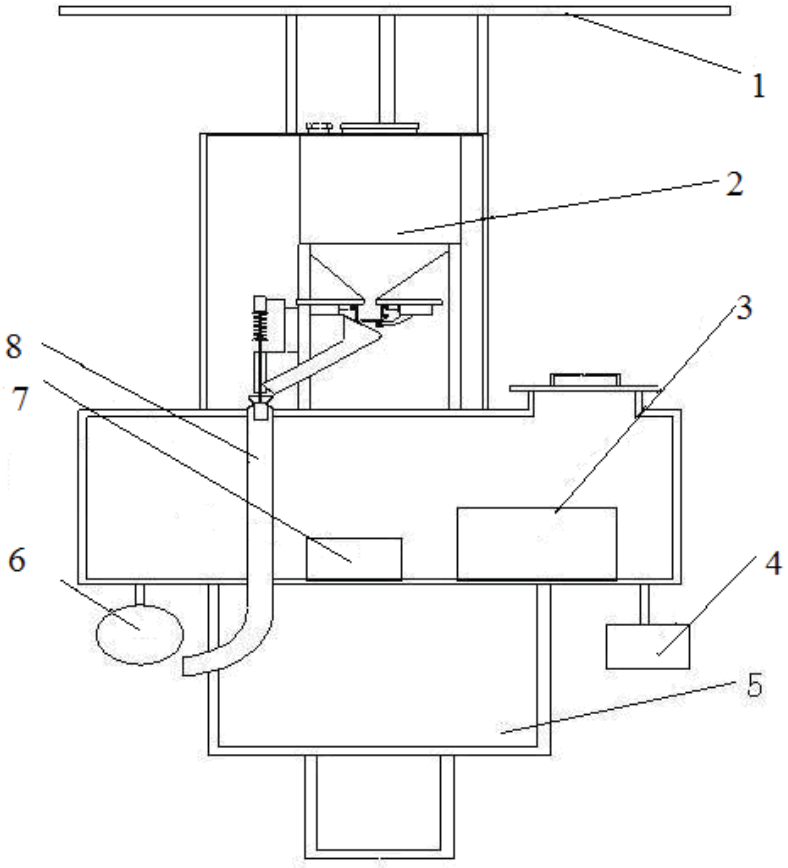

1.Solar Panels 2.Feeder 3.Battery 4.Audio Sound Device 5.Float 6.Underwater Camera 7.51 MCU 89C51 8.Discharging Tube

Fig. 1 the Structure Diagram of Automatic Feeding System

3. The Structure and Function of the System

To improve the efficiency of feeding, before operating, audio sound device which is installed below the float will attract fish around the float, and then underwater camera installed in the lower part of the float collects information on species, quantity, dimension and others to the remote monitoring terminal (PC) through a wireless communication network to determine the quantities of feed for different growth period of fish. By modifying the control program, automatic regular quantitative bait-throwing for all-weather can be achieved. Meanwhile, by the usage of underwater measurement system installed in the lower part of the float for real-time observation of sea water temperature, salinity, dissolved oxygen and other information, scientific basis can be provided for food demands, growth rate and conversion rate of bait.

3.1 Programmable Feeding Machine

The bait feeding machine is the base of the automatic feeding system, which can be either operated alone or centralized controlled through a remote network. With the programmable Ethernet controller, the electromagnet installed in the feeding machine is sequential operated according to the control instruction to realize regular quantitative throwing. It is mainly composed of a quantitative discharging device and sealing device which is used for throwing.

With the increasing development and the consummation of intensive pisciculture technology, especially the application of fish culture in net pen in large area and aquiculture technology of high density in pond, not only the demands of the particle feed is increasing, but the corresponding feeding methods and techniques are also put higher requirements. For example, the feeding habits of different breeds are different, so the feeding time, feeding amount, feeding frequency are also different; The demand of high density cultivation on water quality is higher, thus reducing the pollution of bait to the water will be particularly important.

The automatic bait-feeding machine, as shown in Fig.2, is composed of a case, a container device, a feeding device, a throwing device, a control box and a current detecting device. The container device consists of a material container and a leakage hopper; feeding device includes a feeding tube and a vibrator; the throwing device comprises a motor and a turntable; the control box contains a MCU, real-time clock, an analog-to-digital converter (A / D), button, LED, relay and PCB of current detecting device.

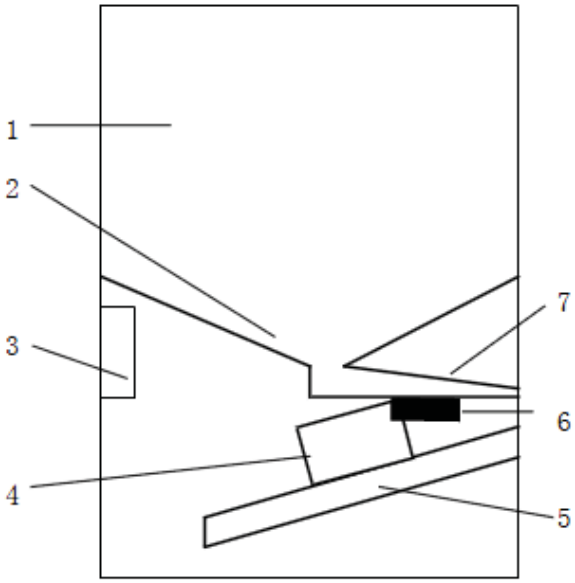

a)

1. Bait Box 2. Leakage Hopper 3. Control box 4. Motor 5. Rotary 6. Shaker 7. Feeding Tube

Fig. 2 the Feeding Machine Structure

3.2 Control Box

The control box is the heart of the programmable feeding machine; its controller (CPU) is the 89C51 of MCS-51 Series. There are 128B data-storage space, 4kb program space, two 16 timer, two external interrupt and 32 I/O port in an 89C51. The control system of the bait-throwing machine is shown in Fig.3. Three buttons are set in it for resuming by alarm, working shift, working time of feeding machine. Resuming by alarm refers to the time of the bait-throwing machine that automatically starts; working shift refers to a process that the combination of feeding time and stopping time, i.e. feeding time and intermittent time; working time is total working hours of feeding machine for a feeding process; electric current detecting device is an important part of the system which provided analysis state of motor, it provide a correct judgment to realize the quantitative feeding (quantitative feeding, bait-throwing machine works irregularly, no feed automatic shutdown) , and it can protect the motor from damage because of short-circuit and excessive rising of temperature ; protection circuit is designed to enhance its ability of anti-jamming.

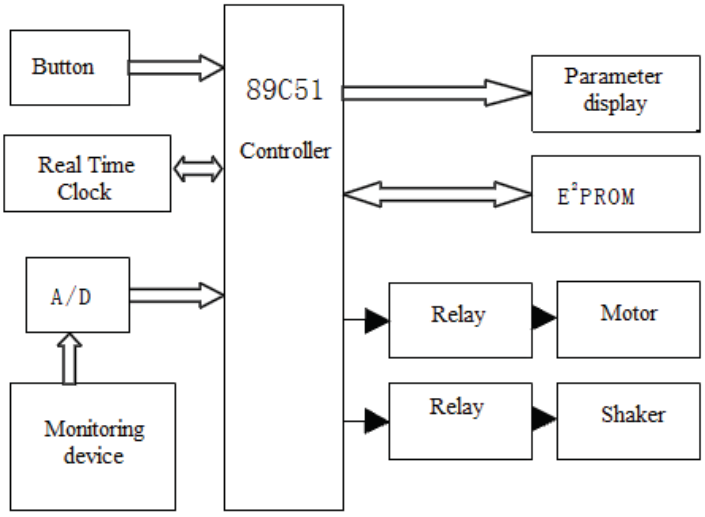

Fig. 3 Block Diagram of Control System

3.3 The Vibrating Feeding Mechanism

The programmable feeding machine adopts the mode of vibration feeding. There is a channel that delivers feed (feeding tube) between the outlet of leakage hopper and the inlet of throwing device, and a horizontal vibrator at the central position is set below the feeding tube. With the vibrator, feed in feeding tube fall into the entrance of throwing device, then throwing out by the thrower. Vibrator's switches are controlled by CPU; the shaking intensity is adjusted by working voltage of the vibrator, the principle of the voltage controller is shown in Fig.4. Once the resistance of the resistor W_1 (which is outside the chassis shell) and the charge and discharge time of capacitance C_1 is changed, the turn-on time of the controlled silicon SCR will be changed, so the working voltage of vibration device can be adjusted (Fig.4 Rc). The circuit provides pulsating DC for the vibrator. Through the bridge rectifier, 220V alternating current forming a pulsating DC current in the A and K poles of SCR; rectifier circuit charging C_1 through the resistor R_1 and the variable resistor W_1; when the voltage of C_1 reached the peak voltage (U_p) of T_1, T1 will resume from dead to conductive and C_1 will be rapidly discharged by the two junctions of T_1 (e, b) and R_2, as a result in R_2 there is a sharp pulse, which will be sent to the control electrode of controlled silicon SCR to conduct the SCR itself. Once the pulsating DC through 0 points, the SCR will be cut off automatically, and the double base diode T_1, C_1 and R_2 will become a relaxation oscillator to trigger circuit of SCR synchronously. The voltage of pulsating DC can be regulated by changing the resistance of the variable resistor W_1. As shown in Fig.4, TVP is a two-way pipe, it can effectively absorb the interference of sharp pulse voltage and lightning superposed voltage.

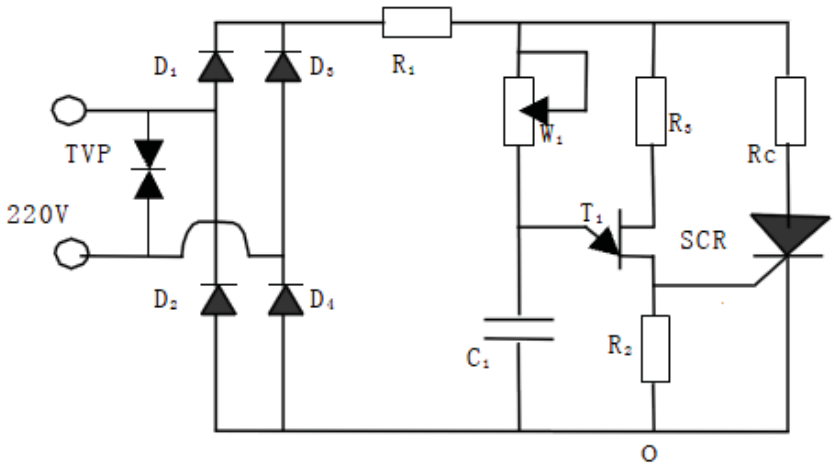

Fig. 4 Voltage Regulating Circuit Diagram

3.4 Brief Introduction of Circuit

As shown in Fig.5 and Fig.6, 89C51 chip is adopted in the system. In P0 port 74LS373 chip is applied as bus isolation one, while there are no isolation chips in the other ports. Three output ends of P1 port (P1.0, P1.1 and P1.2) are used as the inputs of the external circuit of A, B, C; A is used to start or stop V3 (NE555). When V3 works, three feet output square signals of several kilohertz as interval control signals of loudspeaker. C is used for control bipolar SCR, thereby controlling the start of scatters motor (G as shown in Fig.6). To avoid the working influence of the outside circuitry on the microcomputer chip, two power supplies (9V, 5V) is used.

Before starting the machine set the feeding quantity and the feeding frequency sets the parameters, then wait for the luring time, P1.1 foot outputs the high level and low level successively, then the horn sounds about 20 seconds, fishes are concentrated around the feeding machine. In the next stage, the feeding time, P1.2 foot is in low level, it's time for throwing. After a few seconds, it is paused. While P1.2 foot is in high level, it is paused for a few seconds, and then feed is thrown again, so the circulation is repeated until the feeding time (about 30mins) ends. Next will be the interval, which will generally last about 1 ~ 4h, and there is no throwing in it. When the interval time is end, the next round of feeding time will begin. The cycle continues like this. If there is any change during working time, it can be changed at any time as needed.

Because the feeding time and feeding frequency of the machine can be reset, it can save a lot of manpower, and reduce the effect of man's activities on fishes, which is conducive to the growth of fish.

4. The Design of Software System

The software composed by the input and the display of parameter, real-time clock, detection of working current in the motor, motor control, the control of vibrator and fault treatment. Among them, the fault judgment of motor and the state of feeding box is judged by detecting the working current of motor, the flow of the main program is shown in Fig.7.

To improve the reliability and convenience of operation, comprehensive considerations have been made for the software's basic functions and new features, and a variety of functions, such as the parameter setting and access, real-time clock, timing sampling, real-time control of motor and vibratory device, fault display and fault treatment have been set in the system during the design of the software. Based on the on-line testing, continuously strengthening functionality of the software, reliability and capacity of resisting disturbance, further enriching and improving the function of software is needed.

5. Conclusions

In the automatic bait-feeding system, the components (except current detecting device) are nearly the same as the products of current market, just modify the mechanical assembling structure and add a protective circuit, and the circuit design and manufacturing technology are reinforced. The promotion of the product's performance relies on the reasonable and perfect design of software, because it is the core of the whole system.

In the feeding system, a programmable Ethernet controller is adopted as the control core of the system; it realizes timing of sound, automatic regular quantitative feeding and the remote control and modification of the parameters, and the underwater camera outputs video signals to PC machine through the wireless communication network, for users to view or record. Therefore, the system can effectively solve a series of problems, such as precise feeding, acoustic taming, an underwater video and remote monitoring system.

At the same time, according to the breeding area, species and different growing stages, the system can realize scientific feeding by setting the parameters to adjust the quantity of feed, feeding velocity and feeding distance, which can save manpower and feed, reduce the production cost and environmental pollution due to dissolve of feed and sedimentary things.

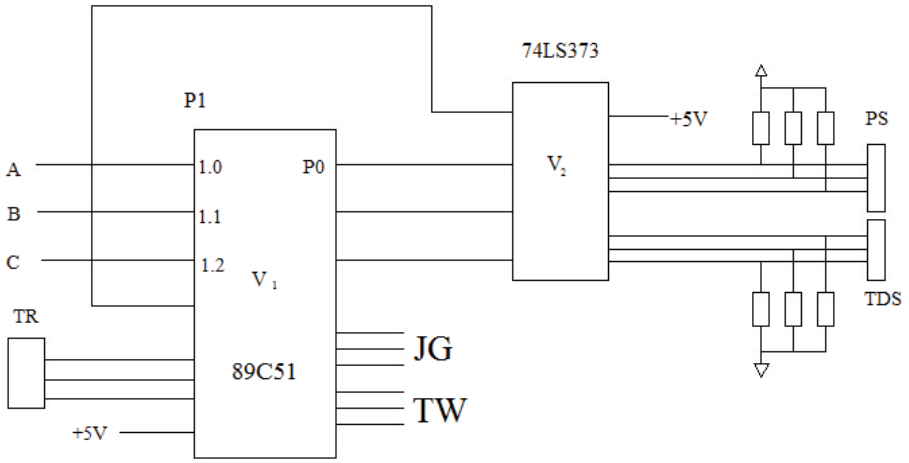

Note: PS, TDS, JG, TW, TR respectively cast time, pause time, feeding time, feeding frequency set input values.

Fig. 5 System Control Chip Chart

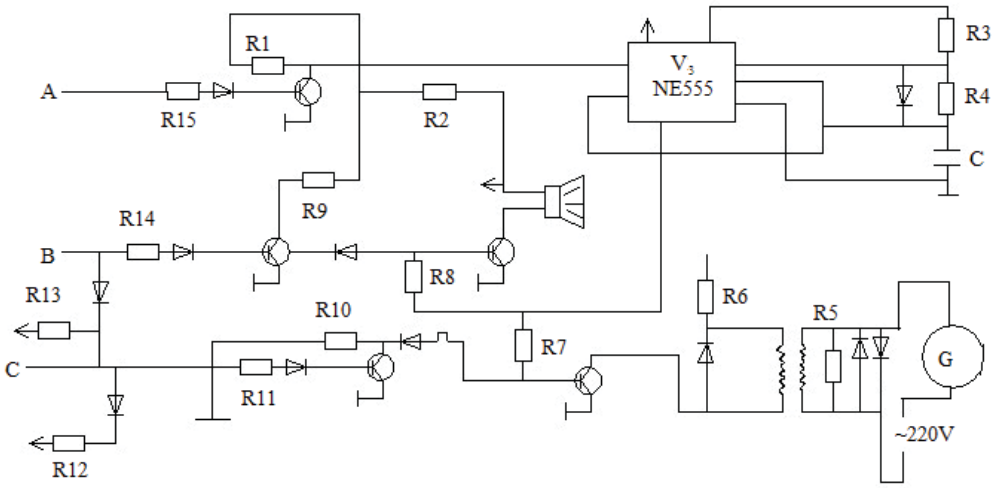

Fig. 6 Motor Circuit Diagram

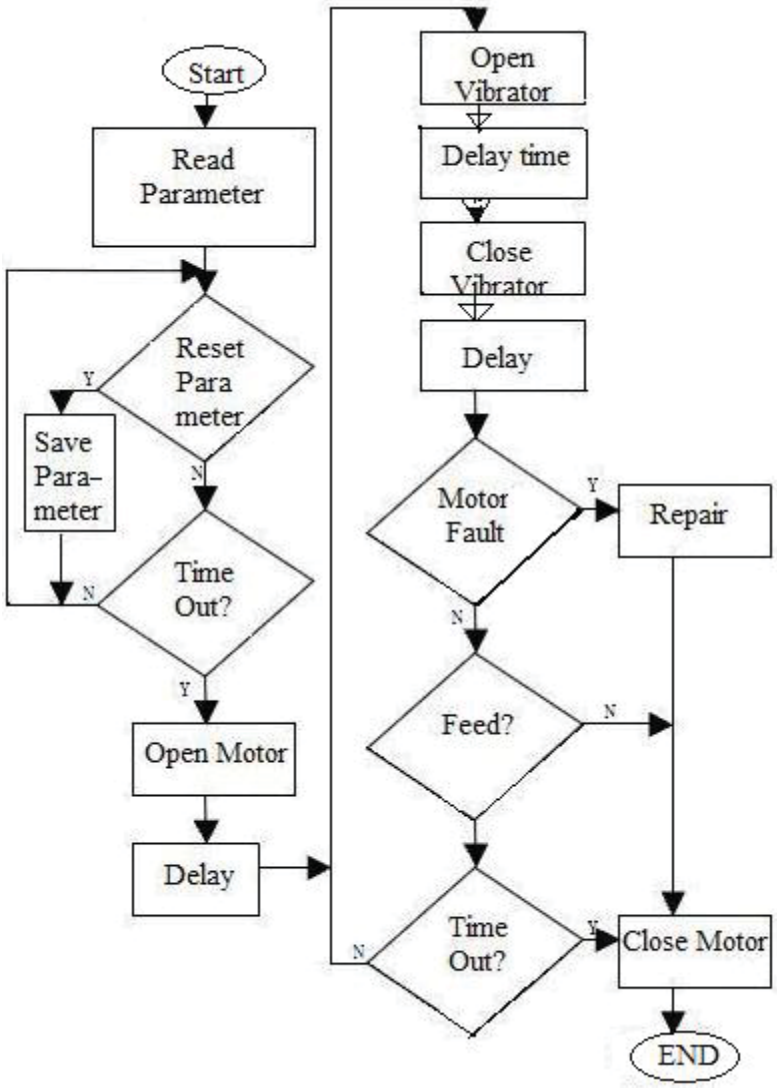

Fig. 7 Flowchart of Main Program

References

[1] J. L Li. Automatic Control System of Fish Feeding Machine based on Single-chip, *Journal of Agricultural Mechanization Research*, pp. 166-168, 2006.

[2] X. Zhong. The Design of Automatic Control System of Programmable Feeding Machine, *Journal of Agricultural Mechanization Research*, pp. 79-82, 2007

[3] A. J RAY, B. L LEWIS, C. L BROWDY and J. W Leffler. Suspended Solids Removal to Improve Shrimp (Litopenaeus Vannamei) Production and an Evaluation of a Plant-Based Feed in Minimal-Exchange, Super Intensive Culture Systems, *Aquaculture*, Vol. 299, No. 1, pp. 89-98, 2010.

[4] L. B Wu. Design of Feeding System with Remote Monitoring in Marine Ranching, *Dalian Ocean University*, pp. 23-25, 2010

International Journal of Comprehensive Engineering
Part C, 2(3), 275-279, 2013
Doi: 10.14270/IJCE2013.2.3.c275
Regular paper

ISSN 2186-2680
e-ISSN 2186-2656
www.iace-journal.org

A Method of Diameter Measurement for Spur Gear Based on Camera Calibration

Ziyue Wu [1], Jinfeng Geng [1], Zhe Xu [1]

[1] College of Engineering, Shang Hai Ocean University, Shang Hai, 201306, China

[#] Corresponding author: zywu@shou.edu.cn; Tel.: 021-61900816

Abstract: The camera calibration is the basis of putting the computer vision technique into practice. This paper proposes a new method based on camera calibration for diameter measurement of gear， and analyses the error from calibration and measurement. Diameter values are gained by this method, which firstly gets the intrinsic parameters and the extrinsic parameters by camera calibration, and then transforms the feature points in image coordinate extracted from the image plane of gear to the 3D world coordinate, lastly compute distance between the sample points and center. The experiment results demonstrate that the method is simple and quick, and easy to implement, highly precise, and rarely limited to the size of target by calibration.

Keywords: Camera Calibration, Median Filter, Addendum Circle, Dedendum Circle.

1. *Received: May 31,2012 / Accepted: May 8,2013 / Published: Sept. 10,2013*

2. Introduction

Gear is the most widely used in various bodies of a transmission device, which pass movement and power between any two axis of space, relied on mutual direct contacting with tooth profiles, so the measurement of gear parameters will directly affect on transfer power and the transmission ratio of the whole organization [1].The traditional measurement methods is too onerous and contain tedious and large computation, While the current measurement method, attached a lot of high technology and complex structure, result in relatively expensive price, and requiring professional operator and high calibration service techniques, thus the range of application is restricted to some degrees [2]. With the rapid development of computer vision technology and widespread application in China, putting the technology of image processing and camera calibration into the measurement of gear parameters has become the need of development [3]. This method has advantages of non-contact, high speed of detection, high accuracy, wide measurement range and relatively low cost. Hence, this method lays foundations for real-time online accurate measurements and detection for gear in the future.

This paper briefly describes the theory and algorithm of the plane camera calibration, and gets the world coordinate position of gear's feature points by taking advantages of the the parameters matrix between 2D image coordinate and 3D world coordinate .The Zhang Zheng you's plane calibration algorithm which is referenced in this paper has been tested in many real date to demonstrate that its operation is simple, flexibility and highly precise, as a result, it greatly facilitates advance of computer vision technology in the field of non-contact measurements [4] .

2. Camera Calibration

2.1 Calibration Theory

According to the pinhole model of camera calibration which is shown in Fig 1, we can establish mathematical model from the relationship between the four coordinates: image coordinate system (origin O_0), the real image coordinate system (origin O_1), the camera coordinate system (origin O), the world coordinate system

(origin O_W), so that we can calculate the following relationship impressed as formula (1) between the image coordinate and the world coordinate:

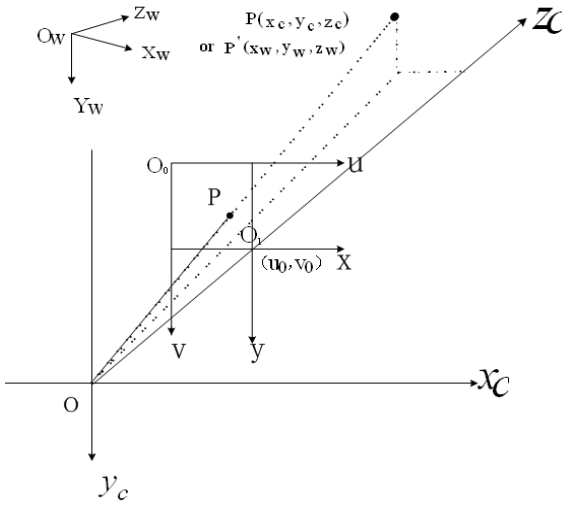

Fig. 1 Coordinate System

$$s\tilde{m} = A[R \quad t]\tilde{M} \tag{1}$$

$$A = \begin{bmatrix} \alpha & \gamma & u_0 \\ 0 & \beta & v_0 \\ 0 & 0 & 1 \end{bmatrix} \tag{2}$$

where $\tilde{m} = [u \quad v \quad 1]^T$ is Homogeneous point on image coordinate. $\tilde{M} = [X_w \quad Y_w \quad Z_w \quad 1]^T$ is Homogeneous point of the 3D world coordinate. S is an arbitrary scale factor. and A, named the matrix of the camera intrinsic matrix ,describe the relationship between image coordinate system and camera coordinate system as shown in formula (2),with (u_0, v_0) the coordinate of the principal point , α, β the scale factor in image u and v axes, and γ the parameter describing the skewness of the two image axes. $[R \quad t]$,called the extrinsic parameters which relates the world coordinate system and the camera coordinate system, is the rotation matrix and translation matrix.

As assumed for the calibration plane, the model plane is on Z=0 of the world coordinate system, namely, (1) can be written as following:

$$s\begin{bmatrix} u \\ v \\ 1 \end{bmatrix} = A[r_1 \quad r_2 \quad r_3 \quad t]\begin{bmatrix} X_w \\ Y_w \\ 0 \\ 1 \end{bmatrix} = A[r_1 \quad r_2 \quad t]\begin{bmatrix} X_w \\ Y_w \\ 1 \end{bmatrix}. \tag{3}$$

$$\begin{bmatrix} X_w \\ Y_w \\ 1 \end{bmatrix} = \lambda * [r_1 \quad r_2 \quad t]^{-1} * A^{-1} * \begin{bmatrix} u \\ v \\ 1 \end{bmatrix}. \tag{4}$$

$$H = A[r_1 \quad r_2 \quad t]. \tag{5}$$

From above, transformational relation can be achieved between image coordinate system and world coordinate system, just matrix H as written in formula (5) (λ as scale factor). Under current case, the lens distortion and the skewness of the two image axes are ignored so as to simplify the process of calibration.

2.2 Camera Calibration

The calibration pattern with black and white squares whose size is 10mm * 10mm is printed on a laser printer and stuck on a glass with a gear measured on the same planar surface. A group of images of plane under different orientations were taken .Next, let begin our calibration process following these steps:

The first step, the corner points in pixel are detected as the intersection of straight fitted to each square. Corresponding points of the world coordinate system are marked in mm according to the sequence of vertical and horizontal squares.

The second step, according to the formula (1) and (5), the simultaneous equations about elements of matrix H are generated on the basis of corner points in pixel and points of the world coordinate system, and results worked out by a nonlinear optimization technique based on the maximum likelihood criterion.

The third step, since R is an orthogonal matrix, according to formula (1) and (5), matrix H of each image is taken into the simultaneous equations. The solution was matrix A, elements of matrix A can provided for the intrinsic parameters.

The forth step. The extrinsic parameters r_1, r_2, t are worked out after bringing A and H into formula (5). So far, the intrinsic and extrinsic parameters of camera have been obtained, that is to say, the process of calibration is over.

2.3 Calibration Result

The following results can be obtained by MATLAB programming according to the algorithm above.

$$A = \begin{bmatrix} 1855.73 & 0.000004 & 36.8 \\ 0 & 1555.1 & 312.27 \\ 0 & 0 & 1 \end{bmatrix};\quad R = \begin{bmatrix} -0.156 & 0.979 & -0.132 \\ 0.986 & 0.162 & 0.038 \\ 0.058 & -0.124 & -0.991 \end{bmatrix};\quad t = \begin{bmatrix} -191.5 \\ -206.0 \\ 1056.9 \end{bmatrix};$$

A is the intrinsic parameters matrix of camera. **R** is rotation matrix. **t** is the translation matrix. Skewness of the two image axes are not taken into our account.

2.4 Error Analysis

In order to verify the accuracy of camera calibration , corner points in image coordinate selected randomly are transformed to the point $[X'_w \quad Y'_w \quad 0]$ in 3D world coordinate in terms of formula (4) .Then error evaluation of calibration process can be got by comparison between actual measured points $[X_w \quad Y_w \quad 0]$ and the points $[X'_w \quad Y'_w \quad 0]$ through calculations. As pictured Fig 2, whether it is the x-axis or y-axis, most of the error percentage is generally about 1%. Including hardware there are some influences on the results as well as software and algorithms, like optical devices. The error variances which X and Y directions respectively are 0.0529 and 0.0471, indicate good stability of error, and the above analysis of calibration results offer a strong support for utilization in the measurement system.

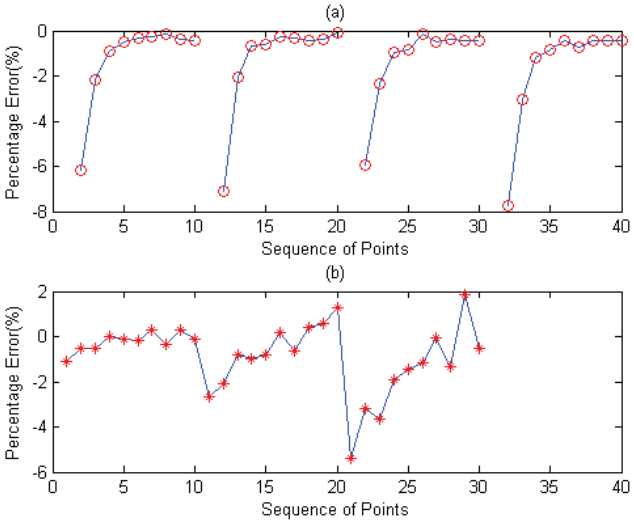

Fig. 2 Error analysis of camera calibration (a) The error of X axis (b) The error of Y axis

3. Diameter Measurement

3.1 Number of Teeth

Median filter is a typical non-linear filter to remove the impulsive noise, actually which is based on the arrangement order and does a better job of preserving sharp edges and details over the low-pass filter. The principle of median filter is that the median or center of the pixel will be placed in the output image in the location corresponding to the center of the window sliding across the pixels of a picture and ranking the pixels in the window in ascending order, and the process is repeated for all the pixels in the image [5,6].

When counting the number of teeth, the size of filter window should be determined suitably by our need ,because that the computation time will be directly affected by the window size as there be more values to sort as a window grow bigger, and the size of window also determines the amount of details that can be filtered out[6]. The number of teeth is equal to the number of regions by subtracting the median filter image from original binary image, as shown in Fig 3 (a).

3.2 Detection of Center

Firstly, in order to get a symmetric and closed area as shown in Fig 3 (b) below, binary image is filtered by the 2D circular mean filter. Then the center of region is quite right to the center of gear marked in the Fig 3 (c).

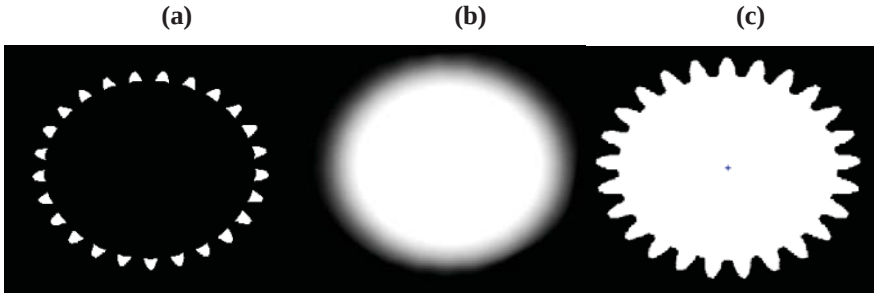

Fig. 3 Images processed (a) Gear Image (b) Image Filtered (c) Marking Center

3.3 Result

In this test, its results N=25 is coincide with the active situation. The feature points in pixel of edge and center from the results of section 2.3 are transformed to the world coordinate according to the formula (4), and there is a part of points listed in the following table 1. Center in pixel is（461.899，221.6885）(pixel)，and after transforming into the world coordinate（36.822，75.828）(mm).Respectively N points are sampled in the addendum circle and dedendum circle. The mean values of distance between center and sample points are regarded as the radius measurement values, so we can get the diameter measurement.

Table 1 Results

Image Coordinate（pixel）	World Coordinate (mm)	Dedendum circle diameter (mm)	Image Coordinate（pixel）	World Coordinate (mm)	Addendum circle diameter (mm)
502.48 129.41	15.568 80.09	43.3548	39.618 48.9234	322.11 245.87	53.9866
502.48 129.41	15.568 80.09	43.3546	39.618 48.9235	322.17 245.99	53.9588
502.48 129.4	15.567 80.089	43.3544	39.618 48.9236	322.2 246.06	53.9544
502.47 129.39	15.566 80.087	43.3548	39.618 48.9237	325.34 186.78	53.9522
…	…		…	…	…
	Measurement（mean）	43.3388mm		Measurement（mean）	54.01816mm

3.4 Error Analysis

The following Fig 4 shows the error percentage between standard value and measurement value in the method proposed in this paper for 30 experiments, where the measurement error of diameter of addendum circle is basically around $^{\pm}$2%, and the measurement error of diameter of dedendum circle is basically around ±5%, but on rare occasions, large disparities emerge more strong than the other. Variances of error by statistic analysis respectively are 0.00067and 0.000557, indicating that the error is basically stable. The most source of error is image processing besides calibration error.

Since the processing of each pixel in image is universal, not related to the specific or individual, error caused inevitably in the course of image processing, so in the future research there should be putted more energy for refining in details.

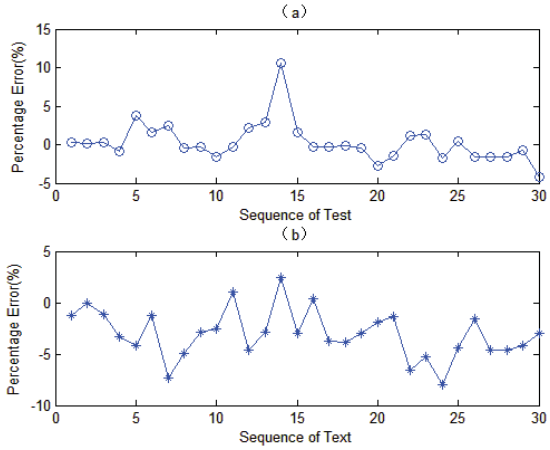

Fig. 4 The error of diameter (a) The error of addendum circle (b) The error of dedendum circle

4. Conclusion

By the analysis mentioned above, compared with literatures [3] and [7], the method to get the diameter of gear based on camera calibration proposed in this paper doesn't only improve the accuracy of measurement, specially, but also not restrict the size of diameter measured from camera calibration. Moreover, there is a problem to explain that sample points in the part of 3 .3 are not uniform distribution in every addendum circle or dedendum circle, and this demonstrate that this gear is not a strict standard, so this offer a basis for testing the precision of gear. But in this paper, the approach is imperfect to estimate the number of sample points according to the number of teeth, and effected by the procedure of image processing. Furthermore, traditional plane calibration algorithm used in this test require calibration pattern all the time, so this impose restriction on the occasions applications of method [8].

Concluded briefly, there are two key issues to solve in the process of putting the computer vision technology into practice, one is camera calibration, the other is image analysis and processing. How to reduce the error from the two sides in our future research and applications will attract more attentions, but give us an idea now.

References

[1] H. Sun, Z. M Chen. *The Theory of Machines and Mechanisms*, Higher Education Press, Bei Jing, pp. 174-180, 2006.
[2] H Rui, R. Lu, N. Liu, S. Li and N. Li. Image Processing Technique for Digital Image Measurement of Involute Spurs, *Tool Engineering*, Vol. 44, No. 9, pp. 90-93, 2010.
[3] W. W Yue. *Research on the Computer Vision Technology for Measurement Gear*, Wuhan University of Technology, 2008.
[4] Z. Y Zhang. A Flexible New Technique for Camera Calibratin, *IEEE Transaction on Pattern Analysis and Machine Imtelligence*, Vol. 22, No. 11, pp. 1330-1334, 2000.
[5] Q. Q Ruan. *Digital Image Processing*(Second Edition), Electronics Industry Press, pp. 334-335, 2007.
[6] Randy Cranm. *Simplified Approach to Image Processing*, Manager Hewlett-Packard Press, pp.95-98, 1997.
[7] H. Du, W. Jin, X. zhang and J. Hu. A Method of Dimension Measurement for Spur Gear Based on Machine Vision, *IEEE International conference on Multimedia and Signal Processing*, pp. 243-246, 2011.
[8] X. R Yang. Progress on Camera Calibration Method in Visual Measurement, *Machinery Design &Manufacture*, Vol. 3, pp. 259-261, 2009.